Chemical and Physical Analysis of Melanin in Complex Biological Matrices

by

Keely E. Glass

Department of Chemistry
Duke University

Date:_____

Approved:

_____
John D. Simon, Co-Supervisor

_____
Stephen L. Craig, Co-Supervisor

_____
Katherine J. Franz

_____
Richard F. Kay

Dissertation submitted in partial fulfillment of
the requirements for the degree of
Doctor of Philosophy in the Department of Chemistry
in the Graduate School of Duke University

2014

ABSTRACT

Chemical and Physical Analysis of Melanin in Complex Biological Matrices

by

Keely E. Glass

Department of Chemistry
Duke University

Date:_____

Approved:

_____
John D. Simon, Co-Supervisor

_____
Stephen L. Craig, Co-Supervisor

_____
Katherine J. Franz

_____
Richard F. Kay

An abstract of a dissertation submitted in partial fulfillment of the requirements for the degree of Doctor of Philosophy in the Department of Chemistry in the Graduate School of Duke University

2014

Abstract

Melanin is a ubiquitous biological pigment found in bacteria, fungi, plants, and animals. It has a diverse range of ecological and biochemical functions including display, evasion, photoprotection, detoxification, and metal scavenging. Two forms of melanin produced from different molecular precursors are present in nature – eumelanin (dark brown-black in color) and pheomelanin (orange-red in color). Both eumelanin and pheomelanin are complex highly cross-linked biopolymers that are found intertwined with proteins, lipids, and metal ions in nature.

Recent reports have used morphological evidence to suggest the presence of melanin in the fossil record. These studies have been met with criticism due to their lack of chemical evidence to support melanin identification. This dissertation describes chemical approaches to unambiguously verify the presence of melanin in the fossil record and characterize the ancient pigment. It also explores the limitations for the survival of melanin in the fossil record and the possibility that melanin acts as a protective matrix to preserve other biomolecules that are embedded in the pigment.

Melanin has unique chemical signatures that are commonly used to characterize and compare the pigment of modern organisms. We applied these chemical approaches to the study of fossil pigmentation. Analysis of the black pigmentation of two > 160 million year old (Mya) Jurassic cephalopod ink sacs provided the first conclusive

evidence for eumelanin in the fossil record. The preserved fossil eumelanin was then compared to modern cephalopod eumelanin from *Sepia officinalis*. Using these chemical approaches we found that fossil eumelanin was chemically and morphologically identical to *S. officinalis* eumelanin.

Although there is mounting chemical evidence for the presence and preservation of melanin in the fossil record, there is very little data constraining its long-term survival. We applied the analytical approaches designed to study fossil melanins and techniques used to study fossil sediments to compare the fossil inks from three deposits of similar age and lithology, but different maturation histories. Specifically, two ~ 180 Mya fossil ink sacs from a site that has entered the oil window in Holzmaden, Germany were compared to the previously analyzed fossil inks from two less mature sites in southern England. The chemistry of eumelanin was shown to alter at the onset of the oil window regardless of the age of the specimen. The decrease in surviving melanin was accompanied by an increase in the relative abundance of organic macromolecular material (kerogen), but no consistent change in melanin morphology.

Finally, the role of melanin as a matrix that enhances the preservation of other biomolecules in the fossil record was considered. Proteins, commonly associated with melanin in modern organisms, were discovered in the aforementioned fossil ink sacs during full-scale chemical analysis. The amino acid profile of the protein in each fossil specimen was determined with an amino acid analyzer and compared to the amino acid

profile the protein in modern *S. officinalis*. Statistical analysis of the amino acid distributions indicated that there is no significant difference between the amino acid profile of modern and fossil melanins. In order to verify the ancient origin of the amino acids in the fossil ink sacs, the ratio of D/L amino acid isomers was determined. While the proteins of living organisms consist of only L-amino acids, post-mortem the amino acids slowly convert from L to D form until they reach equilibrium (D/L = 1). This process is called racemization. The amino acids in the fossil ink sacs were racemized, which suggests their ancient origin. This marks the oldest determination of protein in a fossil system and provides evidence that the longevity of proteins may be enhanced when associated with melanin.

Contents

List of Tables

List of Figures

List of Abbreviations

DHI	5,6-dihydroxyindole
DHICA	5,6-dihydroxyindole-2-carboxylic acid
Mya	million years old
SE	scanning electron microscopy
PDCA	pyrrole-2,3-dicarboxylic acid
PTCA	pyrrole-2,3,5-tricarboxylic acid
isoPTCA	pyrrole-2,3,4-tricarboxylic acid
PTeCA	pyrrole-2,3,4,5-tetracarboxylic acid
HPLC	high-performance liquid chromatography
MS	mass spectrometry
UV-Vis	ultraviolet-visible
EPR	electron paramagnetic resonance
Py-GC-MS	pyrolysis gas chromatography mass spectrometry
FTIR	fourier transform infrared
IR	infrared
XPS	x-ray photoelectron spectroscopy
^{13}C CP-MAS	carbon-13 cross-polarization magic angle spinning
SSNMR	solid state nuclear magnetic resonance

Acknowledgements

To my research advisor Dr. John Simon I give a heartfelt thank you. Without your support, faith, and guidance I would not be in the final stages of my Ph. D. in Chemistry. Your words of encouragement often helped me overcome the greatest challenges in my research and diminished the limitations I set for myself. You have inspired me to teach chemistry and to guide students as you have guided me. Thank you.

This work could not have been completed without the support of my parents, siblings, and husband. Thank you all for giving me the happiest life. Thank you for telling me the hardest truths, listening during the most trying moments, and providing me with a solid support system since the very beginning. Kirstie, thank you for providing the model of a wonderful human being – I know I am older, but you are undoubtedly wiser. To my husband Doug, thank you for being my person. I love you and cannot imagine doing this without you by my side.

For their contributions to my development as a teacher and scientist, I would like to thank Dr. George Dubay, Dr. Todd Woerner, and Dr. Kenneth Lyle. Each of you contributed critically to my Ph. D. experience.

Dr. George Dubay, your kindness and patience as I learned how to use the GC and LCMS will always be remembered. I will miss our daily conversations about science

and life. I thank you for forging a collaboration with the Simon lab and helping the students and I develop new protocols for fatty acid and amino acid analysis.

Dr. Todd Woerner, you taught me how to wield a torch comfortably, how to guide students through research projects, and how to survive graduate school with a touch of humor and a focus on life/work balance. I'll think of you whenever I use fire to fix, fashion, or flame-seal glass and when I interact with students of my own.

Dr. Kenneth Lyle, I will use the demonstrations I've learned through our chemistry outreach work for the rest of my life. I will keep you in mind every time I try a new demonstration, amaze a crowd, and fill up my dewar with liquid nitrogen. I will miss our banter, our work on and off campus, and all of the delicious scientific delicacies we made together.

The past and present members of the Simon Lab inspired me and motivated me to conquer the elusive pigment melanin. I am particularly indebted to Dana Peles for keeping in touch after graduate school and meeting to discuss science and life. Right after starting in the Simon Lab, when I was still a little afraid of the completely new field of research, you gave me a pep talk that I remember to this day. In essence you told me to jump into the research and work directly with the science until I could think of something new. As I wrote my dissertation this "jump-in" philosophy kept me motivated to move forward even when I did not have a clear picture of where to go.

This work could not have been completed without the assistance of exceptional scientists from many disciplines. I wish to thank all of my collaborators and mentors for their contributions to this work. I would also like to thank my undergraduate students for their tireless toils. Thank you all.

1. Introduction to the analysis of biomolecules in fossils

1.1 Biomolecule preservation in fossils

The canonical view that labile soft-tissues break down in the fossil record has been challenged in recent years by the discovery of intact organic constituents in certain fossils (Butterfield, 1990; Stankiewicz et al., 1997; Stankiewicz et al., 1998; Antonio et al., 2011; Cody et al., 2011; Wogelius et al., 2011; Glass et al., 2012; Lindgren et al., 2012). Preservation of these soft-tissues – organismal parts that are not mineralized in life – is rare because degradation by microbes is highly efficient (Briggs et al., 2000; Briggs, 2003; Schweitzer, 2011). Microbes use the carbon and nitrogen within tissues, cells, and proteins for metabolic energy and convert them rapidly to usable forms post-mortem (Butterfield, 1990; Knicker and Hatcher, 1997; Schweitzer, 2011). Even in the case of the most exceptionally preserved soft-tissue fossils, many organic constituents are lost through these processes (Briggs et al., 2000). Tissues that do survive are subject to diagenetic alteration over time whereby their organic constituents polymerize into long chains of hydrocarbons that are resistant to further degradation (Butterfield, 1990; Briggs et al., 2000; Schweitzer, 2011).

Soft-tissues that are preserved have distinctive structural attributes: highly cross-linked structures, large hydrophobic (water-hating) regions, aliphatic or poly-aromatic frameworks, and polymeric backbones (Tegelaar et al., 1989; Butterfield, 1990; Briggs,

1999; Briggs et al., 2000; Schweitzer, 2011). The basis of the degradation resistance of these structural attributes is summarized below. Structures that are highly cross-linked occlude the reactive regions of potential substrates thus protecting from structural degradation (Butterfield, 1990). Poly-aromatic and aliphatic frameworks are less reactive than small, labile organic constituents that contain additional nitrogen and oxygen centers (Tegelaar et al., 1989; Butterfield, 1990). Polymeric backbones are very stable because they must be broken down to their monomeric units at an energetic cost prior to being incorporated by microbes (Butterfield, 1990; Briggs, 1999; Briggs et al., 2000; Schweitzer, 2011). Moreover, polymers composed of different monomeric units or monomer linkages often require more than one type of microbe or enzyme for degradation (Butterfield, 1990). As a result, polymeric structures often survive longer in the fossil record than organic components that degrade more readily (Butterfield, 1990; Schweitzer, 2011). Preservation of soft-tissues is also enhanced when their organic constituents are intimately associated with minerals, incorporated into structural tissues, or encapsulated by degradation-resistant matrices (Butterfield, 1990; Briggs, 1999; Briggs et al., 2000; Schweitzer, 2011).

Collagen, a fibrillar structural protein found in the connective tissues of animals, has many of the structural attributes that confer resilience (Schweitzer et al., 2008). Collagen's relative insolubility in water, frequent tight association with the bone mineral hydroxyapatite, and intermolecular crosslinks lend to its increased survival in the fossil

record (Weiner and Traub, 1986; Traub et al., 1993). Similarly, keratin – a structural protein found in hair, skin, and nails – is composed of cross-linked polymeric fibrils and is often preserved in the fossil record (Fraser and Macrae, 1980; Bonser, 1996; Schweitzer, 2011). Keratin is not biomineralized, but forms abundant inter- and intramolecular crosslinks with other keratin fibers and is composed of numerous hydrophobic amino acids that exclude water and confer long-term stability (Fraser and Macrae, 1980; Schweitzer, 2011). Unlike keratin and collagen, the fossilized carbonaceous tree-resin amber is of interest for both the structures it encases and its own composition (Stankiewicz et al., 1998). Animals and plant matter caught in tree-resin as it is secreted are entombed when the resin hardens to amber (Stankiewicz et al., 1998). Though the encapsulating resin protects the entombed organisms from microbial decay, chemical alteration still occurs slowly in this environment (Knicker and Hatcher, 1997; Stankiewicz et al., 1998; Briggs, 1999).

As scientists have become aware of an increasing number of intact organic constituents in the fossil record over the last few decades, new analytical techniques have been applied to allow them to characterize these residues (Schweitzer et al., 2008; Vinther et al., 2008; Clarke et al., 2010; Li et al., 2010; Wogelius et al., 2011; Glass et al., 2012; Glass et al., 2013). Part of the challenge of this research is to differentiate an organism's original molecules from bacterial degradation products and modern contaminants (Schweitzer et al., 2008; Schweitzer, 2011).

Melanin – a highly cross-linked, insoluble, aromatic biopolymer – has all of the structural attributes of a highly degradation-resist biomolecule (Butterfield, 1990; Glass et al., 2012). As a result, scientists have recently proposed that it survives fossilization (Vinther et al., 2008; Clarke et al., 2010; Li et al., 2010; Vinther et al., 2010; Zhang et al., 2010; Barden et al., 2011; Wogelius et al., 2011; Glass et al., 2012; Lindgren et al., 2012; McNamara, 2013; Lindgren et al., 2014). The study of structures that appear to represent fossil melanin is particularly challenging because the morphology of melanosomes (organelles that contain the pigment melanin) is similar to that of many microbes and minerals found in fossils (Davis and Briggs, 1995; Vinther et al., 2008; Wogelius et al., 2011; McNamara, 2013). Due to these physical similarities, scientist must rely on chemical tools to establish the preservation of melanin in fossils. To develop these tools, an in-depth understanding of the structure and chemical properties of melanin is necessary.

1.2 Introduction to melanin and melanogenesis

Melanin was a term coined in 1840 in reference to black animal pigments (Berzelius, 1840; d'Ischia et al., 2013). Since then the term has been used more broadly to define a class of phenolic-quinone pigments derived from natural and synthetic sources (Riley, 1997; Simon and Peles, 2010; d'Ischia et al., 2013). Natural melanins are nearly ubiquitous; found in some organisms within all kingdoms of life while synthetic melanins are prepared based on methods summarized recently in a review by d'Ischia

and coworkers (Hill, 1992; Wakamatsu et al., 2009; d'Ischia et al., 2013). Although the focus of this dissertation is on natural melanin from modern and ancient cephalopod ink sacs, other notable sources of animal melanin include the feathers of birds and the hair, skin, eyes, brain and inner ears of mammals. Classification of animal-derived melanin into two major types – eumelanin, dark brown-black in color, and pheomelanin, yellow-red in color – occurred in the 1960's following the study of various natural pigments (Prota et al., 1966; Minale et al., 1967; Prota and Nicolaus, 1967a;b; Nicolaus, 1968; Ito, 2003).

The first steps of the biosynthetic pathway for the production of melanin known as "melanogenesis" were established through a series of landmark experiments spanning nearly 100 years (1895-1985) (Ito, 2003). In 1896 Bertrand established that tyrosine is converted by fungal tyrosinase (discovered in 1895) to a black pigment resembling the melanin found in animals (Bourquelot and Bertand, 1895; Bertand, 1896). Henry Raper followed Bertrand's work in 1927 with the isolation of dopa, 5,6-dihydroxyindole (DHI), and 5,6-dihydroxyindole-2-carboxylic acid (DHICA) produced from the oxidation of tyrosine by tyrosinase (Raper, 1927). Through his detailed chemical studies Raper established the primary chemical steps for the enzymatic oxidation of tyrosine to melanin (Raper, 1927). Howard Mason furthered Raper's model in 1948 when he proposed a "polymer" model for melanin following his spectroscopic identification of dopachrome (Mason, 1948). The current understanding of the initial

steps of melanogenesis, called the Raper-Mason scheme in honor of Henry Raper and Howard Mason, is detailed in Figure 1 (Ito and Wakamatsu, 1998).

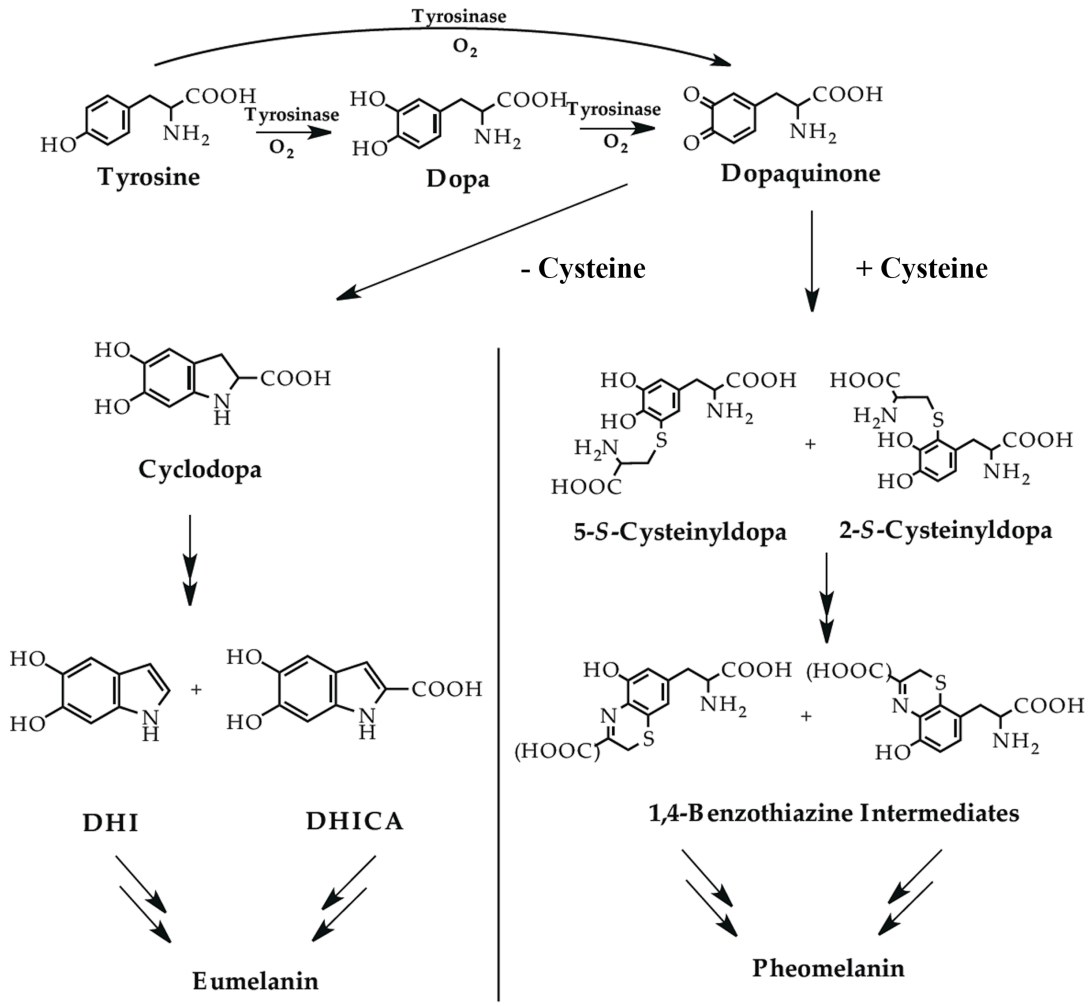

Figure 1: Abridged depiction of the early steps of melanogenesis.

Dopaquinone is the branch point between the formation of eumelanin and pheomelanin. The final pigment formed depends on the concentration of cysteine available. This figure was reproduced with permission (Ito and Wakamatsu, 1998).

As indicated in the Raper-Mason scheme (Figure 1), eumelanin and pheomelanin are produced from different molecular precursors during melanogenesis. The key rate-

determining step for the formation of eumelanin and pheomelanin pigments is the oxidation of L-tyrosine to dopaquinone by the enzyme tyrosinase (Ito, 2003). Dopaquinone is a highly reactive intermediate that rapidly undergoes spontaneous reactions that, in the presence of over 1 μM of cysteine, give rise to sulfurous cysteinyldopa (Land and Riley, 2001; Ito, 2003). Cysteinyldopa then undergoes a series of reactions to form benzothiazine units, which ultimately oxidize to give pheomelanin. In the absence of 1 μM cysteine, dopaquinone is rapidly converted to dopachrome through the intermediate cyclodopa, which is gradually converted to 5,6-dihydroxyindole (DHI) by decarboxylative rearrangement and to 5,6-dihydroxyindole-2-carboxylic acid (DHICA), by tautomerization (Land and Riley, 2001; Ito, 2003). DHI and DHICA are then further oxidized to produce the eumelanin polymer.

In spite of the chemical differences between the reactions responsible for the formation of eumelanin and pheomelanin pigments, both can be found within the same melanocyte (pigment-producing cell) (Ito, 2003; Wakamatsu et al., 2006). In fact, the majority of melanin in animals is a mixture of these two pigment forms (Ito, 2003; Simon and Peles, 2010). Sources of mixed melanins include the hair, skin, eyes, and feathers of animals. Pure eumelanin is also found throughout nature. One notable example of pure eumelanin that will be mentioned throughout this dissertation is the ink of the common cuttlefish, *S. officinalis.* Pheomelanin in contrast, is not found pure in nature.

Melanin is also found naturally in the form of melanin granules. It is important here to clarify the difference between melanin granules and melanosomes. Although both are produced during melanogenesis in which a membrane-bound matrix is formed and melanin is deposited, in vertebrates each melanosome is a single packaged melanin granule (Liu and Simon, 2003). Invertebrate cuttlefish *S. officinalis* in contrast, produces ~30 granules which are released into the ink sac lumen during melanogenesis (Schraermeyer, 1994). To distinguish between the two, ink sac pigment structures are referred to as 'melanin granules' while vertebrate pigment structures are called 'melanosomes' (Schraermeyer, 1994). Both melanin-packages – melanosomes and melanin granules – also contain lipids, metals, and proteins (Prota, 1992). The structure of melanin and the components bound within it contribute to its chemical properties.

1.3 Chemical properties of melanin

Melanin has a diverse range of ecological and biochemical functions: display to attract partners, camouflage and defense to evade predators, photoprotection, anti-oxidant and free-radical scavenging, and binding of metal ions (Hill, 1992; Sarna and Swartz, 2006; Ito et al., 2013b). An excellent summary of the complexity of these various roles of melanin is depicted in the melanin mock-up of the six blind people (scientists) that set out to describe an elephant (melanin) below Figure 2 (Hill, 1992). All of these properties of melanin are important to this thesis and are presented briefly.

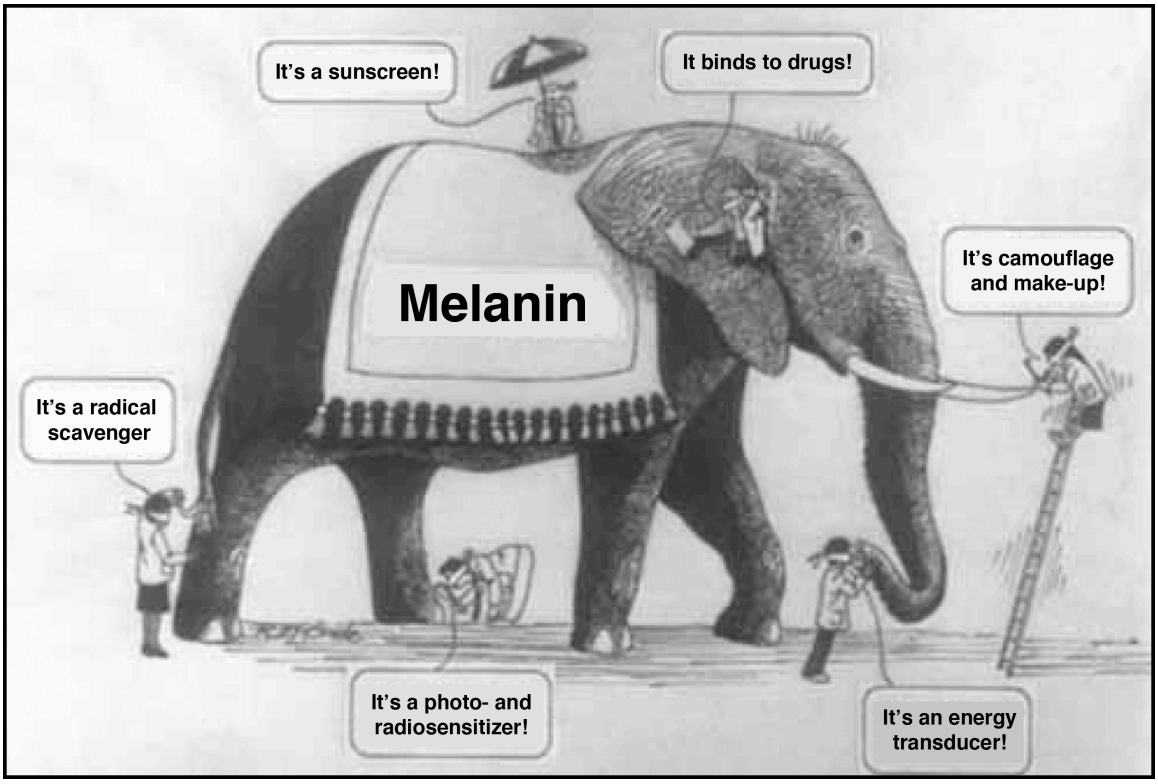

Figure 2: The six scientists examine melanin

Summary of the various roles of melanin reproduced from Hill, 1992. This image details the scientists that study melanin – each with only partial knowledge of its attributes.

Pigments like melanin contain at least one chromophore – a chemical group that can absorb a specific wavelength of visible light. Melanin is unusual in that it can absorb light over a wide spectral range. This absorption is featureless and increases monotonically as wavelengths decrease in the ultraviolet-visible (UV-Vis) range (Crippa et al., 1978; Nofsinger et al., 2002; Simpson et al., 2014). This is likely the result of many chromophores within the heterogeneous aromatic pigment absorbing at overlapping wavelengths through an extended span of the spectra, reflection, and scattering (Nofsinger et al., 2002; Meng and Kaxiras, 2008; Simpson et al., 2014).

The eu- and pheomelanin composition of the melanosomes in an organism is directly related to the coloration observed. Take for example human hair color; all hair colors from black to blond contain a constant level of pheomelanin (0.85-0.99 μg per mg), but varying levels of eumelanin (Ito and Wakamatsu, 2011). The eumelanin to pheomelanin ratio decreases with lighter hair phenotypes and is approximately 26, 17, 12, 10, and 5 for black, dark brown, medium brown, light brown, and blond hair, respectively (Ito and Wakamatsu, 2011). Red hair differs: its eumelanin and pheomelanin concentrations are nearly equal and its pheomelanin concentration is 4.7 μg/mg – much higher than the other hair phenotypes (Ito and Wakamatsu, 2011). The quantity and distribution of pheomelanin and eumelanin is also the predominant control on the coloration of eyes and bird feathers (Prota, 1992; Ito and Wakamatsu, 2003; McGraw and Wakamatsu, 2004; Peles et al., 2009).

The colors imbued by melanin are important in sexual and social display, camouflage, and defense against predators. The feather-melanin distribution of male Mallards for example is effected by the concentration of circulating testosterone (Haase et al., 1995). These elevated testosterone levels are associated with higher pheomelanin concentrations in certain body regions of the male Mallards and has been proposed to increase mating success (Haase et al., 1995; McGraw and Wakamatsu, 2004). One tangible example of defense against predators and camouflage is the black, eumelanin ink spray of cephalopods. In response to a predator approach, cephalopods expel their

ink in the direction of their would-be attacker (Derby and Aggio, 2011). The ink expulsion lends to a rapid escape while the ejected ink cloud obscures the escape route and acts as an intra-specific alarm cue for nearby cephalopods (Derby and Aggio, 2011).

These roles of melanin are of particular interest in the study of fossilized organisms. Resolving the color patterns of extinct species may provide key insights into the natural selection processes at work during crucial evolutionary periods (Wogelius et al., 2011; McNamara, 2013). It may also help discern the functional evolution of melanin and its role in sexual selection, camouflage, and defense mechanisms of ancient organisms (Wogelius et al., 2011; McNamara, 2013).

The broad-band absorption of melanin from the visible range to the UV also plays a critical role in its photoprotective functions (Kollias et al., 1991). Melanin serves as a barrier to decrease UV penetration through the epidermis by scattering UV radiation (Brenner and Hearing, 2008). This UV protection has been linked to the diminished incidence of skin cancer in dark-skinned populations (Halder and Bang, 1988; Gilchrest et al., 1999). In addition to providing a UV filter, melanin also scavenges reactive oxygen species formed during exposure to UV light (Meredith and Sarna, 2006; Sarna and Swartz, 2006; Brenner and Hearing, 2008). As a result, melanin can diminish the negative downstream effects of these reactive oxygen species on cellular processes (Meredith and Sarna, 2006; Sarna and Swartz, 2006; Brenner and Hearing, 2008).

Though its discussion is beyond the scope of this dissertation, it is important to mention that melanin also has photosensitizing properties. Melanin generation of reactive oxygen species is related to the aggregation of the oligomeric constituents of the pigment, unaggregated oligomers are more likely to generate these species upon aerobic photoexcitation than aggregated oligomers (Chedekel et al., 1980; Sarna and Sealy, 1984; Nofsinger et al., 2002). This photosensitization is particularly pronounced for individuals with a high concentration of pheomelanin pigmentation and has been linked to increased sensitivity to skin cancers for light-skinned and haired individuals (Chedekel et al., 1978; Wenczl et al., 1998; Wakamatsu et al., 2012). These photoprotective and photosensitizing roles of melanin thus have interesting evolutionary implications.

Finally, melanin is capable of binding a variety of biologically important metal ions (Potts and Au, 1976; Liu et al., 2004; Liu and Simon, 2005; Hong and Simon, 2006; Hong and Simon, 2007). Metals coordinate to the carboxyl, phenolic hydroxyl, and amine groups inherent to melanin's structure (Hong and Simon, 2006; Hong and Simon, 2007). Eumelanin is an especially efficient metal binder with an affinity for critical metal ions like Ca(II), Cu(II), Fe(II), and Fe(III) (Prota, 1992; Hong and Simon, 2007). Melanin is thought to function in part as a metal reservoir – important for the homeostasis of Ca(II) and as a tight metal binder for toxic metal ions like Cu(II), Fe(II) and Fe(III) that lead to the production of reactive oxygen species when unbound (Sarna, 1992; Zareba et

al., 1995; Boulton, 1998). The ability of melanin to bind relatively high concentrations of these metal ions becomes increasingly important during the search for chemical signatures to identify melanin in fossil organisms herein.

1.4 Overview of this dissertation

In this dissertation the chemical and physical properties of modern melanins were probed and compared to the black pigmentation and associated sediment of four fossilized ink sacs. The pigment and sediment associated with these fossilized ink sacs was analyzed with a diverse array of chemical techniques. **Chapter 2** details the instrumentation used to analyze this pigmentation. An example of the physical and/or chemical data derived from each technique and a summary of the properties they elucidate are described therein.

Chapter 3 presents the analysis of the black pigmentation of two intact > 160 million year old (Mya) Jurassic cephalopod ink sacs from two different sites in the United Kingdom (UK). The chapter details the discovery that the black pigmentation is preserved eumelanin (Glass et al., 2012). The chemical and physical similarities of the fossil ink to modern ink from the common cuttlefish, *S. officinalis*, are also discussed. Differences between the cross-linking of fossil and modern melanins are also detailed and explored (Ito et al., 2013b). The morphology, identity, and quantity of eumelanin in the fossil ink sacs were established by the techniques that follow.

(1) Scanning electron microscopy (SEM) was used to examine the size and overall morphology of the eumelanin from the fossil inks and compare it modern *S. officinalis* ink. (2) Alkaline hydrogen peroxide oxidation was used to identify and quantitate the melanin in the fossil ink and associated sediments by breaking melanin down into distinct chemical markers associated with its monomeric precursors. (3) These markers were further confirmed by exact mass measurements using high-performance liquid chromatography-mass spectrometry (HPLC-MS). (4) The absorbance at 500 nm of melanin solubilized in Soluene-350 was also provided as a rapid alternative to quantitation by alkaline hydrogen peroxide oxidation. (5) Electron paramagnetic resonance spectroscopy (EPR), a technique that probes the electronic properties of a material, was then used to nondestructively verify the presence of eumelanin and absence of pheomelanin.

To provide further insights into the chemistry of the fossil material and to compare it to modern melanin, we performed an additional suite of techniques. (1) To quantitate the amount of key organic residues in fossil – C, N, O, and H – elemental analysis was performed. (2) In order to characterize the preserved organic chemical groups in the fossil melanin, Fourier transform infrared spectroscopy (FTIR) spectra were recorded. (3) X-ray photoelectron spectroscopy (XPS) survey scans and high-resolution carbon scans were then taken to establish the percent of a wider-range of elements on the surface of the fossil material and to identify the binding interactions of

the carbon within. (4) Finally, Carbon-13 Cross-Polarization Magic Angle Spinning Solid-State Nuclear Magnetic Resonance Spectroscopy (^{13}C CP-MAS SSNMR) confirmed that the functional groups established by FTIR and XPS pervaded the bulk of the fossil inks and were not present in similar quantities in the fossil sediments.

Chapter 4 uses the suite of chemical techniques described in **Chapter 2** to compare the melanin of two fossil ink sacs from the UK analyzed in **Chapter 3** to the melanin of two fossils ink sacs from Germany. In this chapter the effect of diagenesis and maturation on the physical and chemical preservation of eumelanin are explored and constraints are proposed for the survival of eumelanin in the fossil record (Glass et al., 2013). To do so, all of the techniques used in **Chapter 3** in addition to the techniques that follow were used to analyze the fossil inks and associated sediments. The techniques used in **Chapter 3** SEM, alkaline hydrogen peroxide oxidation, HPLC-MS, optical absorption at 500 nm, and EPR were performed to determine the presence and morphology of eumelanin in the German fossil inks while elemental analysis, FTIR, XPS, and ^{13}C CP-MAS SSNMR were used to ascertain the chemistry of the fossils. In addition, (1) Pyrolysis-Gas Chromatography-Mass Spectrometry (py-GC-MS) was used to ascertain the extent to which the fossil inks from the UK and Germany were diagenetically modified / transformed relative to modern coleoid ink and (2) Rock-Eval Pyrolysis was used to analyze the sediments associate with each fossil ink and chemically profile their burial sites.

Chapter 5 examines proteins preserved in melanin in fossil melanin. The following techniques are used to analyze the amino acid profile of these proteins. (1) Amino acid analyzer was first used to establish the presence of protein in the fossil melanins analyzed in **Chapter 3** and **Chapter 4**. (2) Statistical analysis of the data indicated that the amino acid composition of fossil ink was not significantly different from that of modern cephalopod ink. (3) Gas chromatography-mass spectrometry (GCMS) of the hydrolyzed proteins from the fossil inks after derivatization with a chiral reagent revealed that the amino acids from the fossil inks have undergone a degree of racemization, which confirmed the ancient origin of the amino acids. After introducing this new field of fossil study, the future research directions and conclusions of this dissertation are presented.

2. Techniques to characterize eumelanin

2.1 Introduction to the techniques commonly used to study eumelanin in modern and fossil systems

Despite many decades of work, the complete macromolecular structure of melanin remains a mystery (Prota, 1992; Meredith and Sarna, 2006; Ito et al., 2011). Melanins form through seemingly random polymerization of known monomeric precursors into complex heterogeneous biopolymers. These biopolymers are insoluble in virtually any solvent, which makes them difficult to analyze using common characterization techniques. As a result, a myriad of alternative techniques have been developed / utilized to study melanin as a solid powder or to break melanin down and study its molecular markers. Many of these techniques are necessary to characterize eumelanin in fossil and modern systems. In this chapter the techniques that will reappear throughout this dissertation are introduced, the instrumentation required is described, and utility of each is detailed. In the materials and methods sections of the specific studies that follow (**Chapter 3** and **4**), the particular conditions used for each technique are detailed.

2.2 Scanning electron microscopy imaging of melanin

Scanning electron microscopy (SEM) is an imaging technique capable of probing the surface of diverse materials with a resolution down to about 1 nm (Zhang, 2009b). This image resolution depends on how the electron probe interacts with a given

specimen (Zhang, 2009b). The high-resolution capability afforded by SEM makes it a convenient method to probe the nanoscopic surface features and microscopic morphology of melanin granules and melanosomes.

Figure 3 shows a schematic of a standard scanning electron microscope (Zhou et al., 2007). At the top of the schematic is an electron gun. The electron gun produces a stream of electrons that are focused by the first condenser lens denoted CL (Zhang, 2009b). A second condenser lens then controls the size of the electron beam and focuses it on the objective lens (OL). The objective lens focuses the electron beam on the sample while the objective aperture eliminates any inappropriately angled electrons from the beam (Zhang, 2009b). Interaction between the electron beam and the sample surface produces three types of signal: secondary electrons (SE), back scattering electrons (BSE), and X-rays.

The most relevant signal for imaging the sample surface with SEM comes from secondary electrons. Secondary electrons are produced when the electron beam hits the surface of the sample (within the top few nanometers) and causes sample atoms to ionize (Zhou et al., 2007). These loosely bound electrons are emitted as a result of the bombardment. The electrons are then collected by the detector and converted into photons by a scintillator (Zhou et al., 2007). The scintillator is coupled to a photomultiplier tube (PMT), an electronic light sensor, which absorbs the photons,

multiplies the resulting current, and gives an output voltage. That voltage is then amplified and displayed as an SEM image (Zhou et al., 2007).

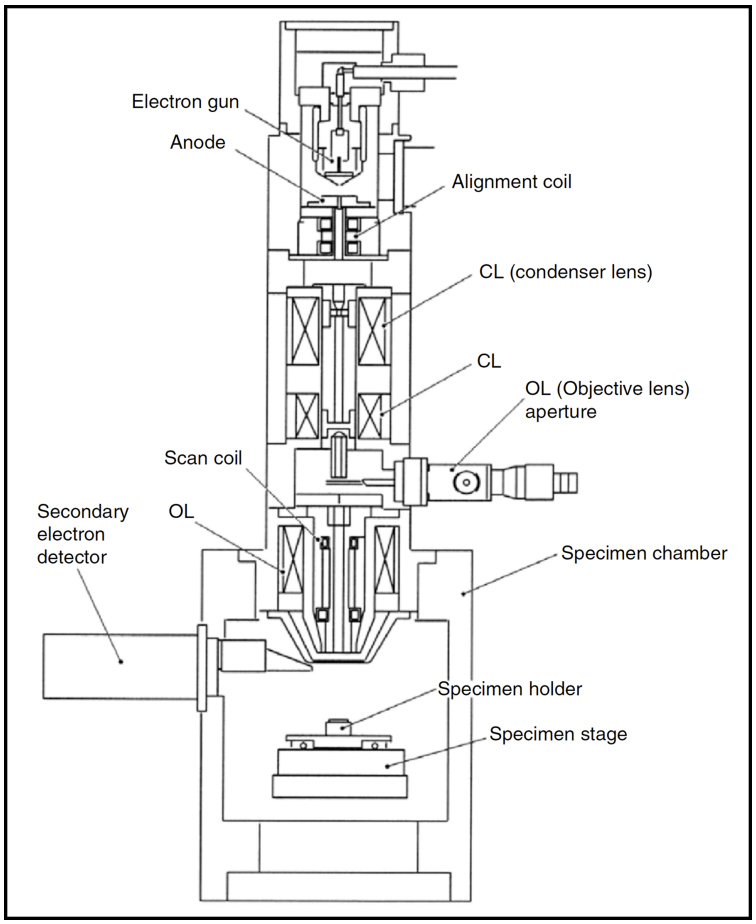

Figure 3: A schematic of a scanning electron microscope

The instrument consists of an electron gun, lens column, scan coils, sample chamber, and detection center. Additional components are labeled on the image above. Reprinted from: Zhou, W.; Apkarian, P.; Wang, Z. L., and Joy, D. (2007) Fundamentals of scanning electron microscopy. In: *Scanning Microscopy for Nanotechnology: Techniques and Applications* (Zhou, W. and Wang, Z. L., Eds.) pp. 1-40. New York: Springer. The original image was provided courtesy of JEOL, USA (Zhou et al., 2007).

Analysis of melanin samples by SEM is complicated by the fact that melanins are relatively nonconductive specimens composed of low atomic number elements (Oliveira

et al., 2000; Zhou et al., 2007). Charge builds up on the surface of these insulating samples when an electron beam scans them because the charge cannot dissipate (Zhou et al., 2007). As a result, the images are blurred and distorted. In order to reduce these effects and increase image contrast, conductive metals like gold (Au) and palladium (Pd) are sputter coated – evaporated as a film layer with controlled thickness – onto the specimen surface in an argon atmosphere (Liu and Simon, 2005; Zhou et al., 2007). The precise methods used to metal-coat and analyze melanin samples are detailed in **Chapter 3** and **4**.

2.3 Introduction to alkaline hydrogen peroxide oxidation

Biopolymers like proteins and polysaccharides are composed of specific monomers interlinked by C-N and C-O covalent bonds that are broken easily through chemical methods (Ito, 2003). Characterization of the structure of melanins is more difficult because melanins are formed by the interlinking of a variety of subunits through intractable C-C bonds (Ito, 2003). Interest in probing the molecular composition of melanin pigments led to the development of protocols that oxidize or reduce melanins to unique degradation markers (Panizzi and Nicolaus, 1952; Prota, 1992; Ito and Wakamatsu, 2003; Ito et al., 2011; d'Ischia et al., 2013). Once identified and quantified, these degradation markers can be related back to the composition of the original pigment.

Analytical methods to determine the molecular composition of melanin in this manner were refined by Shosuke Ito and are currently used to characterize melanin in a wide array of biological samples (Ito and Fujita, 1985; Wakamatsu and Ito, 2002; Ito and Wakamatsu, 2003; Wakamatsu et al., 2009; Ito et al., 2011). Although many different degradation methods have been developed, only alkaline hydrogen peroxide oxidation will be described here. It is important to note that the alkaline hydrogen peroxide oxidation products of melanin discussed below are unique and have never been produced by the alkaline hydrogen peroxide oxidation of any other biological material (Pezzella et al., 1997; Ito et al., 2011).

Alkaline hydrogen peroxide oxidation allows concomitant analysis of the eumelanin and pheomelanin content of a sample (Ito et al., 2011; d'Ischia et al., 2013). When exposed to alkaline conditions of either 1M sodium hydroxide (NaOH) or 1M potassium carbonate (K_2CO_3) with hydrogen peroxide (H_2O_2), eumelanins produce the degradation markers pyrrole-2,3-dicarboyxilic acid (PDCA) and pyrrole-2,3,5-tricarboxylic acid (PTCA) shown in Figure 4 (Piatelli et al., 1962; Ito and Fujita, 1985; Wakamatsu and Ito, 2002; Ito et al., 2011). These markers can be used to infer the distribution of 5,6-dihydroxyindole (DHI) and 5,6-dihydroxyindole-2-carboxylic acid (DHICA), respectively (Figure 1) (Piatelli et al., 1962; Ito and Fujita, 1985; Wakamatsu and Ito, 2002; Ito et al., 2011). Additional alkaline hydrogen peroxide oxidation products of eumelanin, pyrrole-2,3,4-tricarboxylic acid (isoPTCA) and pyrrole-2,3,4,5-

tetracarboxylic acid (PTeCA), have recently been discovered (Ward et al., 2008; Glass et al., 2012; Ito et al., 2013b). IsoPTCA and PTeCA are likely the product of DHI that is cross-linked over time at the C2 and C3 positions or the C3 position alone as mentioned and depicted in **Chapter 3**, Figure 15 (Ito et al., 2013a; Ito et al., 2013b).

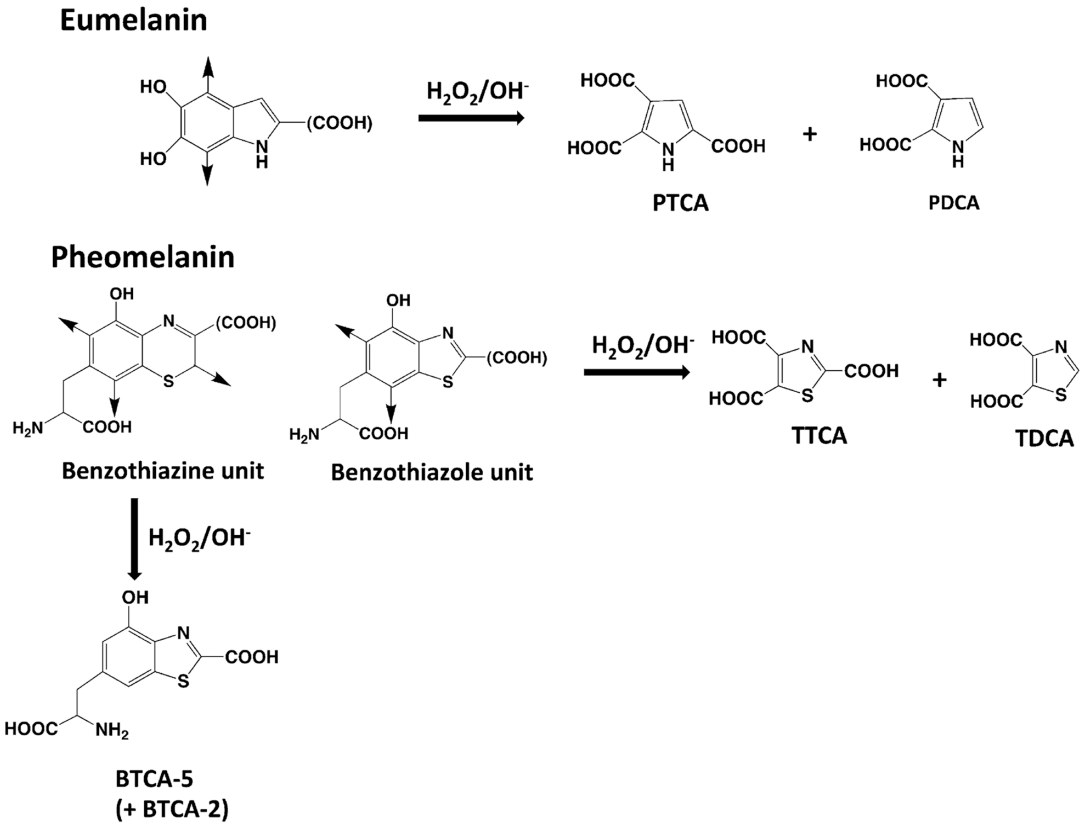

Figure 4: Alkaline hydrogen peroxide oxidation of eumelanin and pheomelanin

On alkaline hydrogen peroxide oxidation, DHI-units of eumelanin give pyrrole-2,3-dicarboxylic acid (PDCA) and DHICA-units give pyrrole-2,3,5-tricarboxylic acid (PTCA). Alkaline hydrogen peroxide oxidation of pheomelanin yields thiazole-2,4,5-tricarboxylic acid (TTCA) and thiazole-4,5-dicarboxylic acid (TDCA) from the component benzothiazole-units and 6-alanyl-2-carboxy-4-hydroxybenzothiazole (BTCA-5) and 7-alanyl-2-carboxy-4-hydroxybenzothiazole (BTCA-2) from the benzothiazine -units. These structures were reproduced with permission (Ito et al., 2011).

Under the same oxidation conditions pheomelanin breaks down to: 6-alanyl-2-carboxy-4-hydroxybenzothiazole (BTCA-5 or BTCA), 7-alanyl-2-carboxy-4-hydroxybenzothiazole (BTCA-2), thiazole-2,4,5-tricarboxylic acid (TTCA), and thiazole-4,5-dicarboxylic acid (TDCA) shown in Figure 4 (Prota, 1992; Ito and Wakamatsu, 2003; Panzella et al., 2007; Greco et al., 2009). While TTCA and TDCA are specific markers for benzothiazole-units, BTCA-5 and BTCA-2 are related to the quantity of benzothiazine-units in pheomelanin pigment (Napolitano et al., 2000; Greco et al., 2009; Wakamatsu et al., 2009; Ito et al., 2011; Wakamatsu et al., 2012).

The concentration of oxidation products of a sample pigment is determined using a high-performance liquid chromatography (HPLC) system equipped with an ultraviolet (UV) detector (Wakamatsu and Ito, 2002; Ito et al., 2011). Briefly, sample degradation mixtures are directly injected onto an HPLC system. To determine the concentration of each degradation marker in a sample mixture, the UV peak areas of synthesized degradation markers at various concentrations are determined and calibration curves are prepared (Ito et al., 2011). Peak areas of the degradation markers in a sample mixture are then determined and compared to the calibration curves to find the concentration of each degradation marker (Ito et al., 2011). These degradation markers can be related back to the molecular composition of the sample pigment. Detailed step-by-step alkaline hydrogen peroxide oxidation protocols are outlined in **Chapter 3** and **4**. Shosuke Ito and Kazumasa Wakamatsu performed all of the alkaline

hydrogen peroxide oxidation experiments mentioned herein at the Fujita School of Health Sciences in Japan. Additional analyses of degradation markers were performed at Duke University (see **Chapter 3**).

2.4 Electron paramagnetic resonance spectroscopy (EPR)

Electron paramagnetic resonance spectroscopy (EPR), also known as electron spin resonance spectroscopy (ESR), is useful for probing the electronic properties of a material. In this form of spectroscopy, molecules that contain unpaired electron spins absorb electromagnetic radiation of microwave frequency (9.5 GHz for the work herein) (Drago, 1992). In EPR, two different energy states ($m_s = \pm ½$) result when the unpaired electron spin moments of a sample align with an applied magnetic field (Drago, 1992). A transition between the energy states occurs when microwave radiation is applied (Figure 5) (Drago, 1992). EPR is based on measuring these transitions (Zhang, 2009b). Most bulk materials are EPR silent – their net electronic spin is zero so no transitions can be measured (Zhang, 2009b). Melanins are unusual in that they exhibit an EPR signal in the bulk – a clear indication that free radical centers are present in the material (Sealy et al., 1982; Meredith and Sarna, 2006).

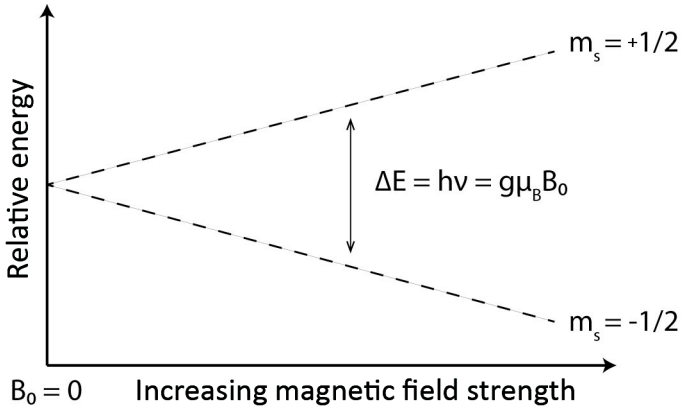

Figure 5: Illustration of electron spin transitions under an external magnetic field

The interaction of unpaired electron spin moments with an applied magnetic field produces two different energy states ($m_s = \pm ½$). The difference between the two energy states ΔE or $h\nu$ is equal to the product of: (1) the g value, a unique property of each paramagnetic material, (2) the Bohr magneton (μ_B), which has a value of 9.274096×10^{-28} Joules (J) per Gauss (G), and (3) the magnetic field applied (B_0) (Drago, 1992; Zhang, 2009b; Brynda, 2010). When no magnetic field is applied the electrons spin states are degenerate.

The principle of EPR is illustrated and the transition energy equation used to characterize a material of interest with EPR is shown in Figure 5. As detailed in the caption of Figure 5, the difference in energy between the electron spin moments when a magnetic field is applied is equal to the product of Plank's constant, 6.626×10^{-34} J sec (h) and the frequency in Hz (ν) (Drago, 1992; Zhang, 2009b; Brynda, 2010). The $h\nu$ in turn is equal to the product of the g value, an intrinsic property of a given paramagnetic material; the Bohr magneton (μ_B), which has a value of 9.274096×10^{-28} J/G; and the magnetic field applied (B_0).

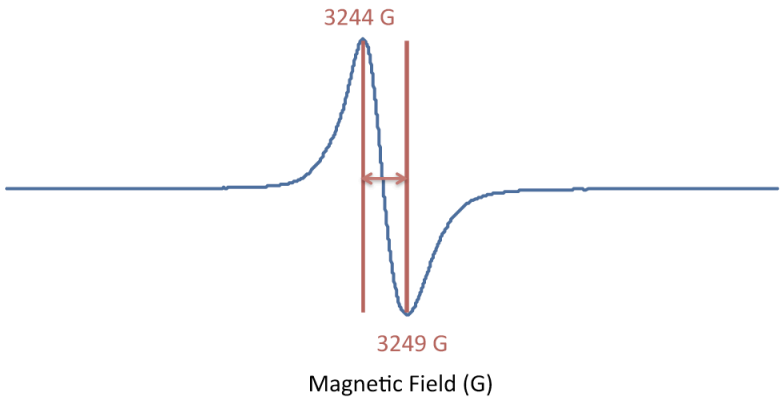

Figure 6: Determination of the linewidth of a *S. officinalis* eumelanin EPR spectrum

The linewidth of an EPR signal, like that of *S. officinalis* eumelanin shown, is the width of the sample's absorption peak.

The EPR experiments used to determine the characteristic g-values and linewidths (Figure 6) of solid melanin samples were carried out at X-band frequency (9.5 GHz). To run the EPR experiment discussed in **Chapter 3** and **4**, small quantities of melanin (~1 mg) were placed in glass EPR tubes. Each melanin sample was exposed to microwaves at the fixed 9.5 GHz frequency while the magnetic field was swept (Drago, 1992). To accurately set the field sweep, a standard of diphenylpicrylhydrazide (DPPH) with a known g-value of 2.0037 ± 0.0002 was used (Drago, 1992). Since the field sweep is assumed to be linear, the g-values of the melanin samples could be calculated relative to this standard (Drago, 1992). The origin of the EPR signal in the melanin samples analyzed, the instrumentation used, and the g-values and linewidths determined are discussed in **Chapter 3** and **4**. Paul Angiolillo and Jeff Rawson helped acquire all of the EPR data.

2.5 Estimation of melanin content with optical absorption

Melanins absorb light throughout the ultraviolet-visible (UV-Vis) range of the electromagnetic spectrum (Kollias et al., 1991; Ozeki et al., 1996b; Wakamatsu and Ito, 2002). The featureless broad absorption spectrum of melanin is unusual for organic chromophores, which typically contain absorbance peaks that correspond to distinct transitions between energy levels of the absorbing species (Wolbarsht et al., 1981; Meredith and Sarna, 2006). The absorption spectrum of melanin is still worth considering. When a sample is not known to contain melanin or instrumentation is limited, a rapid absorption experiment is often performed to estimate the total amount of eumelanin and pheomelanin present (Ozeki et al., 1996b; Wakamatsu and Ito, 2002).

This method is very straightforward. First, the sample of interest is solubilized in 10% water and 90% Soluene-350 – a strong organic base composed of 40-60% toluene, 20-40% N-dodecyl-N,N-dimethyl-1-tetradecanaminium hydroxide, 2.5-10% trioctylmethylammonium chloride, and 2.5-10% methanol (PerkinElmer, 2013). Next, the sample mixture is boiled in a water bath for 45 minutes (Ozeki et al., 1996b). Finally, the absorption spectrum of the solution is recorded from 350 to 800 nm using a UV-Vis spectrophotometer (Ozeki et al., 1996b). Based on a large body of literature (Ozeki et al., 1996a; Ozeki et al., 1996b; Ito and Wakamatsu, 1998; Wakamatsu and Ito, 2002), the absorbance at 500 nm per mg of sample is considered to reflect the total amount of

eumelanin and pheomelanin. Shosuke Ito and Kazumasa Wakamatsu measured the optical absorption of all of the samples in this dissertation (**Chapter 3** and **4**).

2.6 Elemental analysis

Combustion elemental analysis of the carbon (C), nitrogen (N), and hydrogen (H) of a sample is a useful way to access information about the molecular composition of organic constituents. To perform combustion elemental analysis, a sample is first weighed out into a tin capsule and introduced to a furnace at ~1000 °C in the presence of oxygen (Thompson, 2008). When heated in this manner, the carbon in the sample is converted to carbon dioxide (CO_2), nitrogen to nitrogen gas or nitrogen oxides, and hydrogen to water (Thompson, 2008). Next, the combustion products are pushed by an inert gas (typically helium) into a chamber with high purity copper that is heated to 600 °C (Thompson, 2008). The copper converts nitrogen oxides to nitrogen gas and removes any residual / unreacted oxygen from the gaseous sample mixture (Thompson, 2008). Finally, the carbon dioxide, nitrogen gas, and water are separated by gas chromatography and detected by thermal conductivity detection (Thompson, 2008). The resulting peaks are quantified by comparison to calibration curves of high purity standard compounds. Takayuki Sota and Atsushi Nakamura performed the elemental analysis experiments described in this dissertation (**Chapter 3** and **4**).

2.7 Fourier transform infrared spectroscopy (FTIR)

Fourier transform infrared spectroscopy (FTIR) is a versatile chemical technique that is used in **Chapter 3** and **4** to characterize the functional groups in fossil samples, sediments, and related standards. IR spectroscopy is fairly straightforward: a sample is placed in the path of an IR beam, various frequencies of IR light are transmitted through the sample, and the transmitted light is measured (Sherman Hsu, 1997; Zhang, 2009a). Each sample is composed of molecules that have specific vibration frequencies. If the frequency of IR light is equal to the specific vibration of a molecule, then that molecule absorbs the light (Sherman Hsu, 1997).

As a sample absorbs light at different frequencies, the intensity of the transmitted light is reduced. When the intensity of the transmitted light is plotted as a function of frequency it results in a spectrum of sample absorbance (Zhang, 2009a). This spectrum gives information about the specific vibration frequencies of the sample, which can both help identify the functional groups and provide a fingerprint of an unknown sample. Additional details for the IR methodology used herein are provided in **Chapter 3** and **4**. Takayui Sota and Atsushi Nakamura performed all of the FTIR experiments mentioned in this dissertation.

2.8 X-ray photoelectron spectroscopy (XPS)

X-ray photoelectron spectroscopy (XPS), also known as electron spectroscopy for chemical analysis (ESCA), is a useful technique for characterizing the chemical

composition of a sample. XPS is based on the measurement of the kinetic energy and quantity of photoelectrons produced when a sample is bombarded with monochromatic X-rays under ultrahigh vacuum (UHV) (Figure 7) (Schweitzer et al., 2008; Zhang, 2009b). All electrons on the sample surface (top 5-10 nm) that have a binding energy less than the energy of the X-ray radiation are ejected (Swartz, 1973). These photoelectrons are collected by an electron analyzer, which measures their kinetic energies.

Although kinetic energy is measured, the data output of an XPS experiment is binding energy in electron volts (eV). Kinetic energy (KE) is related to binding energy (BE) by the following equation: BE = Energy Final (E_f) – Energy Initial (E_i) = $h\nu - KE$ (Swartz, 1973; Zhang, 2009b). In this equation, the E_i is the energy of an atom prior to excitation with an X-ray photon with energy ($h\nu$) while the E_f is the final energy of the atom following excitation (Zhang, 2009b). Since the photon energy is known based on the X-ray radiation source used – in **Chapter 3** and **4** Al Kα (1486.6 eV) was used for excitation – and the kinetic energy is measured during the course of an experiment, the binding energy can be determined (Zhang, 2009b). By convention, the XPS data is reported in terms of binding energy to facilitate lab-to-lab data comparison.

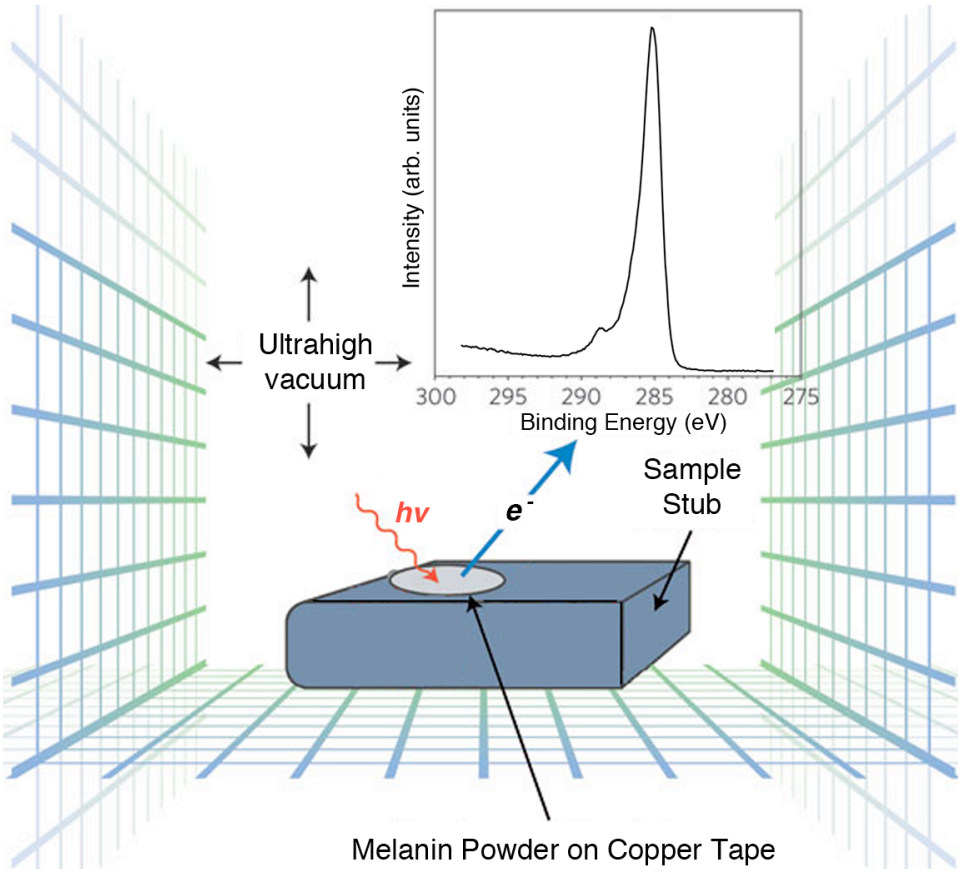

Figure 7: Schematic diagram of an XPS experiment

An X-ray source illuminates a sample and excites atoms within. Following illumination, excited atoms near the surface of the sample (top 5-10 nm) emit photoelectrons, which are analyzed. A high-resolution photoelectron spectrum of carbon in a melanin specimen is shown. Figure was altered and reproduced with permission (Zemlyanov, 2011).

The binding energies of the electron orbitals of an element are specific and characteristic thus the peaks of a photoelectron spectrum correlate with identifiable atoms on the surface of a sample (Zhang, 2009b). Two different types of photoelectron spectra that can be acquired during an XPS experiment were used in the studies outlined in **Chapter 3** and **4**. The first is a survey scan, which identifies the atomic percentage of

all of the elements present on the surface of a sample (Clark et al., 1990). The second is a high-resolution scan of a particular element in a sample. The binding energies of core electrons (i.e. carbon 1s electrons) are affected by the valence electrons and thereby the bonding environment of an atom (Swartz, 1973). The resulting binding energy shifts in the photoelectron spectrum can be used to extract information about the chemical bonding of molecules and the oxidation state of an atom (Figure 8) (Swartz, 1973; Schweitzer et al., 2008; Abbas et al., 2009; Zhang, 2009b).

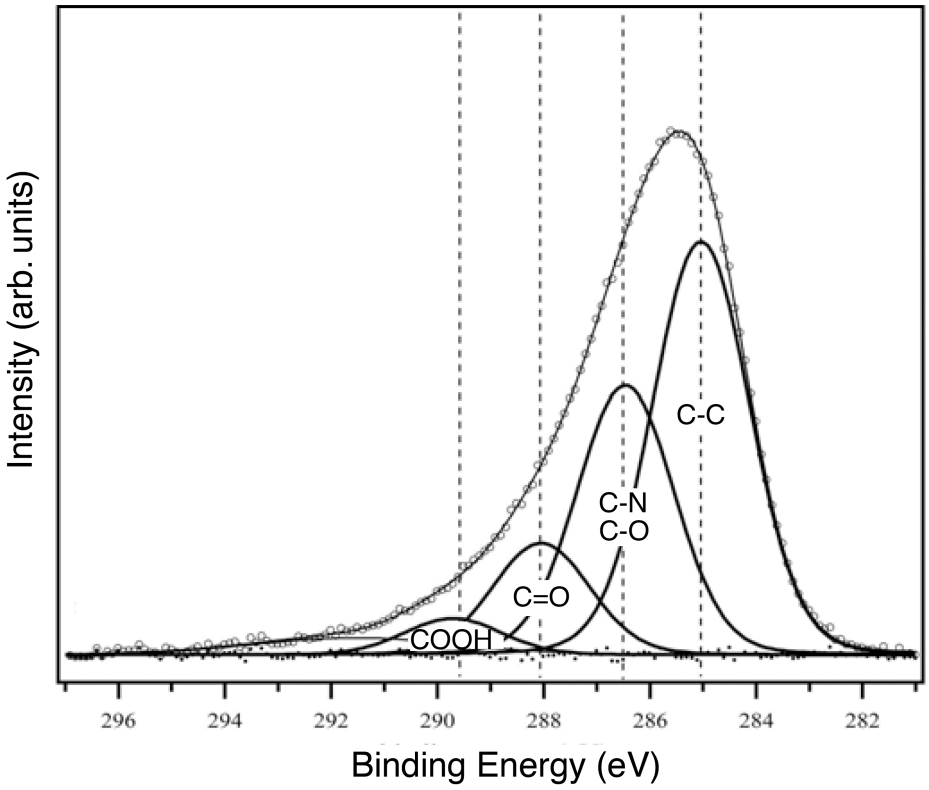

Figure 8: High-resolution C1s scan of synthetic melanin

Deconvolution of an example high-resolution C1s scan of synthetic melanin. The chemical shift and photoemission intensity of the component bonding environments of melanin are shown. Altered and reproduced with permission (Abbas et al., 2009).

2.9 Rock-Eval pyrolysis

Rock-Eval pyrolysis experiments characterize the type and origin of sedimentary organic matter and the thermal maturity of organic rich rocks (Espitalie et al., 1977; Delvaux et al., 1990; Yalçin Erik et al., 2006; McCarthy et al., 2011). Thermal maturity measurements indicate the maximum temperature a rock has experienced and the degree to which organic matter has transformed (McCarthy et al., 2011). Transformation of organic matter occurs in the following order over time under conditions (heat/pressure) that depend on burial site and depth: (1) original organic material, (2) insoluble organic material (kerogen), (3) petroleum and bitumen (thermally degraded kerogen), and (4) simplification of petroleum to oil, wet oil, and finally dry gas (McCarthy et al., 2011). Rock-Eval measurements can indicate the original source of organic material (i.e. lake algae, deep sea plankton, terrestrial plant debris) and screen the petroleum generation and fossil preservation potential of sediments (McCarthy et al., 2011). For fossil preservation, burial sites that have undergone limited maturation are preferred while for petroleum generation, a moderate degree of maturation is optimal.

The first step of a Rock-Eval pyrolysis experiment is pyrolysis – a chemical degradation reaction initiated by thermal energy – of pulverized sediment samples in an inert atmosphere like N_2 (Hübschmann, 2009; McCarthy et al., 2011). The samples analyzed herein were carefully weighed and heated in stages (Glass et al., 2012; Glass et al., 2013). First, they were heated to 300 °C and the temperature was held constant for a

few minutes (Glass et al., 2012). Isothermal heating at 300 °C releases free oil and gas (hydrocarbons) from sample sediments (McCarthy et al., 2011). This produces a peak – S1 – that represents the milligrams of free hydrocarbon generated from one gram of sample (Espitalie et al., 1977; Delvaux et al., 1990; McCarthy et al., 2011).

Then, the samples were heated further to 850 °C at 25 °C/min (Glass et al., 2012). During this heating stage, kerogen and complex organic molecules are broken down to simpler hydrocarbons that are released from the sediment. This produces a peak – S2 – that represents the milligrams of hydrocarbons evolved following thermal breakdown of kerogen / organic constituents per gram of sediment (Espitalie et al., 1977; Delvaux et al., 1990; McCarthy et al., 2011). The temperature at which the maximum amount of hydrocarbon is released (T_{max}) at S2 depends on the level of maturation the organic material in the sediment has undergone. As the heating program temperature approaches 850 °C, a third peak – S3 – that corresponds to the CO_2 released from the kerogen / organic mater is also recorded in mg/g of sediment (McCarthy et al., 2011). The total organic content of the sediments (TOC) was also analyzed to rapidly screen the sediments for their organic richness and fossil preservation potential (McCarthy et al., 2011; Glass et al., 2012). All hydrocarbons were detected with a flame ionization detector (FID) while infrared detectors measured the released CO_2 (Glass et al., 2012).

Each value derived from Rock-Eval pyrolysis gives important information about the sediments. The two measurements that are used in **Chapter 4** to compare fossil

burial sites are the hydrogen index (HI) and the temperature of maximum pyrolysis yield (T_{max}). The HI, defined as 100 x S2 / TOC, is directly related to the amount of hydrogen within sediment kerogen. HI values > 400 mg HC/g TOC indicate the preservation of organic rich matter (Prauss et al., 1991; Glass et al., 2013). For T_{max}, temperatures between 400 °C and 430 °C indicate immature sediments that have not undergone substantial maturation (Espitalie et al., 1977). This is ideal for the preservation of organic material in fossils. A T_{max} between 435 °C - 445 °C represents a mature or oil zone that will generate petroleum, while a T_{max} > 450 °C is indicative of an overmature zone that will neither produce petroleum nor preserve fossils (Espitalie, 1986; Prauss et al., 1991). Other values derived from Rock-Eval pyrolysis are beyond the scope of this dissertation. It is important to note that Suryendu Dutta and Roger E. Summons acquired and analyzed all of the Rock-Eval pyrolysis data discussed herein (**Chapter 4**).

2.10 Pyrolysis gas chromatography—mass spectrometry (Py-GC-MS)

Pyrolysis (Py) is often coupled with gas chromatography-mass spectrometry (GC-MS) to analyze difficult samples (Hübschmann, 2009). As with other varieties of mass-spectrometry, Py-GC-MS exploits the fact that every molecule fragments into a unique chemical fingerprint that can be identified with high-resolution mass analysis (Schweitzer et al., 2008; Hübschmann, 2009). One benefit of Py-GC-MS is that samples do not need to be extracted from their matrix (Schweitzer et al., 2008). However, since

Py-GC-MS only gives information about the bulk sample, signals derived from the matrix cannot be confidently identified without either analyzing the matrix alone or knowledge of related matrices (Schweitzer et al., 2008; Hübschmann, 2009).

In Py-GC-MS, samples are rapidly heated to ~600 °C in order to cleave and volatize their molecular components while minimizing thermally induced side reactions (Schweitzer et al., 2008; Hübschmann, 2009). The sample fragments are then separated by mass using gas chromatography and identified by mass spectrometry (Schweitzer et al., 2008). The components of a sample can either be characterized by individually identifying each pyrolysis product or by comparing sample traces (spectrograms / pyrograms) containing all of the fragment peaks to known standards (Schweitzer et al., 2008; Hübschmann, 2009). Roger E. Summons, Kristen E. Miller, and Suryendu Dutta acquired and analyzed all of the Py-GC-MS data (**Chapter 4**).

3. Chemical evidence for Jurassic eumelanin pigment

3.1 The current state of melanin analysis in the fossil field

Until the last decade, melanin was studied primarily in the feathers, melanoma lesions, and pigmented regions of modern organisms. Melanin was not known to persist in the fossil record – it was presumed lost with other primary organic components (proteins, lipids, DNA etc.) of ancient life (McNamara, 2013). Since scientists learned of melanin's presence in the fossil record, new analytical techniques have been applied to study melanin in ancient life (Vinther et al., 2008; Clarke et al., 2010; Li et al., 2010; Vinther et al., 2010; Zhang et al., 2010; Barden et al., 2011; Wogelius et al., 2011; Glass et al., 2012; Lindgren et al., 2012; Glass et al., 2013; Lindgren et al., 2014).

SEM, an imaging technique that enables morphological analysis of sub-micron structures, has enabled the detection of structures that are morphologically similar to melanin (Vinther et al., 2008; Clarke et al., 2010; Li et al., 2010; Vinther et al., 2010; Zhang et al., 2010; Glass et al., 2012). In 2008, SEM imaging of fossil feathers revealed rod-shaped and spherical microstructures that were interpreted as fossilized melanosomes (Vinther et al., 2008). Since then, structures of approximately the same size and shape as melanosomes and melanin granules have been found in an array of fossils. Using the dimensions of these structures to extrapolate color with discriminant analysis where

rod-shaped structures indicate black-brown eumelanosomes, while spheroidal structures indicate reddish-brown pheomelanosomes the studies appear to offer powerful insights into ancient coloration (Vinther et al., 2008; Clarke et al., 2010; Vinther et al., 2010; Zhang et al., 2010). However, none of these early studies provided definitive chemical evidence to support the claims, leaving the possibility that some of the structures may actually represent the remains of bacteria, remnants of feather-keratin, or other similarly sized microstructures (Davis and Briggs, 1995; Schweitzer, 2011; McNamara, 2013).

In order to meet the demand for chemical evidence to prove the presence of melanosomes and melanin granules in the fossil record, analytical techniques that capitalize on chemical signals associated with melanin have been developed (Wogelius et al., 2011; Lindgren et al., 2012; Manning et al., 2013; Lindgren et al., 2014). Two techniques in particular have received considerable attention: (1) trace-metal analysis of bound ions and (2) time-of-flight secondary ion mass spectrometry (Wogelius et al., 2011; Lindgren et al., 2012; Manning et al., 2013; Lindgren et al., 2014).

Trace-metal analysis involves the spatial detection of metal ions such as calcium, copper, iron, and zinc that are known to bind to melanin (Wogelius et al., 2011). Analysis of modern melanins has shown that melanin tightly binds these metal ions and prevents their circulation through the body (Potts and Au, 1976; Larsson and Tjalve,

1978; Sarzanini et al., 1992; Riley, 1997; Liu et al., 2004; Liu and Simon, 2005; Hong and Simon, 2006; Hong and Simon, 2007). Trace-metal analysis may involve a variety of non-destructive chemical-imaging techniques: synchrotron rapid-scanning x-ray fluorescence (SRS-XRF) gives full sample metal identification whilst x-ray absorption near-edge structure (XANES) and extended x-ray absorption fine structure (EXAFS) provide localized metal-mapping (Wogelius et al., 2011; Manning et al., 2013; McNamara, 2013). The techniques have been successfully applied to the study of melanin in fossil feathers (Wogelius et al., 2011; Manning et al., 2013). By taking advantage of long-lived metal ions that may continue to bind melanin post-mortem, trace-metal analysis provides a new tool for verifying the melanic nature of microstructures identified by SEM. The disadvantage of trace-metal analysis is that microorganisms of similar size and shape to melanosomes are also able to absorb trace metal ions and may be misinterpreted as melanin (Schweitzer, 2011; McNamara, 2013).

In ToF-SIMS, a beam of ions is pulsed over the surface of a sample. Ions from the sample surface (secondary ions) are released and funneled into a mass spectrometer where their masses are analyzed (Lindgren et al., 2012). This technique provides a non-destructive chemical fingerprint of the sample surface. By comparing the chemical fingerprint of a specimen of interest to a related melanin standard, it is possible to determine whether or not a signature consistent with melanin is present (Lindgren et al.,

2012; McNamara, 2013; Lindgren et al., 2014). ToF-SIMS has been successfully applied to the study of melanin in fossilized reptile skin and fish eyes (Lindgren et al., 2012; Lindgren et al., 2014). The only detriment to this technique is that the chemical signatures of melanin in these systems may not differ substantially from melanin derived from other sources including bacteria (Schweitzer, 2011; Glass et al., 2012). Melanin-containing bacteria introduced during decay could replace original melanin components, resulting in false positives.

In this chapter, we analyze cephalopod ink sacs from the Peterborough Member of the Oxford Clay Formation (Middle Jurassic, 162 Ma) at Christian Malford, Wiltshire (UK) and the Blue Lias Formation (Lower Jurassic, 195 Ma) at Lyme Regis, Dorset (UK). SEM images of a specimen from each of these deposits GSM 122841 and GSM 120386 (Figure 9A and B) reveal that the ink is composed of globular granules similar in size and shape to that of modern coleoid *S. officinalis* (Figure 9C-E) (Liu and Simon, 2003). As previously mentioned, the presence of such structures alone is insufficient to prove that melanin pigment is preserved because many microbes and minerals adopt similar morphology (Davis and Briggs, 1995; Schweitzer, 2011).

Fortunately, melanin has a wide range of unique chemical signatures that can be used to identify and characterize its different forms in nature (Riley, 1997; Meredith and Sarna, 2006; Ito et al., 2011). Here we adapt these chemical approaches to verify melanin

in GSM 122841 and GSM 120386 and to compare the preserved pigment to that of melanin from the modern cephalopod *S. officinalis*. These fossils exceed the age beyond which significant diagenetic alteration of organic compounds normally occurs and therefore provide a test for the wider viability of melanin biomarkers in the fossil record (Briggs, 1999).

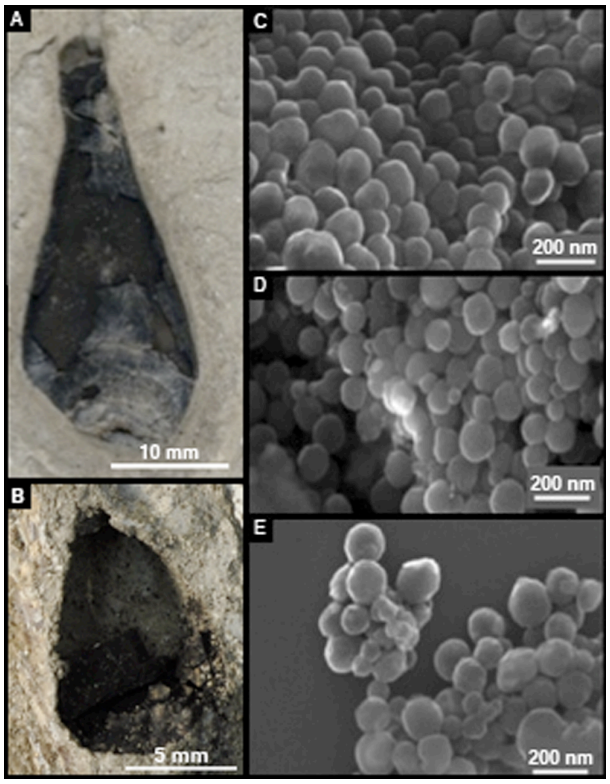

Figure 9: Photographs and SEM images of UK specimens and *S. officinalis*

Photographs of intact Jurassic coleoid ink sac specimens GSM 122841 (A) and GSM 120386 (B). SEM images of *S. officinalis* melanin (C), GSM 122841 (D), and GSM 120386 (E). All SEM images were taken at the same magnification. The average size of the spherical structures shown in C-E is 140 ± 20 nm, 168 ± 30 nm and 156 ± 30 nm, respectively, where ± indicates the standard deviation. All images and data were published previously (Glass et al., 2012).

3.2 Materials and methods

3.2.1 Introduction to the fossil ink sacs from the United Kingdom

GSM 122841 (Figure 9A), *c.* 162 million years old, collected from Peterborough Member of the Oxford Clay Formation (middle Jurassic, Upper Callovian) at Christian Malford, Wiltshire (UK). The Peterborough Member is dominated by fossiliferous organic-rich mudstones (Cox et al., 1992). Based on molecular analysis of the organic matter, Hudson and Martill (1994) suggest that peak palaeotemperature may never have exceeded 40 °C in this area (Hudson and Martill, 1994). Penn and coworkers (1986) suggest that maximum burial in this area was only 200-300m (Penn et al., 1986).

GSM 120386 (Figure 9B), *c.* 195 million years old, collected from Bed 32 of the Blue Lias Formation (early Jurassic, Lower Sinemurian) at Lyme Regis, Dorset (UK), (Lang, 1924). The Blue Lias Formation consists of decimeter-scale cyclical alternations of fossiliferous mudstone and tabular or nodular argillaceous limestones (Lang, 1924). Lyme Regis is located within the Wessex Basin, a Mesozoic fault-bounded depocentre.

Both ink sacs are intact and preserved three-dimensionally. They were each collected *in situ* and exposed by splitting the rock with a knife. Portions of the ink sacs and sediments were removed by etching the surface of the fossils with the tip of a screwdriver. These portions were then ground to a fine powder using a mortar and pestle. *S. officinalis* melanin, isolated from ink sacs of *S. officinalis*, was obtained from

Sigma-Aldrich (St. Louis, MO, USA). DHI and DHICA were prepared as described by Wakamatsu and Ito with minor modifications (Wakamatsu and Ito, 1988). DHI-melanin and DHICA-melanin were prepared by tyrosine oxidation as described by Ozeki and coworkers with minor modifications (Ozeki et al., 1996b).

3.2.2 Scanning electron microscopy

SEM was used to characterize the morphology of fossil and contemporary ink. 0.5 mg samples were suspended in 0.500 mL of ultrapure deionized water and vortexed for 30 s. Prior to dark storage at 4°C, 2 μL of each sample was dropped on a silicon wafer chip (5 mm x 5 mm) and dried in the dark under N_2. Samples were then mounted on a stainless steel peg. To increase resolutions, samples were coated with a 10 nm layer of Au/Pd by applying argon plasma for 3 min at 10 mA using a Hummer V sputter coater. Representative images were captured on an XL-SEG/SFEG SEM operated at 5 - 10 kV in ultra high-resolution mode with a spot size of 1.0 and working distance of 5.0 - 7.5 mm. Dimensions of the structures captured were measured using analySIS XL DOCU software. Images and dimensions of the fossil and *S. officinalis* structures are shown in Figure 9C-E.

3.2.3 Alkaline hydrogen peroxide oxidation

To quantify the production of various pyrrole acids (PDCA, PTCA, isoPTCA, and PTeCA) from melanin samples, alkaline hydrogen peroxide degradation was

performed as described previously (Ito et al., 2011). In brief, ca. 1-4 mg of specimen was taken in a 10 ml screw-capped conical test tube, to which 100 μL water, 375 μL 1 mol/L K_2CO_3 and 25 μL 30% H_2O_2 (final concentration: 1.5%) were added. The mixture was mixed vigorously at 25°C for 20 hr. The residual H_2O_2 was decomposed by adding 50 μL 10% Na_2SO_3 and the mixture was then acidified with 140 μL of 6 mol/L HCl. The reaction mixture was centrifuged at 4,000 g for 1 min, and an aliquot (80 μL) of the supernatant was directly injected into the HPLC system. H_2O_2 oxidation products were analyzed with the HPLC system consisting of a JASCO 880-PU liquid chromatograph (JASCO Co., Tokyo, Japan), a Shiseido C_{18} column (Capcell Pak, Type MG; 4.6 x 250 mm; 5 μm particle size; Shiseido, Tokyo, Japan) and a JASCO UV detector monitored at 269 nm. The mobile phase was 0.1 mol/L potassium phosphate buffer (pH 2.1): methanol, 85:15 (v/v). Analyses were performed at 45°C at a flow rate of 0.7 mL/min. Examples of the resulting HPLC chromatograms for prepared markers of eumelanin and GSM 120386 are shown in Figure 10B and C. The concentration of the degradation markers present in GSM 122841, GSM 120386, the background sediments of each fossil specimen, and *S. officinalis* are tabulated in Table 1.

3.2.4 High-performance liquid chromatography-mass spectrometry

To confirm the identity of the degradation products PDCA, PTCA, isoPTCA, and PTeCA by mass spectrometry, we oxidized 20 mg of fossil ink sac powder (GSM 120386)

in 4.0 mL of 1 mol/L K_2CO_3 with 0.5 mL 30% H_2O_2 for 20 hr., extracted degradation products with ethyl acetate after decomposition of H_2O_2 and acidification to pH 1, and subjected the products to preparative HPLC using a Shiseido C_{18} column (Capcell Pak, Type MG; 20 x 250 mm plus 3.5 mm pre-column; 5 μm particle size; from Shiseido, Tokyo, Japan) at 25°C and at a flow rate of 7.0 mL/min. The mobile phase was 0.4 mol/L formic acid: methanol, 80:20 (v/v). The pyrrole acids were individually collected as described above and then mass spectrometry measurements of each product was performed with high performance liquid chromatography – time of flight mass spectrometry (LC-MS-TOF) as described below.

A 10 μL injection of each degradation product at a concentration of 60 – 80 μM in a 75:25 mixture of LC grade methanol and water solution, was injected onto an Agilent 1200 Series HPLC (Agilent Technologies Inc., Santa Clara, CA, USA) and separated using a Ascents Express 5 cm x 2.1 mm x 2.7 μm C_{18} column (Supelco Analytical, Bellefonte, PA, USA). The HPLC was connected with a standard ESI interface to an Agilent Technologies 6224 time of flight mass spectrometer (MS-TOF) to obtain high-resolution exact mass measurements.

The LC-MS-TOF was operated at a flow rate of 0.3 mL/min using a linear gradient of 0.3% formic acid, 98% water, and 2% acetonitrile (A) and 0.3% formic acid, 98% acetonitrile, and 2% water (B) as the mobile phase. The gradient program started

with 0% B at 0 minutes and increased to 55% B during the 13 minute program. The MS used an electrospray ionization (ESI) source in the negative mode. The desolvation temperature was set to 300 °C using nitrogen as the desolvation gas at 11 L/min at a nebulizer pressure of 227.5 kPa.

Total ion chromatographs and the associated MS spectrum for the isolated PDCA, PTCA, isoPTCA, and PTeCA markers of GSM 120386 are shown in Figure 11, Figure 12, Figure 13, and Figure 14. The quantitative MS data for the parent ion for each degradation product are given in Table 2. These data confirm unambiguously that the degradation products from the fossil melanins are the pyrrole acids characteristic of melanins.

Standards PTCA and PDCA were prepared as described in Ito and Wakamatsu (1998) with minor modifications (Ito and Wakamatsu, 1998). Standard of PTeCA was prepared as described by Ward and coworkers (Ward et al., 2008). The newly identified degradation marker was prepared according to the protocol in **Chapter 3.2.5**.

3.2.5 Preparation of isoPTCA

A standard of isoPTCA was prepared by a chemically straightforward method as follows. A mixture of Cu_2O (104 μmol, 15 mg) and 1,10-phenanthroline (200 μmol, 36 mg) in 4 mL of 1,4-dioxane was prepared and placed under an argon atmosphere. Ethyl isocyanoacetate (2.0 mmol, 220 μL) and diethyl acetylenedicarboxylate (2.4 mmol, 382

μL) were added by syringe to form the reaction mixture. The mixture was heated to 100°C and stirred for 4.5 h. Once the starting material, ethyl isocyanoacetate, was fully consumed, the reaction mixture was cooled to room temperature. The catalyst (Cu_2O) was removed by filtration and the filtrate was concentrated under reduced pressure to give a yellowish-brown oil. Flash column chromatography on silica gel (ethyl acetate/hexane, 1:7 to 1:1) afforded triethyl pyrrole-2,3,4-tricarboxylate as a yellow oil (489 mg, 86% yield). ^{1}H NMR (500 MHz, $CDCl_3$): δ 10.32 (br s, 1H), 7.49 (d, 1H), 4.41 (q, 2H), 4.32 (q, 2H), 4.28 (q, 2H), 1.40 (t, 3H), 1.33 (t, 3H), 1.31 (t, 3H). GCMS (EI): *m*/*z* 283 [$M^{+\bullet}$].

A solution of triethyl 2,3,4-pyrrole tricarboxylate (0.373 mmol, 106 mg) in ethanol (3.2 mL) was refluxed for 20 h following the addition of powdered KOH (3.73 mmol, 209 mg). The reaction was cooled to room temperature, ethanol was removed under vacuum, and the residual product was dissolved in water (2.1 mL). A small amount of ice was added directly to the reaction flask, and the solution was acidified to pH 0.0 – 1.0 by dropwise addition of 12 M HCl. The precipitate was then removed by filtration, washed with water (1 ml) and dried under vacuum overnight. The resulting solid was then purified by HPLC and characterized by mass spectrometry (MS) (10 mg, 14% yield), MS (ESI): *m*/*z* 200 $[M + H]^+$, 198 $[M - H^+]^-$ (Figure 13). This procedure is similar to that used by Ward and coworkers (Ward et al., 2008). The yield was not optimized.

3.2.6 Electron paramagnetic resonance spectroscopy

Eumelanin exhibits a characteristic asymmetric, 4-6 G wide single line EPR spectra with a g value of ~2.004 at X-band (~9.5 GHz), (Meredith and Sarna, 2006). We used a Varian Centuryline E-109 X-band EPR spectrometer interfaced with a PC using a Platform-Independent Data Acquisition Module model 401-012 made by Scientific Software Services (EWWIN 4.21, Plymouth, MI) with frequency measured using an EIP Autohet frequency counter (Model 351D) to acquire the EPR spectra for fossil melanin, fossil sediment and modern melanin samples. The EPR spectra for fossil melanins (Figure 16A and B) are identical to that of *S. officinalis* melanin, and characteristic of the free radical signal associated with melanins. The line widths and g-factors for GSM 122841 and GSM 120386 are 5.6G and 5.7G, and 2.0028 and 2.0026, respectively. The concentration of melanin preserved in the two samples is not known and so the relative intensity of the fossil EPR spectra does not provide information about the relative free radical concentrations. The background sediment however was analyzed on the same quantity of sample and plotted on the same scale as the fossil melanin to provide a qualitative comparison of the melanin present in the pigment and sediment of each sample.

3.2.7 Optical absorption

Optical absorption spectra of melanin are broad and monotonic. The absorbance of fossilized melanin, sediments and *S. officinalis* melanin taken at 500 nm, are compared in Table 4. To prepare the solutions, 0.1 to 5 mg of each specimen was placed in a 10 ml screw-capped conical test tube and 100 μL water and 900 μL Soluene-350 (from Perkin-Elmer, Waltham, MA, USA) were added. The tubes were vortex-mixed and heated at 100°C (boiling water bath) for 15 min. This was subsequently repeated. The mixtures were then centrifuged at 4,000 g for 3 min, and the absorption spectrum of each supernatant was analyzed. The fossil melanins, fossil sediments, and *S. officinalis* melanin all exhibit absorbance at 500 nm. The absorbance at 500 nm (A_{500}) provides an estimate of the total amount of melanin in a sample (Ozeki et al., 1996b).

3.2.8 Elemental analysis

The elemental analysis – C, H, and N – of the fossil melanin, fossil sediment, background standards for hydroxyapatite and calcium carbonate, and modern melanin specimens was performed at The Center for Organic Elemental Microanalysis at Kyoto University using combustion. From these data, the C, H and N ratio of the fossil melanin and organic content of the sediment could be determined (Liu et al., 2005). The results are given in Table 5.

3.2.9 Fourier transform infrared spectroscopy

In preparation for IR, a portion of each sample – fossil and modern – was compressed into a KBr pellet. IR absorption spectra of the pellet were measured using a Fourier transform infrared (IR) spectrometer attached to a microscope (Nicolet 6700/Nicolet Continum; Thermo Scientific Inc., Waltham, MA, US). IR spectra were measured in the wavenumber region from 700 cm^{-1} to 4000 cm^{-1} with resolution of 4 cm^{-1}. The viewing area was 100 x 100 mm. Figure 17A shows the IR absorption spectra of, GSM 122841, GSM 122841 sediment, *S. officinalis* melanin, hydroxyapatite and calcium carbonate with the spectra for GSM 120386 are shown in Figure 17B.

3.2.10 X-ray photoelectron spectroscopy

The surface composition (top 5-10 nm) of fossil sediment, fossil melanin, and contemporary melanin specimens were analyzed and compared using an x-ray photoelectron spectrometer from Kratos Analytical Axis Ultra (Manchester, UK). A circle of each sample (~1 cm diameter) was coated onto copper tape using a plastic spatula. A survey scan of all of the elements available on the surface except for hydrogen (Figure 18A shows the survey scan for the GSM 122841 sample) and a high-resolution spectra of the 1s orbitals of C was obtained at two points on each sample. The relative amounts of C, N, and O were determined using the peak areas and the relative sensitivity factors of the instrumentation to C, N, and O species. The binding energy

charge was corrected by setting the peak corresponding to C bound only to H to 285 eV. The resulting spectra were analyzed using CasaXPS. The deconvolution of the high-resolution scan of the C peak for the GSM 122841 sample and sediment are shown in Figure 18B and C. The percentages of different functional groups bound to carbon, determined by fitting the high-resolution 1s spectra of C with mixed Gaussian (30%)-Lorentzian peaks, is presented for the fossils and *S. officinalis* melanin in Table 6.

3.2.11 ^{13}C cross-polarization magic angle spinning solid state NMR

^{13}CP-MAS SSNMR spectra were acquired on a 600 MHz spectrometer available at the NHMFL AMRIS facility at the University of Florida at Gainesville. Spectra were acquired at a spin rate of 10 kHz using a CP contact time of 2.5 ms and a recycle delay of 0.5 s. Three characteristic spectral regions were identified as follows: 10–90ppm, aliphatic carbons, most likely due to proteinaceous material; 90–160ppm, aromatic carbons, including indole or pyrrole type carbons within the polymer; and 160–225ppm, carbonyl carbon atoms from amides, carboxylates, and quinones which may be associated with the melanin polymer as well as the proteinaceous material. We also ran CP contact time experiments where contact time was shortened to 0.05 ms to further differentiate protonated aliphatic carbon atoms at 90-130 ppm from non-protonated aliphatic carbon atoms at 130 – 160 ppm. The spectrum for the GSM 122841 sample is shown in Figure 19A; that for GSM 120386 is shown in Figure 19C. The sediment spectra

for GSM 122841 and GSM 120386, shown in Figure 19B and D, lack the aromatic carbon and carbonyl carbon peaks found in melanin.

3.3 Results and Discussion

The single unique assay commonly used to identify modern melanins is alkaline hydrogen peroxide oxidation. Under the oxidation conditions described by Ito and collaborators, melanin breaks down into distinct chemical markers associated with its monomeric precursors (Wakamatsu et al., 2009; Ito et al., 2011). A second fundamental method and the most used signature for melanin in physical chemistry EPR, can verify the results of alkaline hydrogen peroxide oxidation. EPR probes the electronic properties of a material nondestructively (Sarna et al., 1976; Sealy et al., 1982).

Alkaline hydrogen peroxide degradation was developed with an understanding of how melanin is naturally synthesized and was refined to identify eumelanin through the presence of specific chemical markers –DHI and DHICA (Figure 4) (Pezzella et al., 1997; Ito and Wakamatsu, 1998). Eumelanin is generated from these chemical building blocks which are derived from the amino acid tyrosine (Figure 1) (Simon et al., 2009). The biologically controlled copolymerization of DHI and DHICA produce eumelanin pigment with an unknown absolute structure (Figure 1) (Palumbo, 2003; Meredith and Sarna, 2006). Alkaline hydrogen peroxide degradation breaks this copolymer into unique markers (Figure 10A), PDCA, PTCA, isoPTCA, and PTeCA (Pezzella et al., 1997;

Ward et al., 2008). These products are common only to eumelanin and have never been produced by the alkaline hydrogen peroxide oxidation of any other biological material (Pezzella et al., 1997; Ito et al., 2011). The chemical degradation of the fossil pigments produces the expected markers for eumelanin (Table 1) and no evidence of the characteristic markers for pheomelanin mentioned in **Chapter 2**. This is consistent with pigment from the ink of *S. officinalis*, which is pure eumelanin. The sediment adjacent to each fossil specimen was also analyzed and yielded small quantities of the degradation markers for eumelanin ranging from 0-4.7% of the eumelanin markers found in each fossil specimen (Table 1). This eumelanin in the background sediment is attributed to a small leak of pigment from the ink sacs.

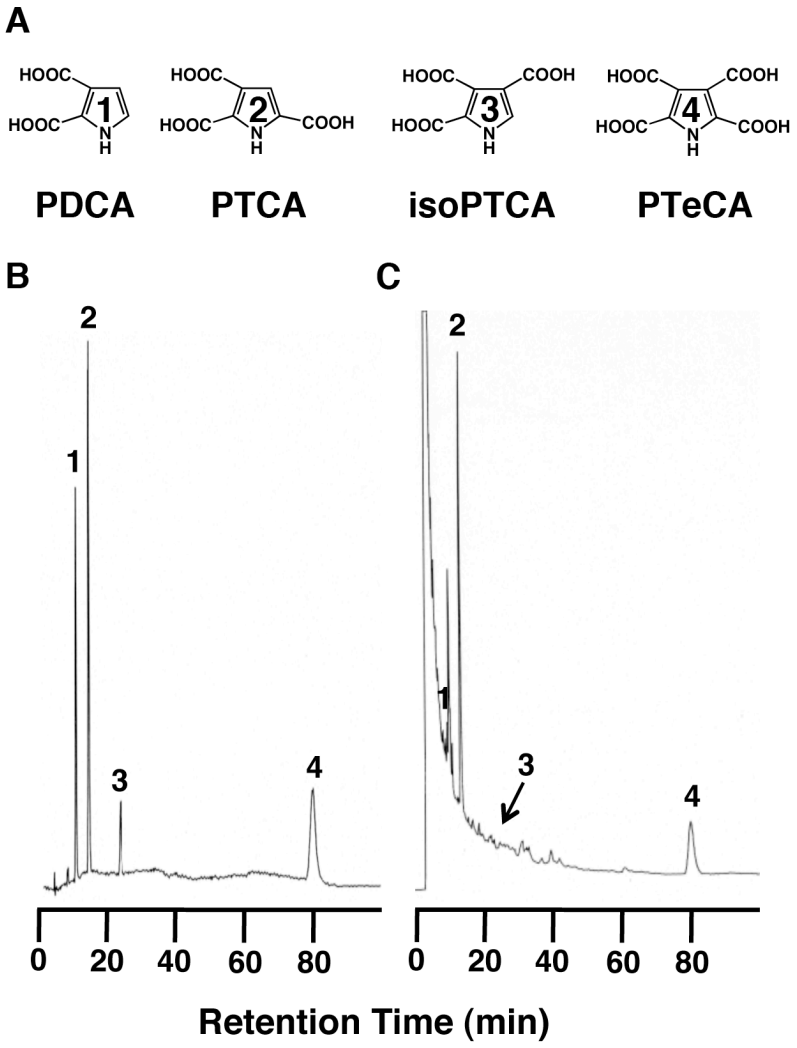

Figure 10: Degradation marker structures and HPLC chromatograms

Chemical structures of the degradation products of eumelanin – PDCA, PTCA, isoPTCA and PTeCA are shown (A). The HPLC chromatograms of prepared standards of these markers (B) and the alkaline hydrogen peroxide oxidation products of GSM 120386(C) are also shown.

Table 1: Quantity of the alkaline hydrogen peroxide oxidation produces from S. officinalis, GSM 122841, GSM 120386 and the fossil sediments

Quantity of melanin markers PDCA, PTCA, isoPTCA, and PTeCA produced by oxidation of *S. officinalis*, GSM 122841, GSM 120386, GSM 122841 sediment, and GSM 120386 in ng/mg. All data was published previously (Glass et al., 2012).

Specimen	PDCA	PTCA	isoPTCA	PTeCA
S. officinalis	704	15710	390	2090
GSM 122841	58	342	47	438
GSM 120386	173	1710	245	2220
GSM 122841 sediment	1.7	2.2	< 2.2	< 1.3
GSM 120386 sediment	2.4	3.2	< 3.9	< 1.5

The identity of each degradation marker from fossil specimen GSM 120386 was confirmed using high-resolution mass spectrometry to obtain exact mass measurements (Figure 11, Figure 12, Figure 13, Figure 14, Table 2). The ratio of PTeCA/PTCA for both GSM 122841 and GSM 120386 is greater than that of modern *S. officinalis* (Table 1). These findings suggest that the PTeCA/PTCA ratio may serve as a good indicator of aging (cross-linking) of eumelanin.

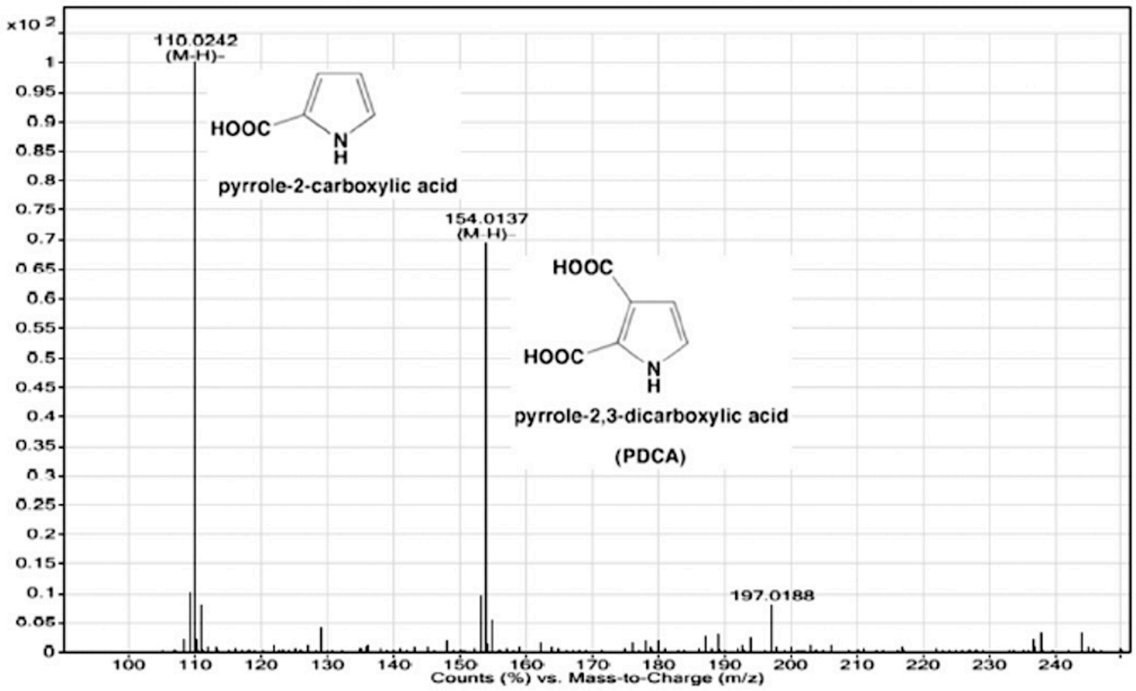

Figure 11: Mass spectrum of the degradation marker PDCA

Mass spectrum for the alkaline hydrogen peroxide oxidation marker PDCA derived from the fossil specimen GSM 120386. The structures associated with the parent ion and the fragment ion of PDCA are shown on the spectrum. Exact mass data is presented in Table 2. This spectrum was published previously (Glass et al., 2012).

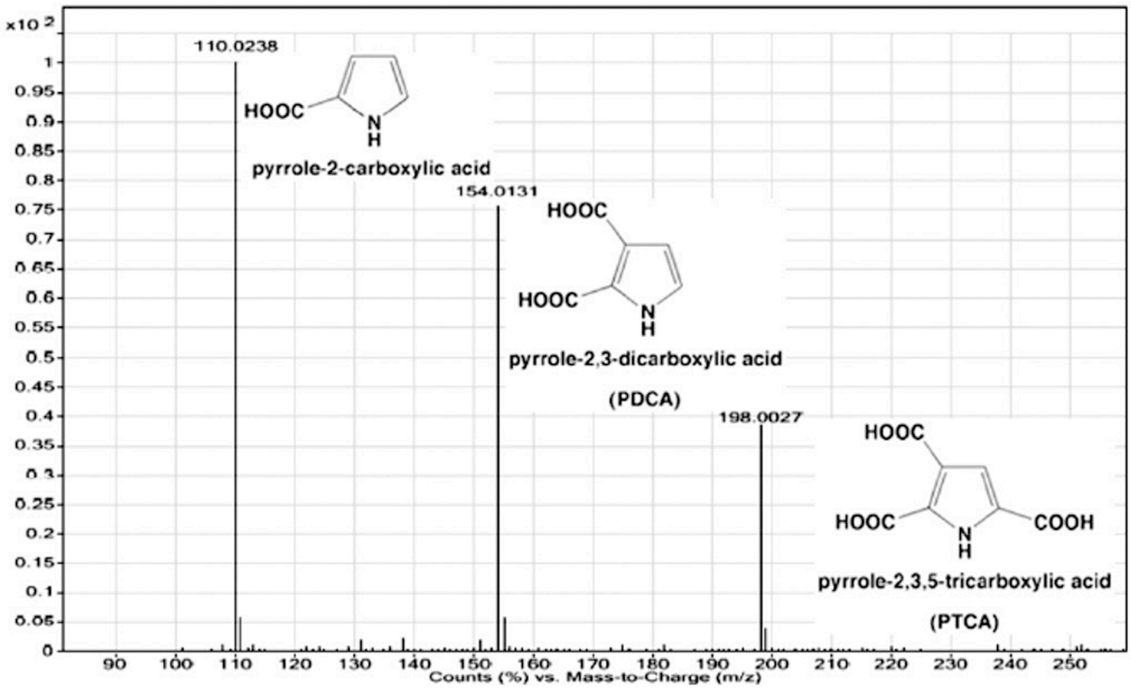

Figure 12: Mass spectrum of the degradation marker PTCA

Mass spectrum for the alkaline hydrogen peroxide oxidation marker PTCA derived from the fossil specimen GSM 120386. The structures associated with the peaks of the parent ion and the fragment ions of PTCA are shown on the spectrum. Exact mass data is presented in Table 2. The spectrum was published previously (Glass et al., 2012).

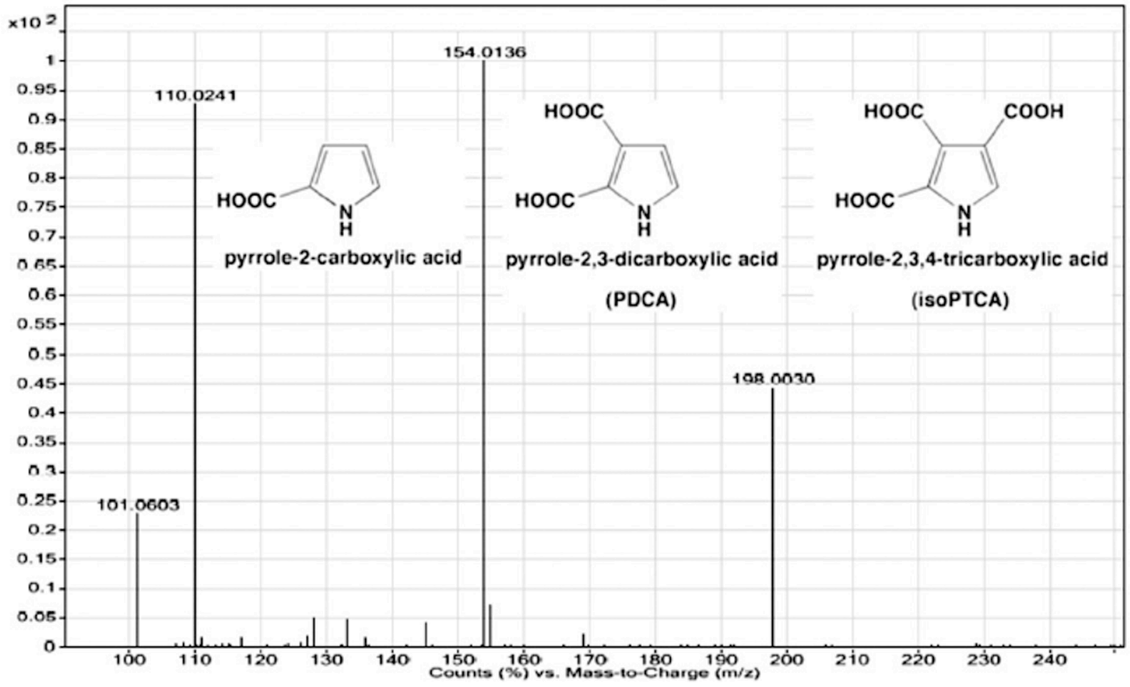

Figure 13: Mass spectrum of the degradation marker isoPTCA

Mass spectrum for the alkaline hydrogen peroxide oxidation marker isoPTCA derived from the fossil specimen GSM 120386. The structures associated with the peaks of the parent ion and the fragment ions of isoPTCA are shown on the spectrum. Exact mass data is presented in Table 2. The spectrum was published previously (Glass et al., 2012).

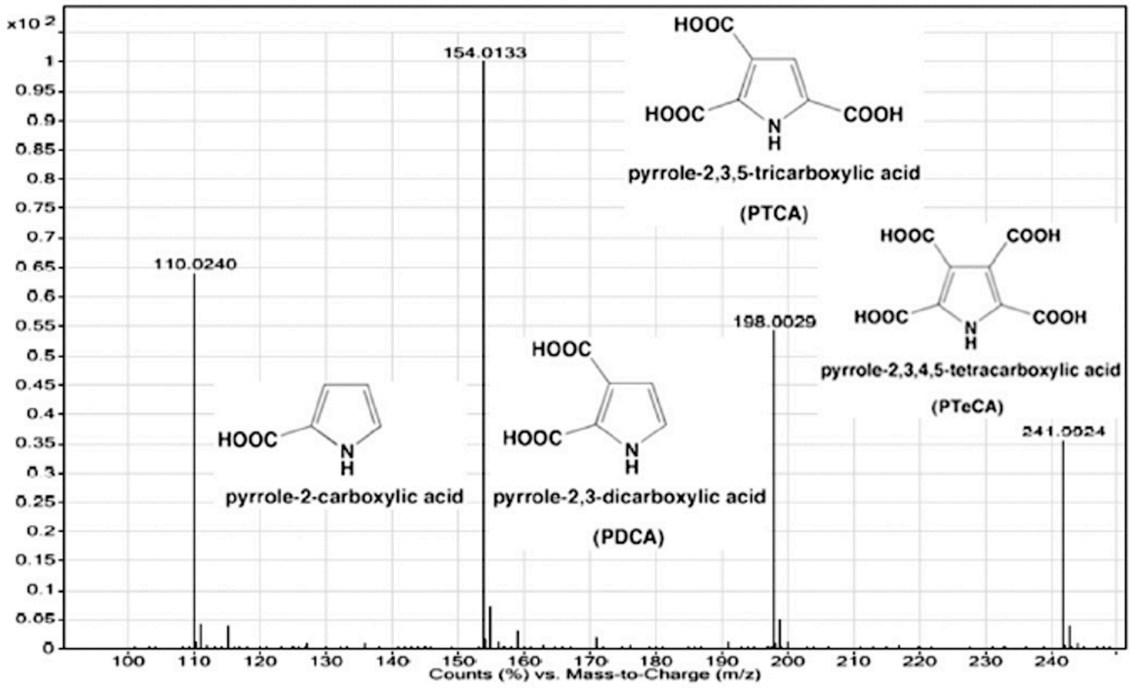

Figure 14: Mass spectrum of the degradation marker PTeCA

Mass spectrum for the alkaline hydrogen peroxide oxidation marker PTeCA derived from the fossil specimen GSM 120386. The structures associated with the peaks of the parent ion and the fragment ions of PTeCA are shown on the spectrum. Exact mass data is presented in Table 2. The spectrum was published previously (Glass et al., 2012).

Table 2: Mass spectral data for the degradation products derived from GSM 120386

Data confirms the presence of PDCA, PTCA, isoPTCA, and PTeCA in fossil specimen GSM 120386. Each decarboxylation results in a decrease in the mass to charge ratio of 44 m/z. Mass spectra are shown in Figure 11, Figure 12, Figure 13, and Figure 14, respectively. All values were published previously (Glass et al., 2012).

	Peak	Formula	Calculated *m*/*z*	Difference in ppm
PDCA	154.0137	$C_6H_5NO_4$	154.0146	5.92
	110.0242	$C_5H_5NO_2$	110.0248	4.95
PTCA	198.0031	$C_7H_5NO_6$	198.0044	6.73
	154.0135	$C_6H_5NO_4$	154.0146	7.26
	110.0241	$C_5H_5NO_2$	110.0248	6.02
isoPTCA	198.0030	$C_7H_5NO_6$	198.0044	6.88
	154.0136	$C_6H_5NO_4$	154.0146	6.53
	110.0241	$C_5H_5NO_2$	110.0248	6.19
PTeCA	241.9942	$C_8H_5NO_8$	241.9942	7.42
	198.0044	$C_7H_5NO_6$	198.0044	7.71
	154.0146	$C_6H_5NO_4$	154.0146	8.17
	110.0248	$C_5H_5NO_2$	110.0248	7.06

Increase in this PTeCA/PTCA ratio also occurs when 1:1 DHI:DHICA synthetic eumelanin is exposed to elevated temperatures for prolonged periods, and so we attribute the increased concentrations of the PTeCA marker in the fossil samples to cross-linking in the eumelanin subunits as a consequence of diagenesis and thermal maturation during sedimentary burial Table 3. A proposed mechanism for this cross-linking developed by Ito and coworkers is summarized in Figure 15 (Ito et al., 2013b).

Table 3: Chemical analysis of synthetic 1:1 DHI:DHICA eumelanin before and after exposure to 100 °C and 40 °C

Analysis of the alkaline hydrogen peroxide oxidation markers for synthetic 1:1 DHI:DHICA eumelanin before and after exposure to 100 °C for 18 days before and after exposure to 40 °C for 70 days. All data was published previously (Glass et al., 2012).

Specimen	PDCA	PTCA	PTeCA	PTeCA/PTCA
Before heating at 100 °C	1690	27710	3180	0.11
After heating at 100 °C	960	8720	9220	1.06
Before heating at 40 °C	1010	27500	2510	0.09
After heating at 40 °C	970	18800	4280	0.23

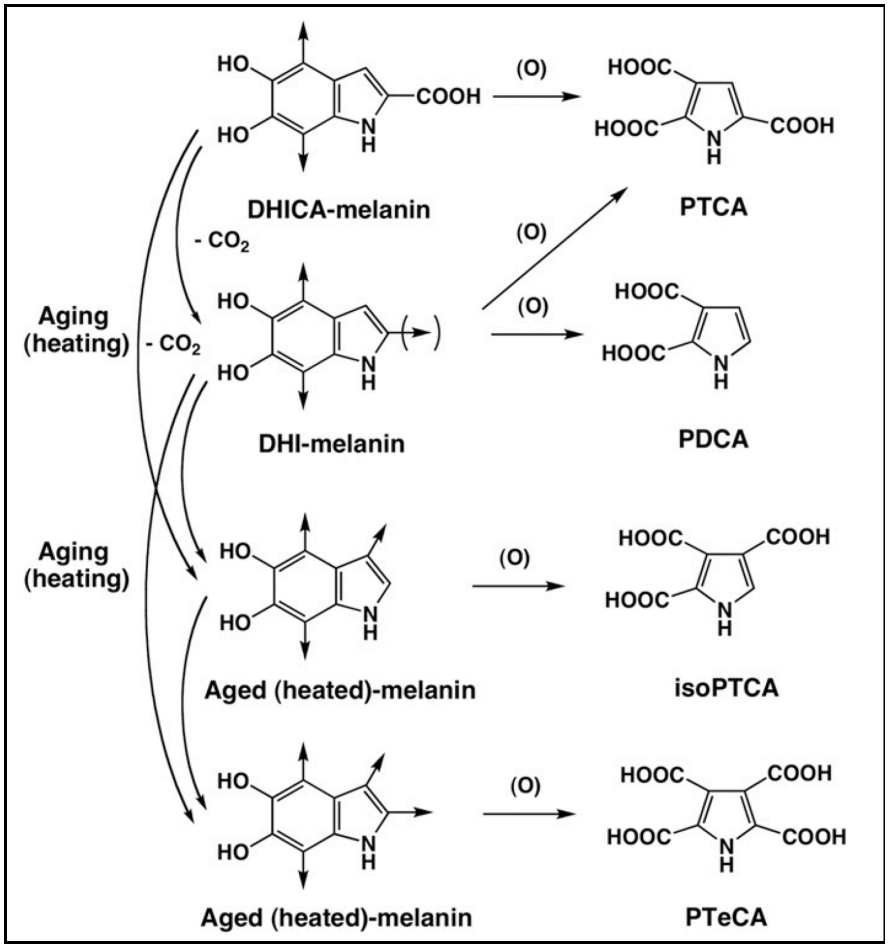

Figure 15: Structural modification of eumelanin during aging (heating) and degradation by alkaline hydrogen peroxide oxidation

On alkaline hydrogen peroxide oxidation [denoted as (O)], the DHICA moiety in eumelanin gives PTCA in a high yield whereas the DHI moiety gives PTCA and PDCA in relatively low yields (Ito et al., 2011). During aging (mimicked by heating), the DHI moiety undergoes cross-linking at either the C2 or C3 position, whereas the DHICA moiety undergoes decarboxylation followed by cross-linking at either the C2 or C3 position. Additional cross-linking affords aged melanin with connections at both the C2 and C3 positions as the final product. These decarboxylated and aged melanins give rise to PDCA, PTCA, isoPTCA and PTeCA. This figure and caption were published previously (Ito et al., 2013b).

Eumelanin also possesses a unique free radical signature that originates from semiquinone species present in the pigment and can be detected by EPR (Sealy et al., 1982). This characteristic signature is an asymmetric 4-6 G wide single line spectra (Figure 6) with a g value of ~2.004 at X-band (~9.5 GHz) (Meredith and Sarna, 2006). X-band EPR spectra of GSM 122841 and GSM 120386 (Figure 16A and B) reveal single band line widths of 5.6 and 5.7G and g-factors of 2.0028 and 2.0026, respectively. This result also confirms the absence of pheomelanin, as the EPR signal of that pigment reveals hyperfine splitting in this frequency range. The diminished EPR signals of the background sediments also confirmed the presence of minimal eumelanin in the sediment of each specimen (Figure 16A and B).

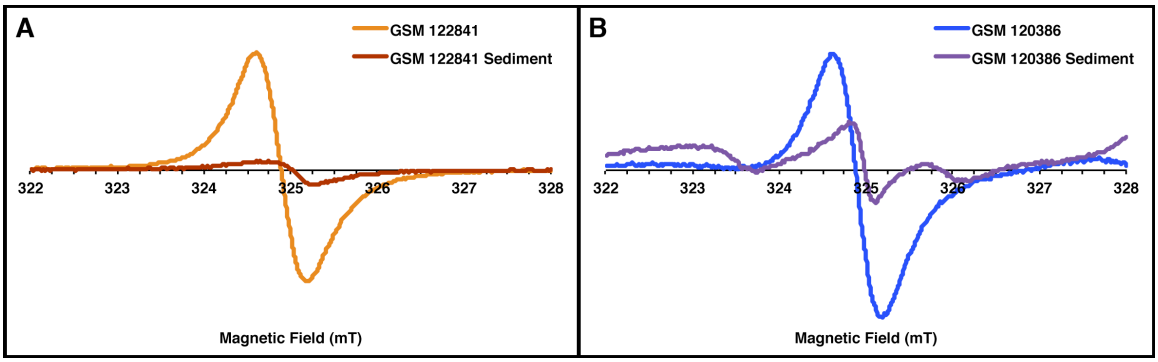

Figure 16: EPR spectra of GSM 122841, GSM 120386, and associated sediments

The EPR spectra of GSM 122841 and GSM 122841 sediment (A) as well as GSM 120386 and GSM 120386 sediment (B) are shown. Both the fossil and their associated sediments exhibited a linewidth and g-factor indicative of eumelanin. The same quantity of the sample pigment and sediment were used to provide a qualitative comparison of the amount of eumelanin present. All data was previously published (Glass et al., 2012).

In addition to the two assays discussed above, melanin solubilization in aqueous Soluene-350 is characterized by a broad, structureless absorption spectrum extending from the UV throughout the visible region (Ozeki et al., 1996b). The absorbance at 500 nm (A_{500}) of the resulting Soluene-350 solution can be used to rapidly estimate the total amount of melanin in a sample (Ozeki et al., 1996b). The A_{500} of the dissolved fossil specimens, background sediments, and *S. officinalis* are shown in Table 4 and further establish the presence of the pigment in the fossil specimens.

Table 4: Absorbance at 500 nm of Soluene-350 solubilized *S. officinalis*, GSM 122841, GSM 120386, GSM 122841 sediment, and GSM 120386 sediment

Values are reported as absorbance at 500 nm per mg of specimen. All values were published previously (Glass et al., 2012).

Specimen	A500 / mg
S. officinalis	5.99
GSM 122841	1.45
GSM 120386	8.13
GSM 122841 sediment	0.135
GSM 120386 sediment	0.100

To gain further insights into the chemistry of the fossilized material, we used: elemental analysis, Fourier transform infrared spectroscopy (FTIR), and x-ray photoelectron spectroscopy (XPS). This is a powerful combination of techniques for identifying structural properties of complex organic constituents.

Elemental analysis can provide a quantitative measure of critical organic residues like carbon (C), hydrogen (H), and nitrogen (N) in each sample (Table 5). GSM 120386 yielded quantities of C, N, and H close to those of DHICA-melanin while the elemental analysis of GSM 122841 provided limited information about its chemical nature. The background sediments showed substantially lower nitrogen content than the fossil pigments (Table 5).

Table 5: Elemental analysis of the C, H, N in synthetic, modern and UK melanins

Percent of C, H, and N in synthetic DHI melanin, synthetic DHICA melanin, *S. officinalis*, GSM 122841, GSM 120386, GSM 122841 sediment, GSM 120386 sediment, and standards of hydroxyapatite and calcium carbonate. Values represent the average of two determinations. All values were published previously (Liu et al., 2005; Glass et al., 2012).

	Elemental Analysis (%)		
Specimen	**C**	**H**	**N**
DHI-melanin	51.52	3.45	7.80
DHICA-melanin	47.43	3.57	6.42
S. officinalis	42.87	2.72	6.57
GSM 122841	16.87	1.69	1.37
GSM 120386	49.40	3.73	5.07
GSM 122841 sediment	14.75	2.27	0.37
GSM 120386 sediment	8.64	0.92	0.18
Calcium carbonate	11.94	0.17	0.00
Hydroxyapatite	1.02	0.50	0.00

To gain insight into the preserved organic chemical groups in the fossil pigment, FTIR spectra were recorded. The FTIR spectrum of *S. officinalis* melanin consists of three major bands centered at 3400 cm^{-1}, 1605 cm^{-1}, and 1371 cm^{-1} (Bardani et al., 1982; Hong and Simon, 2006; Centeno and Shamir, 2008). The band at 3400 cm^{-1} is dominated by absorption due to the stretching mode of the OH bond, while the band at 1605 cm^{-1} is attributed to the carbonyl stretch in indole quinone. The band at 1371 cm^{-1} may consist of absorption bands due to in-plane bending modes of OH and NH bonds combined with various modes of aromatic rings.

The overall FTIR spectral features of *S. officinalis* melanin are also observed in both GSM 122841 and GSM 120386 (Figure 17A and B). The fossil spectra show absorption bands derived from the CH stretching vibration in CH_x functional groups, ~2856 and 2926 cm^{-1}. The absorption bands due to these functional groups are also found in the background sediment spectra where there is no fingerprint of eumelanin. This is consistent with the presence of lipids, which are exceptionally recalcitrant, in both the fossil samples and background sediments. Second, the shoulder at 1711 cm^{-1} becomes more apparent and distinct from the band at 1622 cm^{-1}, suggesting that the content of indole quinone units is lower in fossil eumelanin than in modern melanin. Third, a broad absorption band at less than 1500 cm^{-1} appears, but is accounted for by the background sediment.

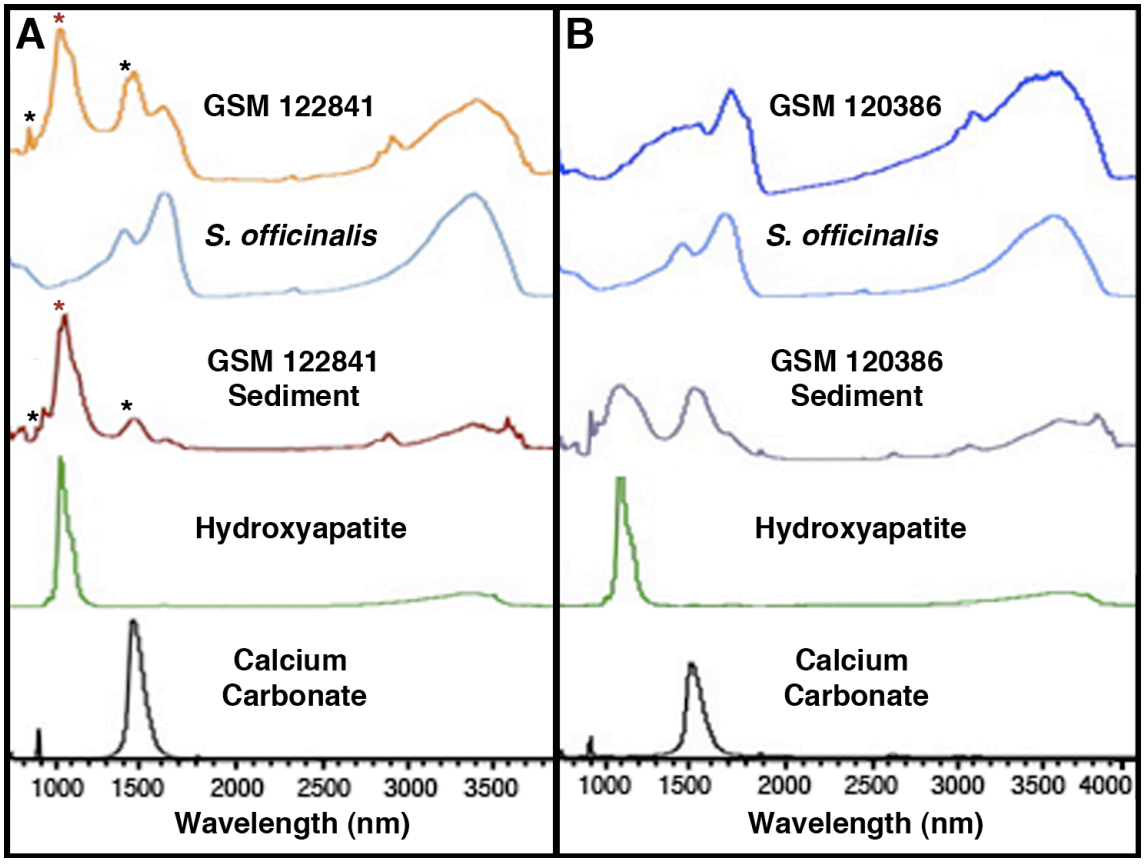

Figure 17: Deconvolution of the FTIR spectra of GSM 122841 and GSM 120386

FTIR absorption spectra for GSM 122841, *S. officinalis*, GSM 122841 sediment, and standards of hydroxyapatite and calcium carbonate (A) and corresponding spectra of GSM 120386 (B). The absorption bands marked by red and black asterisks in (A) are attributed to the phosphate and carbonate group, respectively. This data was published previously (Glass et al., 2012).

The absorption bands indicated by the red and black asterices in the background sediment FTIR spectra of GSM 122841 are due to the phosphate and carbonate groups respectively. It is clear that hydroxyapatite, a common diagenetic mineral, is associated with these fossils, and calcium carbonate, abundant in shell material, is present in the

fossil sediments (Wilby et al., 2004). The carbon and hydrogen in the background sediments is due in part to the calcium carbonate and hydroxyapatite in the sediments (Table 5).

The x-ray photoelectron spectroscopy (XPS) scan shown in Figure 18A corroborates the existence of the organic and mineral residues revealed by FTIR. XPS is not limited to identifying all of the elements present in the top 5-10 nm of a sample, it can also provide information about the binding interactions of a particular element in that sample (Clark et al., 1990). From high-resolution XPS data of the carbon peaks of GSM 122841 and GSM 120386, we determined that carbon participates in CH_x, CNH_2; C-O, C_2NH; C=O; and COO binding interactions (Figure 18B, Table 6). The surface binding interactions of *S. officinalis* melanin and both fossil specimens are identical in type and relative amount. The background fossil sediment participates in many of the same surface binding interactions as the fossil pigment, but the sediment contains carbonate and lacks a carbonyl peak (Figure 18C). It is important to note that calcium carbonate only exhibits two signals, a carbonate (CO_3) signal at ~289.3 eV and a hydrocarbon impurity (CH_x) signal calibrated to 285 eV (Ni and Ratner, 2008).

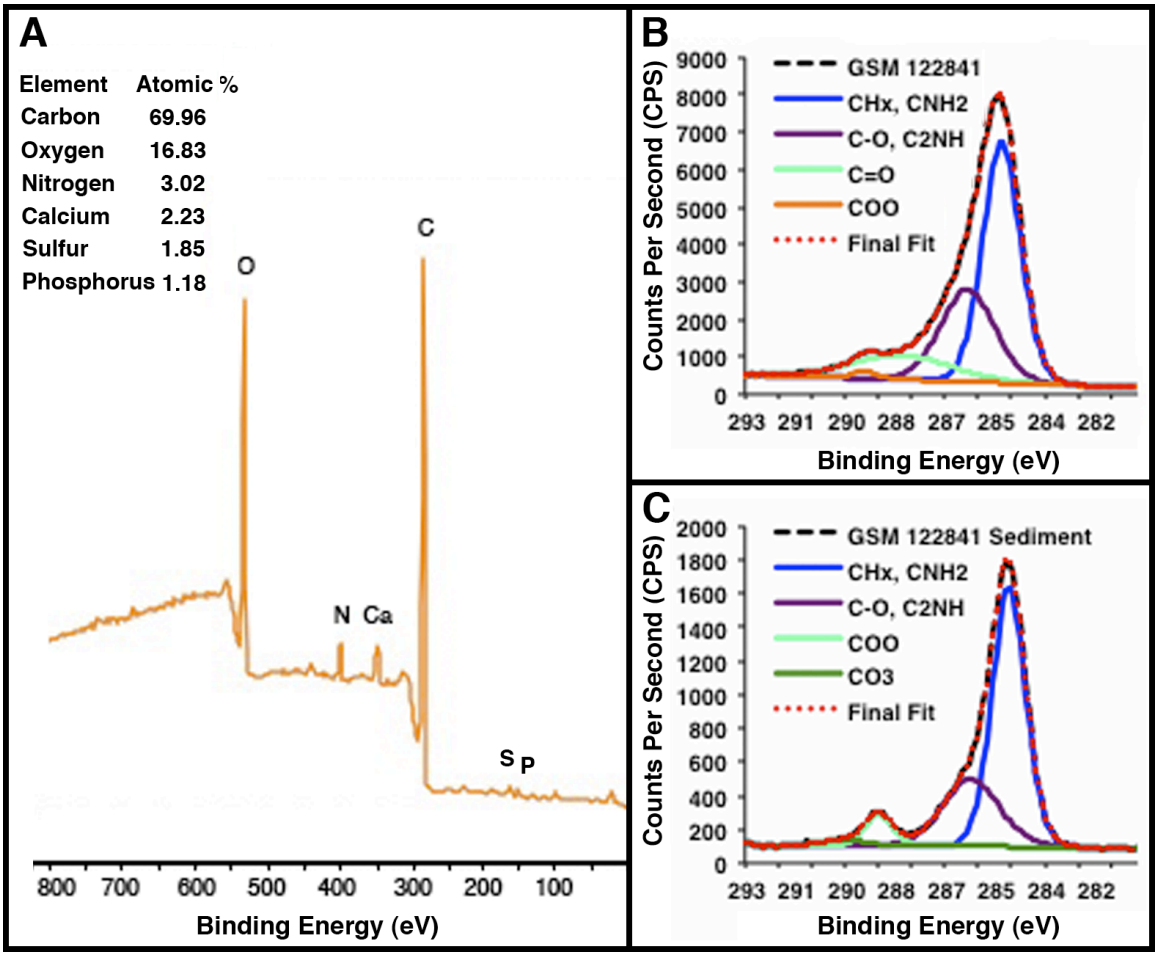

Figure 18: XPS analysis of fossil specimen GSM 122841

XPS survey scan of GSM 122841 (A) revealing the major elements present in the top 5-10 nm of the fossil specimen. Additional elements present in greater than 0.1 atomic% (the detection limit of the instrument) are silicon 2.70, aluminum 2.04, and fluorine 0.18. High-resolution carbon scan of GSM 122841 (B) and GSM 122841 sediment (C) are also shown. The average percent and standard deviation of the functional groups present in the top 5-10 nm of GSM 122841 (B) follow: 54 ± 1, 32 ± 3, 13 ± 4, and 1 ± 1% for CH_x, CNH_2, C-O, C_2NH, C=O, and COO based on fitting with mixed Gaussian (30%) Lorentzian peaks. The functional groups present in GSM 122841 sediment (C): 65 ± 3, 26 ± 2, 6 ± 1, and 3 ± 1% for CH_x, CNH_2, C-O, COO, and CO_3. No C=O peak was present in the GSM 122841 sediment. All data was published previously (Glass et al., 2012).

Table 6: Percent of the different binding interactions of C in *S. officinalis*, GSM 122841, and GSM 120386 determined by XPS

Data is derived from multiple high-resolution carbon scans of each sample calibrated to 285.0 eV for the CH_x, CNH_2 peak. Error indicated is standard deviation. All data was published previously (Glass et al., 2012).

Binding energy (eV)	*S. officinalis*	GSM 122841	GSM 120386
285.0 (CH_x, $CHNH_2$)	52 ± 1	54 ± 1	54 ± 1
286.5 (C-O, C_2NH)	29 ± 1	32 ± 3	27 ± 1
288.2 (C=O)	15 ± 3	13 ± 4	17 ± 2
289.1 (COO)	4 ± 3	1 ± 1	2 ± 1

To verify that the organic functional groups present in the surface of the sample also pervade the bulk of the pigmented fossil, cross-polarization magic angle spinning solid-state nuclear magnetic resonance spectroscopy (CP-MAS SSNMR) was employed. The spectra of GSM122841 (Figure 19A) and GSM120386 (Figure 19C) confirm the presence of aliphatic groups 0-90 ppm (CH_x, CNH_2), aromatic groups 90-160 ppm (CH_x, C-O, C_2NH) and carboxylic acid groups and ketones 160 – 200 ppm (C=O, COO), consistent with those previously reported for *S. officinalis* (Adhyaru et al., 2003). The spectra of the background sediments of GSM 122841 and GSM 120386 lack the aromatic, carboxylic acid and ketone signals present in the fossil pigment (Figure 19B and D). This bulk technique confirms that melanin is not present in the fossil sediments at a level detectable by CP-MAS SSNMR.

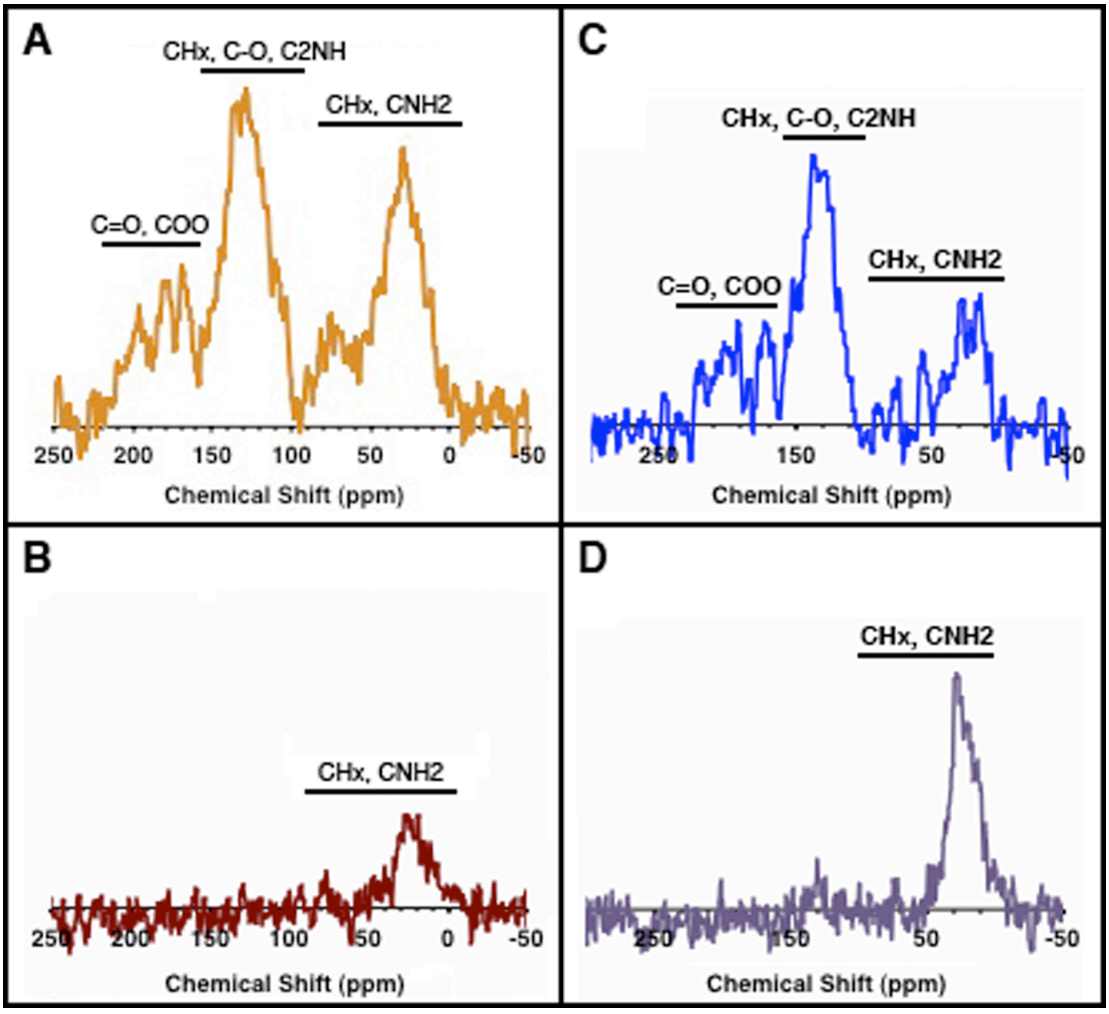

Figure 19: ^{13}C CP-MAS SSNMR spectra of GSM 122841, GSM 120386, and sediments

^{13}C CP-MAS SSNMR spectra of GSM 122841 (A), GSM 122841 sediment (B), GSM 120386 (C), and GSM 120386 sediment (D). All spectra have been published previously (Glass et al., 2012).

3.4 Conclusions

Our results demonstrate that eumelanin persists in the fossil record for at least 160 million years; the oldest determination in the fossil record. Strikingly, within the

limits of the techniques used, the preserved pigment exhibits properties that are chemically similar to modern phylogenetically related *S. officinalis*. The methods discussed here can serve to recognize and understand the distribution of melanin in ancient organisms, but also has important implications for the study of modern life.

For example, preservation of melanin over > 160 million years has implications for the study of stored histological samples associated with benign and cancerous skin tissue. Since concerns related to the decomposition of melanin during storage of these samples are diminished, they may now be analyzed with confidence. The analysis of these histological samples may provide critical information necessary for the early diagnosis of melanoma. Recent studies on historical and modern melanins using pump-probe microcopy provide insights into melanin signatures – this may be a powerful method to study these histological samples (Simpson et al., 2013; Simpson et al., 2014).

For the study of fossil melanins however, there are still many questions to consider. The controls and limitations for the preservation of melanin in the fossil record are unknown. In **Chapter 4** the effect of environmental conditions on the preservation of melanin will be explored through the analysis of four fossil ink sacs from three burial sites.

4. Impact of burial site conditions on the preservation of eumelanin in fossils

4.1 Introduction to factors that may limit eumelanin preservation

The polymeric cross-linked structure and biological ubiquity of melanins mentioned in **Chapter 1** makes them comparable to biomolecules like chitin that are somewhat resistant to microbial degradation and diagenetic alteration (Stankiewicz et al., 1997; Cody et al., 2011). Eumelanins may maintain their integrity for at least ~200 million years in the fossil record (**Chapter 3**) while most other biomolecules lose their original character and polymerize into long chains of hydrocarbons over considerably shorter periods (Briggs et al., 2000).

Recent studies, detailed in **Chapter 3**, have demonstrated the presence of melanin in in ancient organisms (Vinther et al., 2008; Clarke et al., 2010; Li et al., 2010; Vinther et al., 2010; Zhang et al., 2010; Barden et al., 2011; Wogelius et al., 2011; Carney et al., 2012; Glass et al., 2012; Lindgren et al., 2012; Lindgren et al., 2014). A subset of these studies have proposed that the shape of fossil melanosomes correlates with the composition of the pigment (eumelanin and pheomelanin) and this, along with the arrangement of the melanosomes, has been used to infer fossil color (Vinther et al., 2008; Clarke et al., 2010; Li et al., 2010; Vinther et al., 2010; Zhang et al., 2010; Carney et al., 2012). However, little remains known of the physical (temperature, pressure) or

temporal constraints on the long-term survival of melanin and their effects on the morphology and packing of pigment structures.

In this study we explore the effects of diagenesis and maturation on the physical and chemical preservation of eumelanin. For those unfamiliar with the terminology used to describe the chemical and environmental factors that can alter fossil material over time, diagenesis and maturation are described briefly. Diagenesis includes a wide array of molecular alterations that can occur between death to discovery of organic remains: intra- and intermolecular cross-linking, polymerization, deamidation, methylation, decarboxylation, racemization of amino acids, and denaturation of three-dimensional molecular structure (Briggs, 2003; Schweitzer et al., 2008). It is also used in reference to the incorporation of minerals (diagenetic mineralization) from the surrounding environment (Schweitzer et al., 2008).

The depositional / chemical environment (burial site conditions) of a fossil play a role in controlling the rate of diagenesis (Briggs et al., 2000; Schweitzer et al., 2008). Elevated temperatures and pressures accelerate the rate at which organic materials that survived decay (i.e. keratin, collagen, and chitin) are transformed through diagenetic polymerization to a more stable composition (Briggs, 2003). The resulting polymer structures are long-chains of hydrocarbons, similar to some high molecular weight kerogens (Briggs, 2003). Over time these materials can be completely converted to

kerogens with compositions that minimally relate to their organic origin (Briggs et al., 2000; Briggs, 2003). These alterations and the degree to which they have occurred indicate the maturation of the burial site and can be measured and experimentally mimicked (Kenig et al., 1994; Deconinck et al., 2003; Gupta et al., 2006; Ito et al., 2013b; McNamara et al., 2013). It is important to note that sediments that are deemed more mature have undergone a greater degree of alteration than those that are less mature.

In this chapter we report the composition of the coleoid ink from the Posidonia Shale (Early Jurassic, ~ 178-182 million years old) near Holzmaden, Germany – a site that has entered the oil window – and compare it to the ink from two less mature Jurassic mudrock units in southern England discussed in **Chapter 3**.

4.2 Materials and methods

4.2.1 Fossil ink sacs from Germany and the United Kingdom

YPM 221212 and YPM 221210 (Figure 20A and B) were collected from the Koblenzer Bed of the Posidonia Shale Formation (Lower Jurassic, early Toarcian, *tenuicostatum* Zone) near Holzmaden, Baden-Württemberg (Glass et al., 2013). The ink sacs are held in the YPM collections of the Yale Peabody Museum (USA). Melanin has previously been reported in a specimen of *Geotheutis bollensis* from the Posidonia Shale, based on infrared spectroscopy (Beyerman and Hasenmai, 1973). YPM 221212 and YPM 221210 are incomplete specimens, but each is associated with portions of an

undetermined coleoid gladius and/or phosphatized musculature. The Koblenzer Bed consists of calcareous shale with regular alterations of light carbonate-rich laminae and dark organic- and pyrite-rich laminae (Littke et al., 1991; Rohl et al., 2001). Sediment from this region is dominated by Type II (marine) kerogen with a minor contribution from Type III (terrestrial) kerogen (Littke et al., 1991; Prauss et al., 1991).

As stated in **Chapter 3**, GSM 122841 and GSM 120386 (Figure 20C and D) were collected from the Peterborough Member of the Oxford Clay Formation (Middle Jurassic, late Callovian) at Christian Malford, Wiltshire (UK) and from Bed 32 of the Blue Lias Formation (Lower Jurassic, early Sinemurian) at Lyme Regis, Dorset (UK), respectively (Glass et al., 2012). Both ink sacs are held in the GSM collections of the British Geological Survey, Keyworth (UK). The Peterborough Member consists of organic-rich mudstones alternating on a decimeter scale between blocky shelly facies and dark fissile shale (Cox et al., 1992; Wilby et al., 2004). Sediment from this region is dominated by Type II (marine) and Type III (terrestrial) organic matter (Kenig et al., 1994). Based on molecular analysis of the organic matter, Hudson and Martill (1994) suggest that peak palaeotemperature may never have exceeded 40 °C in this area (Hudson and Martill, 1994). Penn et al. suggest that maximum burial in this area was only 200-300m (Penn et al., 1986). The Blue Lias Formation consists of interbedded fossiliferous mudstone and argillaceous limestones (Lang, 1924; Deconinck et al., 2003).

Sediments from the Blue Lias Formation contain primarily Type II (marine) and Type IV (altered) organic material (Deconinck et al., 2003). Both units have experienced a mild thermal history and have not entered the oil window (Kenig et al., 1994; Glass et al., 2012).

Samples of the ink and host sediment associated with each ink sac were removed mechanically and ground to a fine powder using a mortar and pestle. Tyrosinase oxidation was used to prepare synthetic standards of DHI-melanin and DHICA-melanin (Ozeki et al., 1996b; Ito et al., 2013b). Melanin extracted from the ink sacs of the living cuttlefish *Sepia officinalis* was obtained from Sigma-Aldrich.

4.2.2 Scanning electron microscopy

SEM was used to characterize the ultrastructure of the fossil inks as in **Chapter 3**, but with slight variations. A 0.1 mg portion of each sample was suspended in 250 μL of acetone and vortexed for 10 s. 2 μL of each sample was dropped on a silicon wafer chip (5 mm x 5 mm) and dried in the dark under N_2. Samples were then mounted on a stainless steel peg and sputter coated with a 10 nm layer of gold / palladium (Au/Pd) by applying argon plasma for 3 min at 10 mA using a Hummer V sputter coater. Representative images were captured on an XL-SEG/SFEG SEM operated at 5 kV in ultra high-resolution mode with a spot size of 3.0 and working distance of 5.0 mm (YPM 221212 and YPM 221210) and 6.5 mm (GSM 122841 and GSM 120386). Dimensions of the

imaged structures were measured using analySIS XL DOCU software. SEM images of each specimen are shown in Figure 20E-H.

4.2.3 Alkaline hydrogen peroxide oxidation

Alkaline hydrogen peroxide oxidation was performed using the sample protocols mentioned in **Chapter 3**. Briefly, approximately 1-4 mg of each specimen was placed in a 10 mL screw-capped conical test tube, to which 100 μL water, 375 μL 1 mol/L K_2CO_3 and 25 μL 30% H_2O_2 (final concentration: 1.5%) were added. Following vigorous mixing at 25°C for 20 hr., the residual H_2O_2 was decomposed by adding 50 μL 10% Na_2SO_3 and the mixture was then acidified with 140 μL of 6 mol/L HCl. The reaction mixture was centrifuged at 4,000 g for 1 min and an aliquot (80 μL) of the supernatant was injected directly into a high performance liquid chromatography (HPLC) system consisting of a JASCO 880-PU liquid chromatograph (JASCO Co., Tokyo, Japan), a Shiseido C_{18} column (Capcell Pak, Type MG; 4.6 x 250 mm; 5 μm particle size; Shiseido, Tokyo, Japan) and a JASCO UV detector monitored at 269 nm. The mobile phase was 0.1 mol/L potassium phosphate buffer (pH 2.1): methanol, 85:15 (v/v). Analyses were performed at 45°C at a flow rate of 0.7 mL/min.

The chemical markers of melanin in the oxidation mixtures were identified and quantified by comparison to standards of PTCA, PDCA, isoPTCA and PTeCA prepared

as described previously (Figure 21A and B, Table 7) (Ito and Wakamatsu, 1998; Ward et al., 2008; Ito et al., 2013b).

4.2.4 Optical absorption

The absorbance at 500 nm (A_{500}) of melanins performed as aforementioned (**Chapter 3**). To prepare the solutions, 0.1 to 5 mg of each sample were placed in a 10 mL screw-capped conical test tube and 100 μL water and 900 μL Soluene-350 (from Perkin-Elmer, Waltham, MA, USA) were added. The tubes were vortex-mixed and heated at 100°C (boiling water bath) for 15 min. This was then repeated and the mixtures were centrifuged at 4,000 g for 3 min. The absorption spectrum of each supernatant was analyzed (Table 8). All of the samples exhibited some level of absorbance at 500 nm.

4.2.5 Elemental analysis

Elemental analysis of the fossil ink sacs, their associated host sediments, background standards for hydroxyapatite and calcium carbonate, and modern *S. officinalis* melanin was performed at the Center for Organic Elemental Microanalysis at Kyoto University using combustion. The C, H and N ratio of the samples and organic content of the host sediments were determined (Table 9) (Liu et al., 2005).

4.2.6 Fourier transform infrared spectroscopy

In preparation for IR, a portion of each sample was compressed into a KBr pellet. IR absorption spectra of the pellets were measured using a Fourier transform infrared

spectrometer attached to a microscope (Nicolet 6700/Nicolet Continum; Thermo Scientific Inc., Waltham, MA, US). IR spectra were measured in the wavenumber region from 700 cm^{-1} to 4000 cm^{-1} with resolution of 4 cm^{-1} and were compared against hydroxyapatite and calcium carbonate standards (Figure 22A and B). The viewing area was 100 x 100 μm.

4.2.7 X-ray photoelectron spectroscopy

The surface compositions (top 5-10 nm) of the fossil ink specimens were analyzed using an X-ray photoelectron spectrometer from Kratos Analytical Axis Ultra (Manchester, UK) (**Chapter 3**). A circle of each sample (~1 cm diameter) was coated onto copper tape using a plastic spatula. A survey scan of all of the elements heavier than boron was obtained at three points on two circles of each sample. The resulting spectra were analyzed using CasaXPS. Results are tabulated in Table 10.

4.2.8 ^{13}C cross-polarization magic angle spinning solid state NMR

^{13}C CP-MAS SSNMR spectra were acquired on a Bruker Advance 600 MHz spectrometer located in the National High Magnetic Field Laboratory for Advanced Magnetic Resonance Imaging and Spectroscopy (AMRIS) facility at the University of Florida, Gainesville. Spectra were acquired at a spin rate of 10 kHz using a CP contact time of 2.5 ms with a ramped Hartmann-Hahn matching condition and a recycle delay of 0.5 s (Figure 23A-D).

4.2.9 Pyrolysis-gas chromatography-mass spectrometry

Py-GC-MS serves as a powerful technique for the chemical characterization of melanin without any pretreatment of the sample (Stepien et al., 2009). Pyrolysis experiments were performed using a CDS Analytical 5250 pyroprobe equipped with an autosampler. CDS quartz sample tubes were packed with a quartz filler rod, followed by a plug of quartz wool, ~300 to 700 μg of sample and a second quartz wool plug. The samples were then loaded in the autosampler which sequentially dropped them into the pyrolysis chamber where they were held at 50 °C for 5 s and then heated at 10 °CmS^{-1} to 600 °C and held for 20 s. The valve oven and transfer line were held at 300 °C throughout the analyses. Released volatiles were transferred directly to a GC column held at 40 °C.

GCMS analysis of the volatiles released during pyrolysis was conducted using an Agilent 6890N gas chromatograph coupled to a Micromass Autospec-Ultima mass spectrometer. The GC was equipped with a DB-5MS column (60m x 0.25mm x 0.25um) and was operated in split mode with a 10:1 split and 1 mL/min He flow rate. The GC was held at 40 °C for 2 min and then heated to 310 °C at 6 °C min^{-1} where it was held for 20 min. The MS was operated in electron impact mode at 70 eV and scanned m/z 50-600 once per second. Py-GC-MS data for *S. officinalis*, GSM 120386, YPM 221210, and YPM 221212 are shown in Figure 24A-D.

4.2.10 Rock-Eval pyrolysis

Rock-Eval pyrolysis experiments were conducted using a Rock-Eval-6 standard pyrolyzer manufactured Vinci Technologies. Fossil samples were first pyrolyzed under inert N_2 atmosphere. The residual carbon was subsequently burnt in an oxidation oven. A flame ionization detector (FID) was used to detect the amount of hydrocarbons released during pyrolysis, while online infrared detectors continuously measured the released CO and CO_2. The samples were first pyrolyzed from 300 °C to 650 °C at a rate of 25 °C/min. The oxidation phase starts with an isothermal stage at 300 °C, followed by an increase to 850 °C at a rate of 25 °C/min to oxidize all of the residual carbon.

4.3 Results and Discussion

The presence and preservation of eumelanin in the fossil record was demonstrated in **Chapter 3** using a wide range of chemical techniques on fossil ink from the Oxford Clay (GSM 122841) and Blue Lias formations (GSM 120386). Eumelanin identified in these specimens by its unique chemical markers (alkaline hydrogen peroxide oxidation), was compared morphologically with modern melanin from *S. officinalis* (SEM) and was differentiated from other components in the sample matrices (elemental analysis, FTIR, XPS, and ^{13}C CP-MAS SSNMR). These fossil inks are compared below to the inks of two coleoids from the Posidonia Shale formation (YPM 221212 and YPM 221210) (Figure 20A-D).

The constituent granules of the inks exhibit considerable variation in size: those in YPM 221212 and YPM 221210 (Figure 20E and F) from the Posidonia Shale have diameters of 542 ± 49 nm and 213 ± 30 nm, respectively, whilst those in GSM 122841 and GSM 120386 (Figure 20G and H) from the Oxford Clay and Blue Lias formations are 168 ± 30 nm and 156 ± 30 nm, respectively (Glass et al., 2012). These dimensions are broadly comparable to the range of granule sizes recorded in living *S. officinalis* (~100 – 250 nm) (Liu and Simon, 2003). The size of modern melanin granules is known to be pH dependent: lower pH promotes aggregation, which is reversible as pH rises (Bridelli, 1998). Actualistic decay experiments indicate that subtly different conditions (including pH) may be generated in and around individual carcasses during decomposition (Kear et al., 1995). This provides a plausible explanation for the significantly larger granules observed in specimen YPM 221212 from the Posidonia Shale in comparison to those in YPM 221210 from the same unit. Differences in granule size may also have been facilitated by variations in the extent of diagenetic mineralization (Briggs, 2003), an explanation supported by XPS data for the samples from each of the deposits (see below).

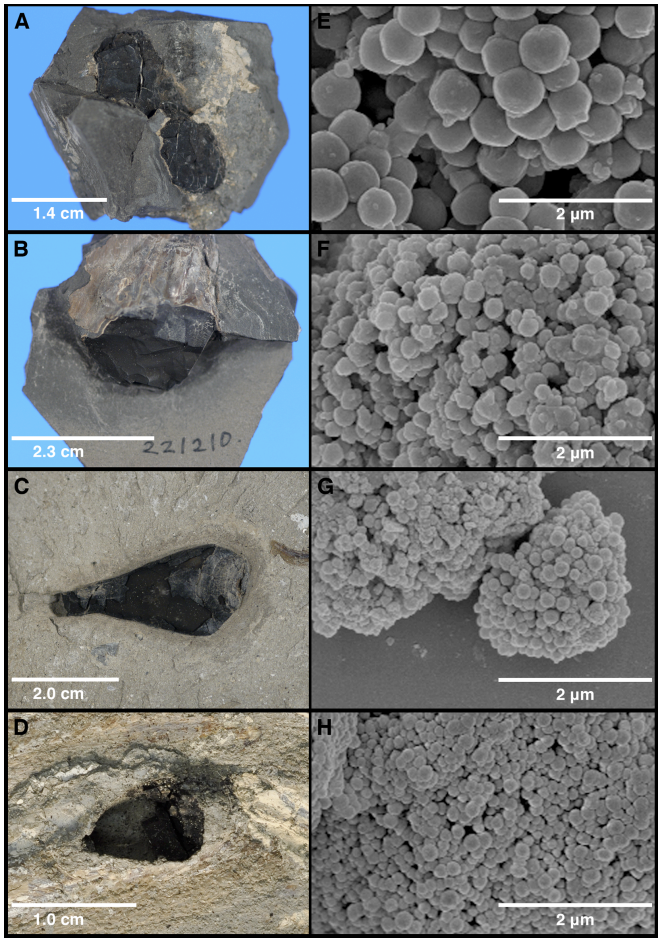

Figure 20: Photographs and SEM images of German and UK specimens

Photographs of YPM 221212 (A), YPM 221210 (B), GSM 122841 (C) and GSM 120386 (D). SEM images of YPM 221212 (E), YPM 221210 (F), GSM 122841 (G), and GSM 120386 (H). All SEM images were taken at the same magnification. The average size of the spherical granules shown in E-H are 542 ± 49 nm, 213 ± 30 nm, 168 ± 30 nm, and 156 ± 30 nm respectively, where ± indicated the standard deviation. All photographs and SEM images were published previously (Glass et al., 2012; Glass et al., 2013).

Alkaline hydrogen peroxide oxidation of YPM 221212 and YPM 221210 yielded only markers for eumelanin (Figure 21A): no markers for pheomelanin were detected. This is consistent with the ink from GSM 122841 and GSM 120386 (Figure 21B), and with

pigment from the ink sac of *S. officinalis* (Glass et al., 2012). Overall, the quantity of eumelanin present in the Posidonia Shale specimens is *ca* 1% of the quantity present in the fossil specimens from the Oxford Clay and Blue Lias formations, and 0.1% of that in modern *S. officinalis* based on a comparison of the amount of PTCA yielded from each specimen (Table 7). Host sediment adjacent to each Posidonia Shale ink sac revealed minuscule quantities of the eumelanin markers, consistent with previous findings for the host sediments of the Oxford Clay and Blue Lias formations (Table 7) (Glass et al., 2012).

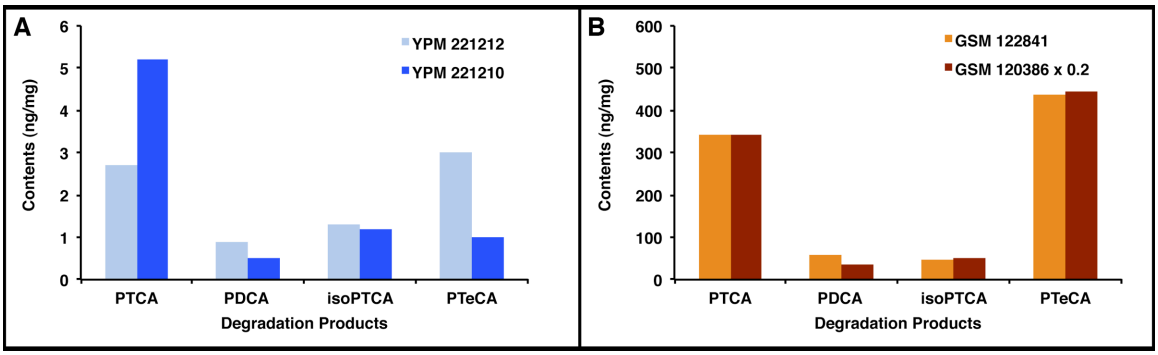

Figure 21: Alkaline hydrogen peroxide oxidation of fossil ink

Quantification of eumelanin markers produced following alkaline hydrogen peroxide oxidation of fossil specimens YPM 221212 and YPM 221210 (A) and GSM 122841 and GSM 120386 (B). The quantity of each eumelanin marker derived from GSM 120386 was multiplied by 0.2. Note the difference in the between the Y-axes. All alkaline hydrogen peroxide oxidation data was published previously (Glass et al., 2012; Glass et al., 2013).

Table 7: Degradation products from *S. officinalis*, fossil melanin, and fossil sediment

Quantity of melanin alkaline hydrogen peroxide oxidation products PDCA, PTCA, isoPTCA, and PTeCA produced by oxidation of *S. officinalis*, YPM 221212, YPM 221210, YPM 221212 sediment, YPM 221210 sediment, GSM 122841, GSM 120386, GSM 122841 sediment, and GSM 120386 sediment in ng/mg. All data was published previously (Glass et al., 2012; Glass et al., 2013).

Specimen	PDCA	PTCA	isoPTCA	PTeCA
S. officinalis	704	15710	390	2090
YPM 221212	0.9	2.7	1.3	3.0
YPM 221210	0.5	5.2	1.2	1.0
YPM 221212 sediment	< 0.1	0.3	< 0.5	< 0.4
YPM 221210 sediment	< 0.1	0.4	< 0.5	< 0.5
GSM 122841	58	342	47	438
GSM 120386	173	1710	245	2220
GSM 122841 sediment	1.7	2.2	< 2.2	< 1.3
GSM 120386 sediment	2.4	3.2	< 3.9	< 1.5

The A_{500} of all of the fossil ink sacs, their host sediments, and of modern *S. officinalis* are shown in Table 8. These values confirm that the host sediment adjacent to each fossil ink sac contains significantly less melanin than the ink itself, demonstrating again that the source of melanin is endogenous.

Table 8: Absorbance at 500 nm of Soluene-350 solubilized *S. officinalis*, UK fossils, German fossils, and fossil sediments

Values are reported as absorbance at 500 nm per mg of specimen. All absorbance data was published previously (Glass et al., 2012; Glass et al., 2013).

Specimen	A500 / mg
S. officinalis	5.99
YPM 221212	0.73
YPM 221210	2.06
YPM 221212 sediment	0.065
YPM 221210 sediment	0.068
GSM 122841	1.45
GSM 120386	8.13
GSM 122841 sediment	0.135
GSM 120386 sediment	0.100

Elemental analyses reveal that YPM 221212 and YPM 221210 have very similar C, N, and H ratios, despite differences in the dimensions of their granules (Table 9). The fossil specimens from the Oxford Clay and Blue Lias formations have substantially different C, N, and H ratios from these specimens and from each other. The stoichiometric ratios of C and H in all of the fossil specimens were higher than modern *S. officinalis* and synthetic DHI and DHICA-melanin. The comparatively elevated levels of carbon and hydrogen in the Posidonia specimens appear to be derived, in part, from calcium carbonate and hydroxyapatite replacement of the fossils (as revealed by FTIR

and XPS analyses). Nitrogen abundance therefore provides a better proxy for the quantity of organic material preserved.

Table 9: Elemental analysis of the C, H, N in synthetic, modern, and fossil melanins

Percent of C, H, N in synthetic DHI-melanin, synthetic DHICA melanin, *S. officinalis* melanin, YPM 221212, YPM 221210, GSM 122841, GSM 120386, and standards of hydroxyapatite and calcium carbonate. Values represent the average of two determinations. All values were published previously (Glass et al., 2012; Glass et al., 2013).

	Elemental Analysis (%)		
Specimen	**C**	**H**	**N**
DHI-melanin	51.52	3.45	7.80
DHICA-melanin	47.43	3.57	6.42
S. officinalis	42.87	2.72	6.57
YPM 221212	37.58	3.24	2.24
YPM 221210	36.59	3.14	2.29
GSM 122841	16.87	1.69	1.37
GSM 120386	49.40	3.73	5.07
Calcium carbonate	11.94	0.17	0.00
Hydroxyapatite	1.02	0.50	0.00

FTIR spectra for YPM 221212 and YPM 221210 (Figure 22A and B) exhibit diminished absorption bands at 3400 cm^{-1}, 1605 cm^{-1}, and 1371 cm^{-1} compared to *S. officinalis* and to the specimens from the Oxford Clay and Blue Lias formations (Figure 22A and B), consistent with them preserving lower quantities of melanin (Bardani et al.,

1982; Hong and Simon, 2006; Centeno and Shamir, 2008; Glass et al., 2012). These absorption bands are attributed to the stretching mode of the OH bond at 3400 cm^{-1}, the carbonyl stretch of indole quinone at 1605 cm^{-1}, and the various aromatic rings and in-plane bending modes of OH and NH bonds. The most pronounced absorption band at 3400 cm^{-1} is clearly above the host sediment, but is less pronounced than the absorption bands derived from the CH stretching vibration in the CH_x functional groups ~ 2840 and 2912 cm^{-1}, which are attributed to lipids. The absorption bands at ~2840 and 2912 cm^{-1} are also found, at lower levels, in the host sediment. By contrast, in the inks from the Oxford Clay and Blue Lias formations (Glass et al., 2012) the absorption band at 3400 cm^{-1} is approximately three times more pronounced than the CH stretching vibration of the CH_x functional groups, indicating lower lipid content.

A shoulder at 1710 cm^{-1} is present in all of the fossil ink sac spectra, suggesting a decrease in the preservation of indole quinone units relative to eumelanin from modern *S. officinalis* ink (Glass et al., 2012). Apatite and calcite, both minerals commonly associated with fossil ink sacs (Kear et al., 1995), are also associated with these fossils. Hence some of the carbon and hydrogen present in the elemental analysis can be accounted for by the presence of these diagenetic phases (Table 9).

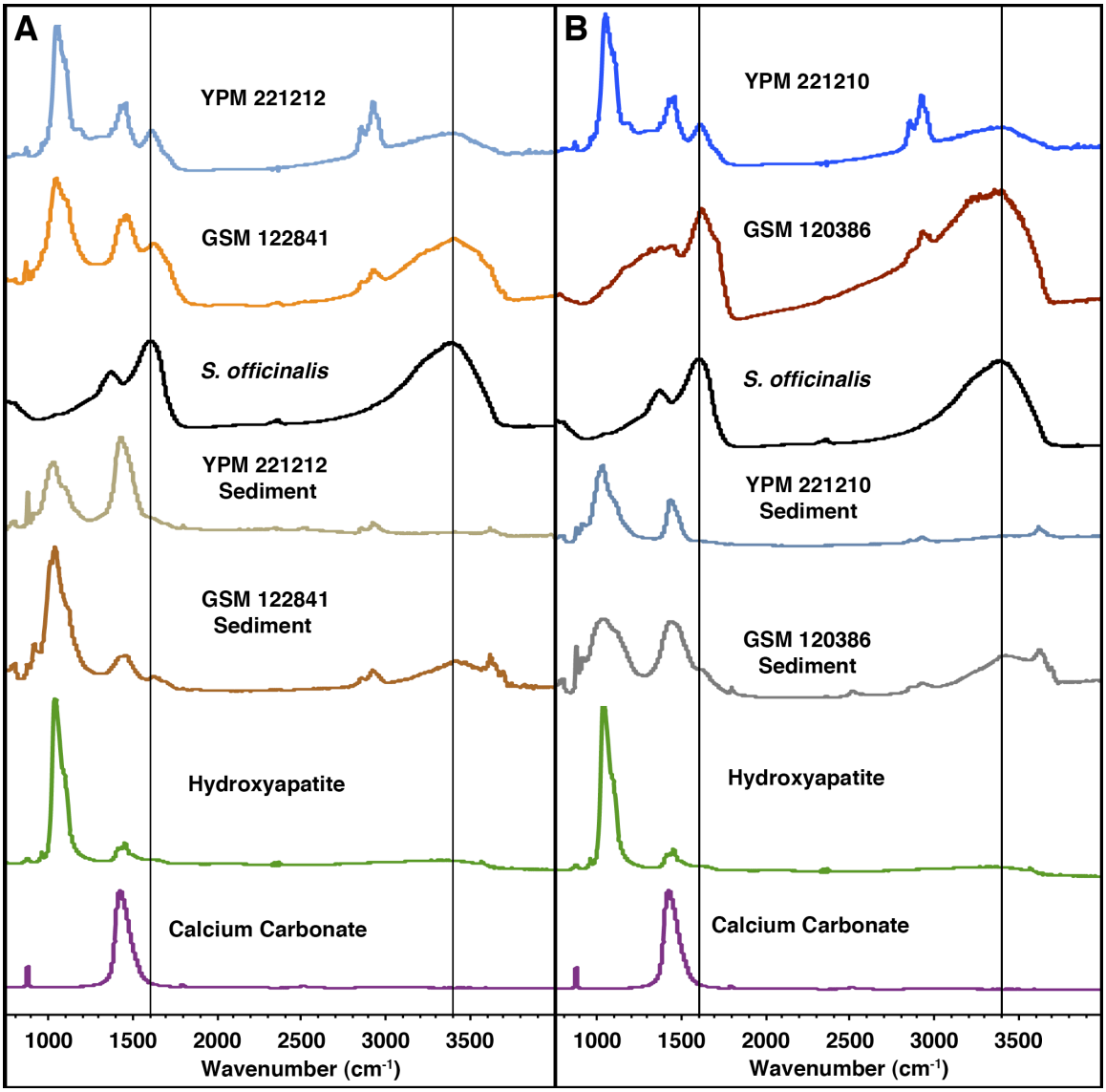

Figure 22: Deconvolution of the FTIR spectra of fossil inks and sediments

FTIR absorption spectra for YPM 221212, GSM 122841, *S. officinalis*, YPM 221212 sediment, GSM 122841 sediment, and standards of hydroxyapatite and calcium carbonate (A) and YPM 221210, GSM 120386, *S. officinalis*, YPM 221210 sediment, GSM 120386 sediment, and standards of hydroxyapatite and calcium carbonate (B). Lines on the spectra denote bands that appear to correspond melanin. All spectra were published previously (Glass et al., 2012; Glass et al., 2013).

XPS survey scans of the fossil inks (Table 10) provide the information required to compare their respective degrees of diagenetic mineralization. Although the atomic percent of carbon in YPM 221212 and YPM 221210 (70.59 ± 4.63 and 64.56 ± 0.29) is similar to that of GSM 122841 (70.88 ± 0.51) and GSM 120386 (69.51 ± 0.82), calcium carbonate ($CaCO_3$) accounts for a portion of the carbon scanned (Glass et al., 2012). The atomic percent of calcium, which is also a component of hydroxyapatite $Ca_{10}(PO_4)_6(OH)_2$, is much greater in the specimens from the Posidonia Shale (5.59 ± 2.40 and 6.28 ± 0.11) than the Oxford Clay (2.54 ± 0.27) or Blue Lias (1.16 ± 0.04) formations. Phosphorus is also higher in the former (3.43 ± 1.65 and 3.62 ± 0.06) than in the Oxford Clay (1.22 ± 0.11) and Blue Lias (not detected) formations. These differences indicate a greater degree of diagenetic mineralization in the Posidonia Shale specimens.

Table 10: XPS survey of the elements present in the German and UK fossil specimens

XPS survey scan data of the major elements present in the top 5-10 nm of the ink in fossil specimens YPM 221212, YPM 221210, GSM 122841, and GSM 120386. Atomic percentages are accurate to 0.1%. Data represents the average of four measurements; the standard deviation (±) is indicated. All survey scan data was published previously (Glass et al., 2012; Glass et al., 2013).

	Atomic (%)			
Elements	**YPM 221212**	**YPM 221210**	**GSM 122841**	**GSM 120386**
Carbon	70.59 ± 4.63	64.56 ± 0.29	70.88 ± 0.51	69.51 ± 0.82
Nitrogen	0.89 ± 0.16	2.27 ± 0.27	2.54 ± 0.27	3.32 ± 0.04
Oxygen	17.70 ± 1.72	21.60 ± 0.46	17.37 ± 0.31	18.32 ± 0.25
Calcium	5.59 ± 2.40	6.28 ± 0.11	2.19 ± 0.21	1.16 ± 0.04
Phosphorus	3.43 ± 1.65	3.62 ± 0.06	1.22 ± 0.11	N/A
Silicon	1.11 ± 0.54	0.63 ± 0.06	2.82 ± 0.06	4.08 ± 0.49
Fluorine	0.69 ± 0.33	1.04 ± 0.27	0.08 ± 0.09	N/A
Aluminum	N/A	N/A	0.97 ± 1.13	1.86 ± 0.50
Sulfur	N/A	N/A	1.93 ± 0.18	1.75 ± 0.12

^{13}C CP-MAS SSNMR spectra of ink from YPM 221212 and YPM 221210 (Figure 23A and B) clearly show aliphatic groups 0-90 ppm, aromatic groups 90-160 ppm and carbonyl groups 160 – 200 ppm consistent with those for *S. officinalis* and the fossil inks from the Oxford Clay and Blue Lias (Figure 23C and D) formations (Glass et al., 2012). Acquisition of ^{13}C CP-MAS SSNMR spectra involves cross-polarization transfer of ^{1}H nuclear spin magnetization to ^{13}C nuclei, which enhances the signal of the lower

abundance ^{13}C nuclei. Minerals like calcite and apatite that lack either hydrogen or carbon cannot undergo cross-polarization and are thus not detected. This simplifies interpretation of signals in the 160-200 ppm range.

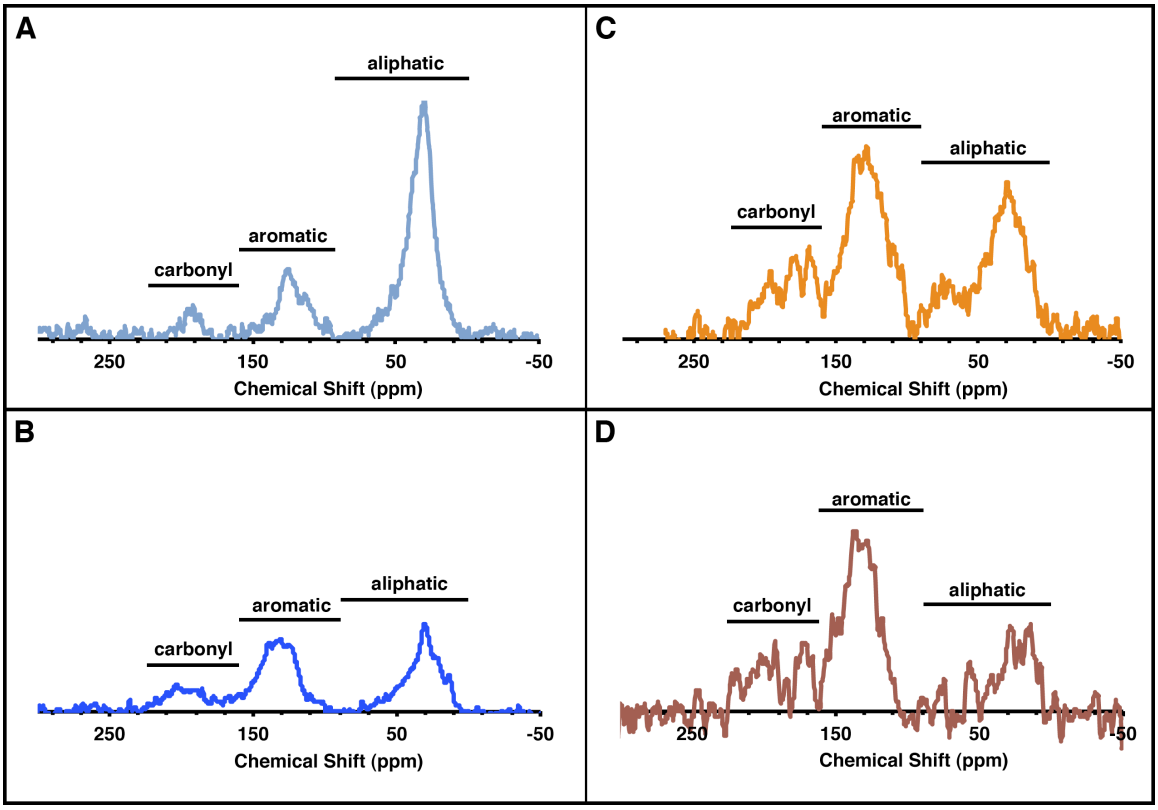

Figure 23: ^{13}C CP-MAS SSNMR spectra of German and UK fossil specimens

^{13}C CP-MAS SSNMR spectra of YPM 221212 (A), YPM 221210 (B), GSM 122841 (C), and GSM 120386 (D). All spectra have been published previously (Glass et al., 2012; Glass et al., 2013).

Aromatic and carbonyl groups are present at similar levels in both of the Posidonia inks, but the proportion of aliphatic groups is greater in YPM 221212 than YPM 221210. This reflects a higher content of hydrocarbons and a lower content of

pigment, corroborating the lower PTCA and A_{500} values for this specimen (Table 7 and Table 8). The ratio of aliphatic to aromatic constituents is greater in both Posidonia specimens than for the inks from the Oxford Clay and Blue Lias formations.

Pyrolysis spectra of the fossil inks (Figure 24B-D) serve as an indication of the extent to which they have been diagenetically modified/transformed relative to modern coleoid ink (Figure 24A). The pyrolysis products of both the modern and fossil inks show no trace of the C_{16} and C_{18} fatty acids noted as possible non-melanin contaminants. Thiophene and its alkylated derivatives, which are abundantly present in the pyrolysates of the fossil inks, are absent or occur below detection limit in *S. officinalis* ink (Glass et al., 2012). The presence of thiophenes in the fossil inks is consistent with the incorporation of sulfur into the geomacromolecule as a result of sulfide generation in the sediments. High-sulfur geopolymers are formed in low iron marine paleoenvironments where the sulfide produced by sulfate-reducing bacteria can react preferentially with organic matter (Damste and Leeuw, 1990).

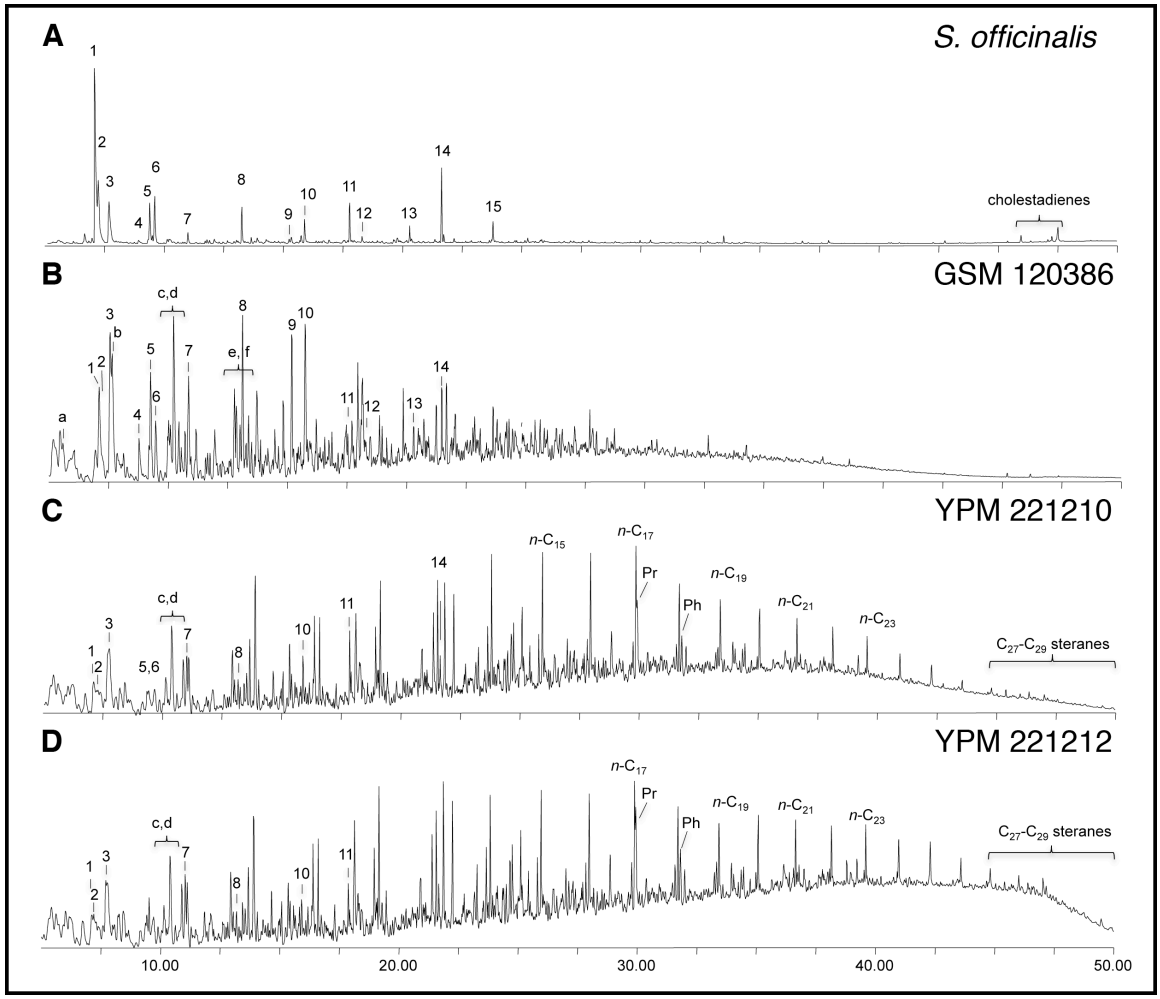

Figure 24: Py-GC-MS chromatograms of modern and fossil melanins

Total ion chromatograms following pyrolysis of *S. officinalis* (A), GSM 120386 (B), YPM 221210 (C), and YPM 221212 (D). The numbers indicate the major pyrolysis products of melanin while the letters indicate their diagenetic products: **1** pyridine, **2** pyrrole, **3** toluene, **4** C_1-pyridine, **5** C_1-pyrrole, **6** C_1-pyrrole, **7** styrene, **8** phenol, **9** C_1-phenol, **10** C_1-phenol, **11** 2-phenylacetonitrile, **12** C_2-phenol, **13** 3-phenylpropanenitrile, **14** indole, **15** C_1-indole, **a** thiophene, **b** C_1-thiophene, **c** C_2-benzene, **d** C_2-thiophene, **e** C_3-thiophene, and **f** C_3-benzene. The melanin also contained cholestadiene isomers. Other diagenetic products in the fossil samples include C_{15-30} *n*-alkanes, acyclic isoprenoids pristine (Pr), phytane (Ph), and C_{27-29} styrene isomers. These chromatograms were published previously (Glass et al., 2012; Glass et al., 2013).

Py-GC-MS reveals that the composition of ink from the Posidonia Shale differs considerably from that from the Blue Lias. GSM 120386 contains comparatively few diagenetic products while YPM 221210 and YPM 221212 have abundant *n*-alkyl residues indicative of significant transformation of original organic constituents from the fossil material. The enhanced aliphatic component of the Posidonia Shale specimens indicated by ^{13}C CP-MAS SSNMR and py-GC-MS is likely a consequence of polymerization of free fatty acids (Stankiewicz et al., 2000; Gupta et al., 2006). This can occur over time, as evidenced by the progressive transformation of macromolecules in natural resins, such as amber (Stankiewicz et al., 1998) or collagenous and chitinous fossils (Gupta and Briggs, 2011). Significantly, however, all of the ink samples are from the Jurassic (they span a maximum period of *ca* 17 million years), indicating that age is not the dominant control on eumelanin preservation.

Rock-Eval pyrolysis analyses of bulk sediment samples from the Posidonia Shale near where the two ink sacs were collected indicate that the sedimentary organics are approaching early maturation (Prauss et al., 1991). Analysis of the Posidonia Shale from the Bisingen / Zimmern 1002 borehole sited near Holzmaden gave a total organic content (TOC) of 6-8% and a temperature of maximum pyrolysis yield (T_{max}) of 435 °C (Prauss et al., 1991; Rohl et al., 2001). This T_{max} is within the 435 °C-445 °C range that indicates the onset of the oil window. The samples had a hydrogen index (HI) of

approximately 540 mg HC/g TOC, where HI values > 400 mg indicate the preservation of hydrogen-rich organic matter (Prauss et al., 1991). In comparison, the fossil ink sacs from the Oxford Clay and Blue Lias formations, which preserve substantially greater quantities of pigment, are associated with immature sedimentary organic material with TOC values of 11.9% and 4.5%, T_{max} 411 °C and 424 °C, and HI 694 mg HC/g TOC and 330 mg HC/g TOC (Glass et al., 2012).

4.4 Conclusions

The structure of eumelanin renders it unusually resilient. Comparison of its chemistry in coleoid ink sacs from Jurassic mudrocks with differing burial histories indicate that maturation is the dominant control on its survival in the fossil record. Sediments that have undergone significant maturation are unlikely to yield biomarkers for eumelanin within current detection limits. This is broadly consistent with the results of short-term maturation experiments, which have shown temperature to be the primary determinant on the physical preservation of melanosomes (McNamara et al., 2013).

It is important to note that chemical preservation of fossil eumelanin does not correlate with its macroscopic- or microscopic- morphological preservation (Dutta et al., 2010): all of the ink sacs are three-dimensional and retain evidence of pigment granules. Chemical preservation is also independent of the visible color, which is black in all specimens. Early diagenetic apatite and/or calcite is associated with each of the

examined ink sacs, and may plausibly enhance the size of the pigment granules, but based on our current data has no impact on eumelanin preservation.

5. Preservation of proteins in ancient ink sacs

5.1 Introduction to the analysis of proteins in the fossil record

Under geochemical conditions biomolecules of evolutionary value degrade as described in **Chapter 1.1**. As a result, the recent discovery of chemically and morphologically preserved eumelanin in ~ 200 Mya cephalopod ink sacs was unexpected (**Chapter 3**). Although the pigment has many attributes indicative of high degradation resistance, its shape, size, and distribution originally led researchers to misidentify it as a microbial biofilm in the fossil record (Davis and Briggs, 1995; Moyer et al., 2014). Studies following the identification of intact melanin in fossils demonstrated that melanin is preserved in a wide-range of ancient specimens (Barden et al., 2011; Wogelius et al., 2011; Lindgren et al., 2012; Lindgren et al., 2014) and set limits on the environments likely to yield melanin-containing fossils (**Chapter 4**).

In addition to expanding the range of biomolecules known to survive in the fossil record, these studies have called into question previous estimates of the longevity of biomolecule preservation. Specifically, the temporal limits proposed (Lindahl, 1993; Qian et al., 1993; Collins et al., 1995; Bada et al., 1999; Hoss, 2000; Nielsen-Marsh, 2002)

for the survival of other biomolecules with particular evolutionary value were reexamined (Collins et al., 2000; Salamon et al., 2005; Asara et al., 2007; Schweitzer et al., 2007a; Schweitzer et al., 2007b; Schweitzer et al., 2009; Lindqvist et al., 2010).

Previously, theoretical kinetics and laboratory experiments designed to emulate the degradation of proteins and DNA over time predicted that proteins would not survive in the fossil record beyond a few million years and that DNA would degrade within approximately 100,000 years in optimal conditions (Qian et al., 1993; Bada et al., 1999; Collins et al., 2000; Hoss, 2000). These predictions did not account for the association or cross-linking of DNA and proteins with degradation resistant matrices like amber, some mineral phases, and bone (Antonio et al., 2011). In recent studies of fossil specimens, these proposed limitations for protein and DNA survival have been surpassed (Collins et al., 2000; Salamon et al., 2005; Schweitzer et al., 2007a; Schweitzer et al., 2007b; Schweitzer et al., 2009; Lindqvist et al., 2010; Antonio et al., 2011). The time range over which critical biomolecules are retained are now known to depend in part on the matrix in which they are contained (Butterfield, 1990; Briggs, 1999; Briggs et al., 2000; Schweitzer, 2011).

Although melanin's role in coloration is often cited, the role of melanin as a matrix for the preservation of other biomolecules has not been considered. Melanin in modern organisms contains intact proteins (5-10% by weight) thought to be tightly

associated with the polymer matrix (Hong and Simon, 2007; d'Ischia et al., 2013). In this Chapter we demonstrate that the preserved melanin in four fossil cephalopod ink sacs (**Chapter 3** and **4**) contain endogenous proteins with an amino acid composition that is not significantly different from modern cephalopod ink. We also prove that the amino acids in two of the fossil ink sacs have undergone a degree of racemization (see **Chapter 5.2.3**) consistent with their ancient history and unusual melanin-matrix.

5.2 Techniques and methods to analyze fossil amino acids

5.2.1 Fossil and Modern Specimens

All fossil specimens analyzed were introduced in **Chapter 3** and/or **4**. As stated, GSM 122841 and GSM 120386 (shown in Figure 9A and B as well as Figure 20C and D) were collected from the Peterborough Member of the Oxford Clay Formation (Middle Jurassic, late Callovian) at Christian Malford, Wiltshire (UK) and from Bed 32 of the Blue Lias Formation (Lower Jurassic, early Sinemurian) at Lyme Regis, Dorset (UK), respectively (Glass et al., 2012). Both ink sacs are held in the GSM collections of the British Geological Survey, Keyworth (UK). YPM 221212 and YPM 221210 (Figure 20A and B) were collected from the Koblenzer Bed of the Posidonia Shale Formation (Lower Jurassic, early Toarcian, *tenuicostatum* Zone) near Holzmaden, Baden-Württemberg (Glass et al., 2013). The ink sacs are held in the YPM collections of the Yale Peabody Museum (USA).

Samples of the ink and host sediment associated with each ink sac were removed mechanically and ground to a fine powder using a mortar and pestle. *S. officinalis* melanin, isolated from ink sacs of *S. officinalis*, was obtained from Sigma-Aldrich (St. Louis, MO, USA).

5.2.2 Amino acid analyzer

An amino acid analyzer is an instrument designed to separate, identify, and quantify the amino acid composition of proteinaceous specimens that have been hydrolyzed. Many different hydrolysis methods are used to break apart the amide bonds that connect the amino acids within a protein chain (Schweitzer et al., 2008). In the first portion of this study, vapor-phase hydrolysis was used prior to amino acid analysis.

Vapor-phase hydrolysis is the hydrolysis of a sample with a strong hydrolyzing acid in a sealed, evacuated vessel (Rutherfurd and Gilani, 2001; Higbee et al., 2003). Unlike many liquid hydrolysis methods, sample in vapor-phase hydrolysis is not placed directly in the hydrolyzing acid (Rutherfurd and Gilani, 2001). Instead, multiple samples are placed in small open tubes that fit within a hydrolysis vessel (i.e. the PicoTag reaction vial in Figure 25). A small quantity of the hydrolyzing acid, typically 6 M hydrochloric acid (HCl), is then added to the bottom of the vessel (Rutherfurd and Gilani, 2001). When the hydrolysis vessel is sealed under vacuum, the vapor pressure of HCl is reduced (Rutherfurd and Gilani, 2001; Higbee et al., 2003). When the reaction

vessel is heated, the HCl vapor interacts with each sample. Over time at the appropriate temperature, the proteinaceous component of each sample is hydrolyzed. There are multiple benefits of vapor-phase hydrolysis: first, multiple samples can be hydrolyzed concurrently; second, impurities including metals in the hydrolyzing acid do not interfere with hydrolysis; and third, the inert atmosphere prevents the oxidative loss of some amino acids (Rutherfurd and Gilani, 2001; Higbee et al., 2003). All of these benefits are particularly important when analyzing samples with minute quantities of proteinaceous material.

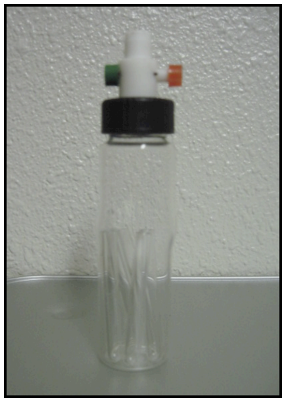

Figure 25: Vapor hydrolysis reaction chamber

The PicoTag reaction vial shown was used for the vapor phase hydrolysis of the protein fraction of melanin samples and fossil sediments. This photograph was provided by Shosuke Ito.

Vapor-phase hydrolysis was used to hydrolyze melanin from *S. officinalis*, GSM 122841, GSM 120386, YPM 221212, and YPM 221210 inks thought to contain protein. It was also used to hydrolyze the sediments associated with GSM 122841, GSM 120386,

YPM 221212, and YPM 221210 fossils. 1 mg of each modern / fossil ink and 2-3 mg of each fossil sediment were weighed into hydrolysis tubes, which were then placed inside a Waters PicoTag reaction vial (Figure 25). A small amount of 6M HCl was then placed into the PicoTag reaction vial surrounding the hydrolysis tubes. The reaction vial was then filled with nitrogen and evacuated under vacuum. The vial was heated on a heating block at 110 °C for 24 hours. After cooling, the hydrolysis tubes were dried under vacuum. The residuals of the specimens were dissolved in 120 μL of pH 2.2 lithium loading buffer for amino acid analysis (Mitsubishi, Japan). For analysis, 80 μL each solution was injected into the amino acid analyzer.

The amino acid analyzer used in this study was a Hitachi High Speed Amino Acid Analyzer L-8500, Hitachi Ltd., Japan. Injected amino acids were first separated by ion exchange chromatography (Higbee et al., 2003). After the amino acids were separated, they were automatically derivatized with ninhydrin and identified with visible detection (440 nm / 570 nm) (Boucher et al., 1997; Higbee et al., 2003). The areas under the detected peaks were determined and compared to calibration curves of amino acid standards to establish the concentrations of the amino acids. This method of quantitation is similar to that used in **Chapter 2.3** to quantify alkaline hydrogen peroxide oxidation markers. Shosuke Ito and Kazumasa Wakamatsu performed all vapor-phase hydrolysis and amino acid analyzer experiments.

Following amino acid determination, the glutamic acid concentration of each specimen was set to one to enable specimen-to-specimen comparison of the remaining amino acids. Both parametric (ANOVA test) and nonparametric (Kruskai-Wallis rank sum test) statistical analyses were performed to examine whether or not the amino acid profile of modern cephalopod melanin differed significantly from that of preserved fossil melanins. Jae Lee performed all of the statistical tests at the University of Virginia.

5.2.3 Vacuum hydrolysis of melanin samples

The second form of hydrolysis used in this study was vacuum hydrolysis. Vacuum hydrolysis is a liquid hydrolysis method in which the sample is placed directly into hydrolyzing acid (amino acid analysis grade 6 M HCl from Sigma Aldrich) in special hydrolysis tubes that can connect to a vacuum line (Rutherfurd and Gilani, 2001). In this study, the specialized hydrolysis tubes were made by flame-fusing glass adapters to empty pre-scored glass ampules. The air in *S. officinalis*, GSM 122841, GSM 120386, GSM 122841 sediment, and GSM 120386 sediment samples (0.5 – 1.5 mg) suspended in HCl (0.5 – 1.5 mL) was carefully bubbled out under vacuum. Once samples were fully degassed, the tubes were flame-sealed / melted shut under vacuum to seal them from air. The samples were then heated for 24 hours at 110 °C.

After the samples were hydrolyzed, the tubes were cooled and opened along the score-line. Samples suspended in HCl were then mixed, removed using sterile long-

stemmed glass pipettes, and placed in 4 mL amber vials. The vials were uncapped, covered with three layers of parafilm that were then perforated 6 times with a syringe tip, and frozen in liquid nitrogen. After freezing, the vials were placed in a lyophilizer chamber and the remnant HCl was removed using a lyophilizer (freeze-dryer). The samples were then derivatized and analyzed by GCMS as described in the next section.

5.2.4 Analysis of D and L amino acids by GCMS

Amino acids are the monomeric units of proteins. Of the twenty amino acids that commonly occur in living organisms, nineteen are chiral; the four groups surrounding their central carbon are distinct and can arrange into either a levorotary (L) or dextrorotary (D) formation (Figure 26) (Schweitzer et al., 2008). The proteins of living organisms are composed of L- amino acids, but post-mortem the L-amino acids are converted to D-amino acids. This conversion or racemization of amino acids proceeds until equilibrium, which occurs when the D/L amino acid ratio is one.

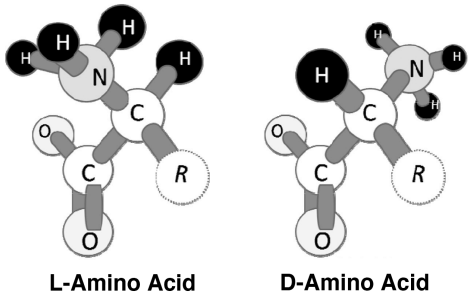

Figure 26: Schematic of chiral amino acids

Generic left (L) and right (D) chiral amino acid isomers are shown. Images of the L and D isomers were reproduced with permission (Schweitzer et al., 2008).

Chiral amino acid analysis is a useful way to gauge whether or not the amino acids from fossil specimens are endogenous or from a more recent contamination (Schweitzer et al., 2008). One main assumption of this technique is that the amino acids derived from original fossil material are older and have undergone more racemization than modern contaminants (Bada and Schroeder, 1975). Although many techniques are available to determine the ratio of D to L amino acids, in this study we derivatized D and L amino acid enantiomers to their diastereomers (LD and LL), separated them by achiral gas chromatography, and identified them with mass spectrometry using the methods that follow.

Samples of *S. officinalis*, GSM 122841, GSM 120386, GSM 122841 sediment, and GSM 120386 were first vacuum hydrolyzed and dried in 4 mL amber vials using the methods presented in **Chapter 5.2.2**. The hydrosylates were then derivatized using published methods with a few modifications (Kvenvolden et al., 1971; Bada et al., 1979). A mixture of 4M HCl in 2-(+)-butanol, prepared by bubbling a known mass of HCl gas into 2-(+)-butanol purchased from Sigma Aldrich, was then added to each hydrosylate based on the mass prior to hydrolysis (1 mL per 1 mg). Following chiral acid addition, the vials were capped and heated at 100 °C in an oil bath for 3 hours and then cooled. The unreacted 2-(+)-butanol / HCl was removed under vacuum (ice/water). The resulting esters were then acylated with pentafluoropropionic anhydride. 0.3 mL of

pentafluoropropionic anhydride in 0.5 mL of dichloromethane (DCM) per 0.5 mg of specimen was added to the reaction vials. The reaction vials were then capped and placed on a shake plate at room temperature to react for 2 hours. Residual pentafluoropropionic anhydride / DCM was then removed under N_2 flow.

To determine the retention time of the diastereomeric derivatives of the amino acids of interest, derivatized amino acid standards were resolved on an HP-5 column using the 50.28 min run program detailed in Table 11. A list of the additional system parameters follows: solvent cut time 6.30 min, ion source temperature 200 °C, detector voltage 0.3kV, interface temperature 250 °C, and threshold 250. These conditions provided full separation of all of the amino acid derivatives analyzed.

To prevent interference from background and matrix ions during the analysis of fossil, sediment, and modern specimens, selected ion monitoring (SIM) was used. In SIM, the retention time and fragment ions of interest can be selectively monitored while interfering ions are left undetected. SIM allows unambiguous determination of multiple peaks at different time segments. The time segments and monitored mass fragments selected for this study are detailed in Table 12. The rest of the program was identical to the one used to analyze derivatized amino acid standards above. Quantitation of the amino acid enantiomers was achieved by measuring peak heights on the resulting gas chromatograms.

Table 11: Gas chromatography-mass spectrometry run program

The gas chromatograph-mass spectrometry program details the conditions necessary to elute and resolve all of the amino acid peaks. Notice that though the hold time is zero between the first and final segment, the rate of temperature change varies.

Rate (°C / min)	Final Temperature (°C)	Hold Time
–	70	2.3
15	130	0
2	132	0
0.5	138	0
2	147	0
1	151	0
2	159	0
0.5	163	0
2.5	325	4

Table 12: Selected ion monitoring program

In select ion monitoring, multiple mass fragments can be monitored during a given timeframe. The following program was used to identify peaks associated with amino acids and to determine their peak areas. The monitored fragments were determined by analysis of amino acid standards.

Time Segment (min)	Monitored Fragments
6.40 – 7.15	119, 147, 176, 190, 191, 204, 218
7.15 – 7.95	119, 188, 202, 203, 248
7.95 – 8.50	119, 160, 164, 188, 189, 202, 218, 219,
8.50 – 10.50	119, 164, 190, 218, 232, 233, 260
10.50 – 11.90	103, 119, 190, 220, 266
11.90 – 14.20	119, 189, 216, 217, 244, 261
14.20 – 16.50	119, 189, 202, 203, 221, 230, 231, 277
16.50 – 19.50	119, 189, 234, 262, 318
19.50 – 21.50	103, 119, 148, 204, 266
21.50 – 24.00	119, 202, 230, 248, 276
24.00 – 26.50	119, 176, 190, 230, 231, 253, 310
26.50 – 38.20	119, 131, 170, 187, 243, 305, 333

5.3 Results and Discussion

The presence of intact eumelanin in the fossil record was established in **Chapter 3** using a wide range of chemical techniques. Limitations for the preservation of eumelanin in fossils were then determined using site-specific chemical data in **Chapter 4**. These studies have been validated by the discovery of intact eumelanins in fossils throughout the world (Barden et al., 2011; Wogelius et al., 2011; Lindgren et al., 2012; Lindgren et al., 2013; Lindgren et al., 2014). Although the presence and preservation of eumelanin in fossils is well established, implications for the survival proteins associated with the pigment have not been considered. In this study we determine whether the fossil inks from the Oxford Clay (GSM 122841), Blue Lias (GSM 120386), and Posidonia Shale Formations (YPM 221212 and YPM 221210) analyzed in **Chapter 3** and **4** contain preserved protein material. We also compare amino acid profile of the fossil inks to that of modern *S. officinali*s ink.

Amino acid analysis with an amino acid analyzer is an efficient way to determine the distribution of amino acids in modern and fossil inks. For this type of amino acid analysis, samples of *S. officinalis*, GSM 122841, GSM 120386, YPM 221212, and YPM 221210 melanins were hydrolyzed with vapor phase hydrolysis as described in **Chapter 5.2.2** (Rutherfurd and Gilani, 2001; Higbee et al., 2003). The hydrolyzed material was then injected onto the amino acid analyzer where the amino acids were separated by ion

exchange chromatography, derivatized with ninhydrin, and detected and quantified with a UV-Vis detector as outlined in **Chapter 5.2.2** (Boucher et al., 1997; Higbee et al., 2003). The amino acid data from the modern and fossil inks was normalized to glutamic acid for comparison (Figure 27). The background sediments of the fossil specimens are not shown because they did not contain appreciable amounts of amino acids. The percent of amino acids in each specimen are tabulated in Table 13.

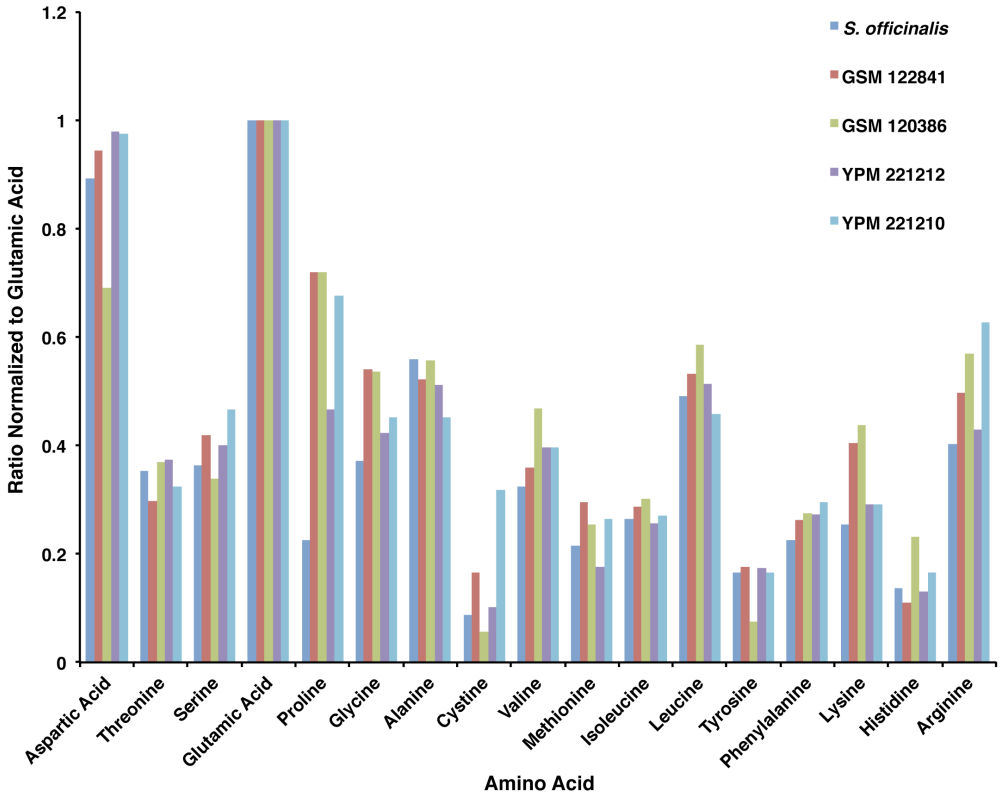

Figure 27: Profile of the amino acids in modern and fossil melanins

Determination of the concentration of amino acids in *S. officinalis*, GSM 122841, GSM 120386, YPM 221212, and YPM 221210 inks with an amino acid analyzer. All of the amino acid data was normalized to glutamic acid to enable cross-specimen comparison.

Table 13: Total percentage of amino acids in each specimen

The total percentage of amino acids per one mg of specimen was determined based on the amino acid analysis data. Shosuke Ito and Kazumasa Wakamatsu performed this experiment and data analysis.

Specimen	Percent of Amino Acids
S. officinalis	6.46
GSM 122841	0.086
GSM 120386	0.224
YPM 221212	0.048
YPM 221210	0.113

The amino acid data was compared statistically using parametric (ANOVA) and nonparametric (Kruskal-Wallis rank sum) tests. The ANOVA test was used to compare the mean concentrations of the amino acids in modern and fossil inks (McDonald, 2008). The ANOVA test relies on a few critical assumptions about a data set: (1) the samples are independent, (2) there is a normal distribution of the error in the sample measurements, and (3) the populations tested have the same variance (McDonald, 2008; Tiemann, 2010). The result of the ANOVA test is an F-value that gives a measure of how spread out the sample data is (variance) (McDonald, 2008). If the variance of the samples is close to equal then the F-value is close to one (Tiemann, 2010). An F-value close to one indicates that the mean of the amino acid concentrations from the samples do not vary

significantly (McDonald, 2008; Tiemann, 2010). The F-value of the amino acid analyzer data was 0.859. Although this F-value suggests similarities between the amino acid distributions of the specimens, it is not conclusive.

In order to account for any oversimplification of the dataset due to assumptions required for the ANOVA test, the Kruskal-Wallis rank sum test was performed. The major advantage of the Kruskal-Wallis rank sum test is that it does not assume that the data is normally distributed (McDonald, 2008). For this test there must be a nominal variable (ink sac source) and a measurement variable (amino acid concentrations) (McDonald, 2008). The test began by ranking each measurement value, the smallest value was ranked one while the next largest was ranked two and so on (McDonald, 2008). Consider for example the alanine concentration of each specimen (Figure 27), YPM 221210 has the smallest alanine concentration and was ranked 1. The other specimens received the following ranks: YPM 221212 (rank 2), GSM 122841 (rank 3), GSM 120386 (rank 4), and *S. officinalis* (rank 5). The sum of the ranks for all of the amino acid concentrations of each specimen were then calculated and the test statistic H – the variance of the ranks among specimens – was determined (McDonald, 2008). For the Kruskal-Wallis rank sum test, a significant result indicates that the amino acid distribution of specimens are significantly different (McDonald, 2008). The results of the Kruskal-Wallis rank sum test were not significant (H: 2.3897, 4 d.f., P=0.6645), which

clearly demonstrates that the amino acid distributions of the modern and fossil melanins are not significantly different. Additional equivalence tests are necessary to determine whether or not the amino acid distributions are identical.

Although this amino acid data is very useful for comparison of the amino acid profile of modern to fossil inks, it does not give information about the origin of the amino acids. It is unlikely due to the similarity between the amino acid profiles of the fossil and modern melanins, but the fossil amino acids could be derived from a modern contamination rather than an ancient melanin proteins (Bada and Schroeder, 1975). One method to determine whether or not the amino acids are due to a modern contamination is to determine their D/L isomer ratio (Schweitzer et al., 2008). In living organisms, it is rare to find D-amino acids. Once an organism dies however, amino acids in the constituent proteins of the organism begin to convert from L to D isomers until the ratio of L to D isomers is equal (Schweitzer et al., 2008). This process is known as racemization.

In the absence of contaminating amino acids, full racemization is thought to occur in < 5-10 million years in cold environments and < 1 million years at approximately room temperature (Schroeder and Bada, 1976; Bada et al., 1999). It is important to note that these rates represent the minimum timeframe for amino acid racemization and do not take into account either the environment fossil, matrix of the

protein, or the protein's amino acid composition (Eglinton and Logan, 1991; Schweitzer et al., 2008). To determined degree of racemization of fossil specimens GSM 122841 and GSM 120386 and modern *S. officinalis* eumelanin, the specimens were first hydrolyzed using vacuum hydrolysis (**Chapter 5.2.3**). The resulting hydroslyate was then esterified in acidified chiral 2-(+)-butanol and acylated with pentafluoropropionic anhydride in DCM using established methods (Kvenvolden et al., 1971; Bada et al., 1979). The diastereomeric derivatives of the amino acids were resolved on an HP-5 column using the GC run program outlined in Table 11 and identified using selected ion monitoring of the ion sets shown in Table 12 and Table 14. These ion sets are identical to those used in other GCMS studies of the same amino acid derivatives (Brückner, 2000).

Table 14: Selected ion monitoring of amino acid mass fragments (*m*/*z*)

The diastereomers LD and LL of the amino acids standards were separated by gas chromatography and eluted at the peak retention times below. In the SIM program (outlined in Table 12), ions sets were chosen based on the fragmentation patterns of derivatized amino acid standards. Ions characteristic of specific amino acids are noted below. The parent ion of each amino acid derivative ($\mathbf{M^{+\bullet}}$) is also indicated.

	Retention Time (min)			
Amino Acid	**LD**	**LL**	**$M^{+\bullet}$**	**Characteristic Ions**
Alanine	6.495	6.612	292	190, 218
Valine	8.052	8.178	319	218
Aspartic Acid	17.620	17.763	392	234, 262

Quantitation of the amino acid enantiomers was obtained by measuring the gas chromatogram peak areas. The D to L ratio of the alanine, valine, and aspartic acid in L-

amino acid standards, GSM 122841, GSM 120386, and *S. officinalis* are listed in Table 15. These amino acids were chosen because they have the slowest, median, and fastest racemization rates of the nineteen chiral amino acids common to proteins and they are frequently used to analyze the degree of racemization of fossil systems (Bada and Schroeder, 1975; Schroeder and Bada, 1976; Bada et al., 1979; Bada, 1985; Bada et al., 1999). Before considering the racemization data, it is critical to take into account the racemization caused by sample processing (Bada, 1985). For example, the D/L ratios of the L-amino acids provide information about the optical impurity of the chiral derivatizing agent, 2-(+)-butanol. Based on the L-amino acid data, the optical impurity of 2-(+)-butanol leads to an artificial derivatization-induced D/L ratio of ~ 0.05. Since the standard L-amino acids do not undergo hydrolysis, their D/L ratios do not account for hydrolysis-induced racemization. Based on previous studies, hydrolysis of proteins induces a small amount of racemization that results in a D/L ratio of ~ 0.15 (Bada and Schroeder, 1975; Schroeder and Bada, 1976; Bada, 1985). Together the protein hydrolysis and derivatization with 2-(+)-butanol result in a baseline D/L ratio of ~ 0.20.

Table 15: Comparison of the racemization of modern and fossil melanins

The D/L ratios shown are based on the peak areas of each specimen's derivatized amino acids. The peaks were identified by their retention time and ion profile (Table 14).

	Enantiomer Ratios (D/L)			
Amino Acid	**L-Standards**	***S. officinalis***	**GSM 122841**	**GSM 120386**
Alanine	0.05	0.12	1.33	1.41
Valine	0.05	0.20	1.99	3.08
Aspartic Acid	0.04	0.42	0.90	1.05

First, consider the racemization of *S. officinalis* while keeping the ~ 0.20 baseline racemization in mind (Table 15). While aspartic acid of *S. officinalis* exhibits a degree of racemization, alanine and valine show no racemization. Due to the modern origin of the *S. officinalis* melanin, this result was unexpected. Consider however, that *S. officinalis* melanin was purchased from Sigma Aldrich. Since Sigma's *S. officinalis* melanin is from a bulk batch that was extracted from *S. officinalis* over 15 years ago, the aspartic acid may have begun to convert from the L to D form. Sigma *S. officinalis* melanin was stored in a plastic container exposed to surface conditions; without a protective biological or sediment matrix, a degree of racemization could occur. Aspartic acid is known to have the fastest racemization rate of the three amino acids analyzed, thus the fact that valine and alanine are not racemized does not detract from the possibility that racemization has begun (Bada, 1985).

Since Sigma *S. officinalis* melanin is chemically and morphologically identical to the melanin of fossils GSM 122841 and GSM 120386 (**Chapter 3**) and the amino acid profile of *S. officinalis* is not significantly different from that of the fossil melanins, the racemization rate of its proteins provides an excellent standard for comparison to fossil proteins. It is clear from comparison of the racemization rates of the amino acids from fossil melanin to those of *S. officinalis* melanin that the fossil amino acids have D/L ratios that are significantly higher (Table 15). Hence, the fossil amino acids are more fully racemized and is not due to a modern contamination, which would have a D/L ratio of ~ 0.2. In addition, since all of the fossil amino acids have a D/L ratio significantly higher than 0.2, the racemization is not due to the sample processing.

One concern when considering the fossil data is that the L-valine to D-valine has exceeded equilibrium D > L for both fossil specimens. Since the distribution of the protein bound to melanin in modern and fossil organisms is unknown, it is difficult to surmise the reason for the D/L ratio of valine. If the valine residues of the protein are exposed to the surface of the melanin granules – known to bind metal ions – then their racemization rates may be affected by chelation by metal ions (Bada, 1985; Hong et al., 2004; Liu et al., 2004; Liu and Simon, 2005; Hong and Simon, 2006; Hong and Simon, 2007). To understand how chelation by metal ions could effect the conversion of L to D amino acids, it is important to know the mechanism of amino acid racemization.

Amino acid racemization occurs when the hydrogen on the alpha carbon of an amino acid is removed, resulting in the formation of a planar carbanion (Neuberger, 1948; Cram, 1964; Bada and Schroeder, 1975; Bada, 1985). The stability of the carbanion, as determined by resonance stabilizing capacity and the electron withdrawing groups of an amino acid, controls the rate of racemization (Neuberger, 1948; Bada, 1985). A more stable carbanion racemizes more rapidly than a less stable one (Bada, 1985). Chelation by positively charged metal ions is known to greatly stabilize the carbanion intermediate (Bada, 1985).

Based on pump-probe analysis of GSM 120386 and *S. officinalis* by Simpson and collaborators, the fossil specimen contains a high proportion of bound iron similar to that of *S. officinalis* artificially loaded with melanin (Simpson et al., 2013). X-ray photoelectron spectroscopy data (Table 10) also indicates that a substantial amount of calcium is associated with the melanin in GSM 122841 and GSM 120386. If valine is on the surface of the melanin granules, then these metal ions could stabilize the carbanion, speed up racemization, and potentially shift the D/L ratio towards the D isomer (Bada, 1985). Another possibility is that vacuum hydrolysis for 24 hours does not release all of the amino acids or hydrolyze all of the protein bound within melanin granules. If that is the case, than the D/L ratio of valine may be an artificial reflection of surface bound or

surface associated amino acid. Additional studies are needed to elucidate the source of these high valine ratios.

5.4 Conclusion of the analysis of fossil specimens

This study demonstrates that the amino acid profile of fossil melanin ink is not significantly different from that of modern *S. officinalis* melanin. It also shows that the amino acids derived from the fossil melanins are not due to a modern contamination. This preservation of protein in fossil melanins 160 Mya marks the oldest determination of amino acids in a fossil specimen. The fact that these proteins are found associated with melanin suggests that the melanin may provide a protective matrix for the protein. Since melanin is found in every kingdom of life, the survival of proteins in melanin has promising implications for biologic investigations of extinct animals.

Overall this dissertation establishes the presence and preservation of eumelanin in the fossil record, sets limits on the environments likely to yield intact eumelanin, and demonstrates the preservation of ancient amino acids associated with the eumelanin in fossils. The persistence of these endogenous materials over geological time is unprecedented and indicates that there are many organic moieties still hidden in the fossils.

References

Abbas, M.; D'Amico, F.; Morresi, L.; Pinto, N.; Ficcadenti, M.; Natali, R.; Ottaviano, L.; Passacantando, M.; Cuccioloni, M.; Angeletti, M. and Gunnella, R. (2009) Structural, electrical, electronic and optical properties of melanin films. *European Physical Journal E,* **28**: 285-291.

Adhyaru, B. B.; Akhmedov, N. G.; Katritzky, A. R. and Bowers, C. R. (2003) Solid-state cross-polarization magic angle spinning C-13 and N-15 NMR characterization of Sepia melanin, Sepia melanin free acid and Human hair melanin in comparison with several model compounds. *Magnetic Resonance in Chemistry,* **41**: 466-474.

Antonio, J. D. S.; Schweitzer, M. H.; Jensen, S. T.; Kalluri, R.; Buckley, M. and Orgel, J. P. R. O. (2011) Dinosaur Peptides Suggest Mechanisms of Protein Survival. *Plos One,* **6**.

Asara, J. M.; Schweitzer, M. H.; Freimark, L. M.; Phillips, M. and Cantley, L. C. (2007) Protein sequences from mastodon and Tyrannosaurus rex revealed by mass spectrometry. *Science,* **316**: 280-285.

Bada, J. L. and Schroeder, R. A. (1975) Amino acid racemization reactions and their geochemical implications. *Naturwissenschaften,* **62**: 71-79.

Bada, J. L.; Darling, H. D.; Dungworth, G.; Kessels, H. J.; Kvenvolden, K. A. and Blunt, D. J. (1979) Amino acid racemization dating of fossil bones, I. Inter-laboratory comparison of racemization measurements. *Earth and Planetary Science Letters,* **43**: 265-268.

Bada, J. L. (1985) Racemization of amino acids. In *Chemistry and Biochemistry of the Amino Acids* (Barrett, G.C., Eds.) pp. 399-414. New York: Chapman and Hall.

Bada, J. L.; Wang, X. Y. S. and Hamilton, H. (1999) Preservation of key biomolecules in the fossil record: current knowledge and future challenges. *Philosophical Transactions of the Royal Society of London Series B-Biological Sciences,* **354**: 77-86.

Bardani, L.; Bridelli, M. G.; Carbucicchio, M. and Crippa, P. R. (1982) Comparative mossbauer and infrared-analysis of iron-containing melanins. *Biochimica Et Biophysica Acta,* **716**: 8-15.

Barden, H. E.; Wogelius, R. A.; Li, D.; Manning, P. L.; Edwards, N. P. and van Dongen, B. E. (2011) Morphological and Geochemical Evidence of Eumelanin Preservation in the Feathers of the Early Cretaceous Bird, Gansus yumenensis. *Plos One*, **6**.

Bertand, G. (1896) Sur une nouvelle oxydase, ou ferment soluble oxydant, d'origine vegetale. *Comptes Rendus des séances de la Société de Biologie (Paris)*, **112**: 1215-1217.

Berzelius, J. J. (1840) Dritte ungearbeitete und vermehrte Original Auflage. *Lehrbuch der Chemie*, **9**: 22-24.

Beyerman, K. and Hasenmai, D. (1973) Identification of 180 million years old, probably unchanged melanine. *Fresenius Zeitschrift Fur Analytische Chemie*, **266**: 202-205.

Bonser, R. H. C. (1996) The mechanical properties of feather keratin. *Journal of Zoology*, **239**: 477-484.

Boucher, J. L.; Charret, C.; Coudray-Lucas, C.; Giboudeau, J. and Cynober, L. (1997) Amino acid determination in biological fluids by automated ion-exchange chromatography: performance of Hitachi L-8500A. *Clinical Chemistry*, **43**: 1421-1428.

Boulton, M. (1998) Melanin and the Retinal Pigment Epithelium. In *The Retinal Pigment Epithelium: Function and Disease* (Marmor, M.F. and Wolfensberger, T.J., Eds.) pp. 68-85. New York: Oxford University Press.

Bourquelot, E. and Bertand, G. (1895) Le bleuissement et le noircissement des champignons. *Comptes Rendus des séances de la Société de Biologie (Paris)*, **2**: 582-584.

Brenner, M. and Hearing, V. J. (2008) The protective role of melanin against UV damage in human skin. *Photochemistry and Photobiology*, **84**: 539-549.

Bridelli, M. G. (1998) Self-assembly of melanin studied by laser light scattering. *Biophysical Chemistry*, **73**: 227-239.

Briggs, D. E. G. (1999) Molecular taphonomy of animal and plant cuticles: selective preservation and diagenesis. *Philosophical Transactions of the Royal Society B-Biological Sciences*, **354**: 7-16.

Briggs, D. E. G.; Evershed, R. P. and Lockheart, M. J. (2000) The biomolecular paleontology of continental fossils. *Paleobiology*, **26**: 169-193.

Briggs, D. E. G. (2003) The role of decay and mineralization in the preservation of soft-bodied fossils. *Annual Review of Earth and Planetary Sciences*, **31**: 275-301.

Brückner, H. (2000) Determination of free D-amino acids in mammalia by chiral gas chromatography-mass spectrometry. *Journal of High Resolution Chromatography*, **23**: 576-582.

Brynda, M. (2010) Introduction to electron paramagnetic resonance spectroscopy. In *Biomedical applications of biophysics* (Jue, T., Eds.), 3: pp. 59-98. New York: Humana Press.

Butterfield, N. J. (1990) Organic preservation of non-mineralizing organisms and the taphonomy of the Burgess Shale. *Paleobiology*, **16**: 272-286.

Carney, R. M.; Vinther, J.; Shawkey, M. D.; D'Alba, L. and Ackermann, J. (2012) New evidence on the colour and nature of the isolated Archaeopteryx feather. *Nature Communications*, **3**.

Centeno, S. A. and Shamir, J. (2008) Surface enhanced Raman scattering (SERS) and FTIR characterization of the sepia melanin pigment used in works of art. *Journal of Molecular Structure*, **873**: 149-159.

Chedekel, M. R.; Smith, S. K.; Post, P. W.; Pokora, A. and Vessell, D. L. (1978) Photodestruction of pheomelanin - role of oxygen. *Proceedings of the National Academy of Sciences of the United States of America*, **75**: 5395-5399.

Chedekel, M. R.; Agin, P. P. and Sayre, R. M. (1980) Photochemistry of pheomelanin - action spectrum for superoxide production. *Photochemistry and Photobiology*, **31**: 553-555.

Clark, M. B.; Gardella, J. A.; Schultz, T. M.; Patil, D. G. and Salvati, L. (1990) Solid-state analysis of eumelanin biopolymers by electron-spectroscopy for chemical-analysis *Analytical Chemistry*, **62**: 949-956.

Clarke, J. A.; Ksepka, D. T.; Salas-Gismondi, R.; Altamirano, A. J.; Shawkey, M. D.; D'Alba, L.; Vinther, J.; DeVries, T. J. and Baby, P. (2010) Fossil Evidence for Evolution of the Shape and Color of Penguin Feathers. *Science,* **330**: 954-957.

Cody, G. D.; Gupta, N. S.; Briggs, D. E. G.; Kilcoyne, A. L. D.; Summons, R. E.; Kenig, F.; Plotnick, R. E. and Scott, A. C. (2011) Molecular signature of chitin-protein complex in Paleozoic arthropods. *Geology,* **39**: 255-258.

Collins, M. J.; Riley, M. S.; Child, A. M. and Turnerwalker, G. (1995) A basic mathematical simulation of the chemical degradation of ancient collagen. *Journal of Archaeological Science,* **22**: 175-183.

Collins, M. J.; Gernaey, A. M.; Nielsen-Marsh, C. M.; Vermeer, C. and Westbroek, P. (2000) Slow rates of degradation of osteocalcin: Green light for fossil bone protein? *Geology,* **28**: 1139-1142.

Cox, B. M.; Hudson, J. D. and Martill, D. M. (1992) Lithostratigraphic nomenclature of the Oxford Clay (Jurassic) *Proceedings of the Geologists' Association London,* **103**: 343-345.

Cram, D. J. (1964) Fundamentals of Carbanion Chemistry. In *Organic Chemistry A Series of Monographs* (Blomquist, A.T., Eds.), 4: pp. New York: Academic Press.

Crippa, P. R.; Cristofoletti, V. and Romeo, N. (1978) Band model for melanin deduced from optical-absorption and photoconductivity experiments. *Biochimica Et Biophysica Acta,* **538**: 164-170.

d'Ischia, M.; Wakamatsu, K.; Napolitano, A.; Briganti, S.; Garcia-Borron, J. C.; Kovacs, D.; Meredith, P.; Pezzella, A.; Picardo, M.; Sarna, T.; Simon, J. D. and Ito, S. (2013) Melanins and melanogenesis: methods, standards, protocols. *Pigment Cell & Melanoma Research,* **26**: 616-633.

Damste, J. S. S. and Leeuw, J. W. (1990) Analysis, structure and geochemical significance of organically-bound sulfur in the geosphere - state-of-the-art and future-research. *Organic Geochemistry,* **16**: 1077-1101.

Davis, P. G. and Briggs, D. E. G. (1995) Fossilization of feathers. *Geology,* **23**: 783-786.

Deconinck, J. F.; Hesselbo, S. P.; Debuisser, N.; Averbuch, O.; Baudin, F. and Bessa, J. (2003) Environmental controls on clay mineralogy of an Early Jurassic mudrock (Blue Lias Formation, southern England). *International Journal of Earth Sciences,* **92**: 255-266.

Delvaux, D.; Martin, H.; Leplat, P. and Paulet, J. (1990) Comparative Rock-Eval pyrolysis as an improved tool for sedimentary organic matter analysis. *Advances in Organic Geochemistry,* **16**: 1221-1229.

Derby, C. D. and Aggio, J. F. (2011) The Neuroecology of Chemical Defenses. *Integrative and Comparative Biology,* **51**: 771-780.

Drago, R. S. (1992) Electron paramagnetic resonance spectroscopy. In *Physical Methods for Chemists* (Field, C.; Vondeling, J. and Bortel, J., Eds.) pp. 360-401. Orlando: Saunders College Publishing.

Dutta, S.; Hartkopf-Froeder, C.; Mann, U.; Wilkes, H.; Brocke, R. and Bertram, N. (2010) Macromolecular composition of Palaeozoic scolecodonts: insights into the molecular taphonomy of zoomorphs. *Lethaia,* **43**: 334-343.

Eglinton, G. and Logan, G. A. (1991) Molecular preservation. *Philosophical Transactions of the Royal Society of London Series B-Biological Sciences,* **333**: 315-328.

Espitalie, J.; Laporte, J. L.; Madec, M.; Marquis, F.; Leplat, P.; Paulet, J. and Boutefeu, A. (1977) Rapid method for source rocks characterization and for determination of petroleum potential and degree of evolution. *Revue De L Institut Francais Du Petrole,* **32**: 23-42.

Espitalie, J. (1986) Use of Tmax as a maturation index for different types of organic matter. Comparison with vitrinite reflectance. In *Thermal Modelling in Sedimentary Basins* (Burrus, J., Eds.) pp. 475-496. Paris: Technip.

Fraser, R. D. and Macrae, T. P. (1980) Molecular structure and mechanical properties of keratins. *Symposia of the Society for Experimental Biology,* **34**: 211-246.

Gilchrest, B. A.; Eller, M. S.; Geller, A. C. and Yaar, M. (1999) The pathogenesis of melanoma induced by ultraviolet radiation. *New England Journal of Medicine,* **340**: 1341-1348.

Glass, K.; Ito, S.; Wilby, P. R.; Sota, T.; Nakamura, A.; Bowers, C. R.; Vinther, J.; Dutta, S.; Summons, R.; Briggs, D. E. G.; Wakamatsu, K. and Simon, J. D. (2012) Direct chemical evidence for eumelanin pigment from the Jurassic period. *Proceedings of the National Academy of Sciences of the United States of America,* **109**: 10218-10223.

Glass, K.; Ito, S.; Wilby, P. R.; Sota, T.; Nakamura, A.; Bowers, C. R.; Miller, K. E.; Dutta, S.; Summons, R. E.; Briggs, D. E. G.; Wakamatsu, K. and Simon, J. D. (2013) Impact of diagenesis and maturation on the survival of eumelanin in the fossil record. *Organic Geochemistry,* **64**: 29-37.

Greco, G.; Wakamatsu, K.; Panzella, L.; Ito, S.; Napolitano, A. and d'Ischia, M. (2009) Isomeric cysteinyldopas provide a (photo)degradable bulk component and a robust structural element in red human hair pheomelanin. *Pigment Cell & Melanoma Research,* **22**: 319-327.

Gupta, N. S.; Michels, R.; Briggs, D. E. G.; Evershed, R. P. and Pancost, R. D. (2006) The organic preservation of fossil arthropods: an experimental study. *Proceedings of the Royal Society B-Biological Sciences,* **273**: 2777-2783.

Gupta, N. S. and Briggs, D. E. G. (2011) Taphonomy of Animal Organic Skeletons Through Time. In *Taphonomy: Process and Bias through Time, Second Edition* (Allison, P.A. and Bottjer, D.J., Eds.) pp. 199-221.

Haase, E.; Ito, S. and Wakamatsu, K. (1995) Influences of Sex, Castration, and Androgens on the Eumelanin and Pheomelanin Contents of Different Feathers in Wild Mallards. *Pigment Cell Research,* **8**: 164-170.

Halder, R. M. and Bang, K. M. (1988) Skin-cancer in blacks in the United States. *Dermatologic Clinics,* **6**: 397-405.

Higbee, A.; Wong, S. and Henzel, W. J. (2003) Automated sample preparation using vapor-phase hydrolysis for amino acid analysis. *Analytical Biochemistry,* **318**: 155-158.

Hill, H. Z. (1992) The function of melanin or six blind people examine an elephant. *Bioessays,* **14**: 49-56.

Hong, L.; Liu, Y. and Simon, J. D. (2004) Binding of metal ions to melanin and their effects on the aerobic reactivity. *Photochemistry and Photobiology*, **80**: 477-481.

Hong, L. and Simon, J. D. (2006) Insight into the binding of divalent cations to sepia eumelanin from IR absorption spectroscopy. *Photochemistry and Photobiology*, **82**: 1265-1269.

Hong, L. and Simon, J. D. (2007) Current understanding of the binding sites, capacity, affinity, and biological significance of metals in melanin. *Journal of Physical Chemistry B*, **111**: 7938-7947.

Hoss, M. (2000) Ancient DNA - Neanderthal population genetics. *Nature*, **404**: 453-454.

Hübschmann, H.-J. (2009) Sample Preparation. In *Handbook of GC/MS: Fundamentals and Applications* (Wiley-VCH, Eds.) pp. 63-70. Weinheim: Wiley-VCH.

Hudson, J. D. and Martill, D. M. (1994) The Peterborough Member (Callovian, middle Jurassic) of the Oxfod Clay formation at Peterborough, UK. *Journal of the Geological Society*, **151**: 113-124.

Ito, S. and Fujita, K. (1985) Microanalysis of eumelanin and pheomelanin in hair and melanomas by chemical degradation and liquid chromatography. *Analytical Biochemistry*, **144**: 527-536.

Ito, S. and Wakamatsu, K. (1998) Chemical degradation of melanins: Application to identification of dopamine-melanin. *Pigment Cell Research*, **11**: 120-126.

Ito, S. (2003) A chemist's view of melanogenesis. *Pigment Cell Research*, **16**: 230-236.

Ito, S. and Wakamatsu, K. (2003) Quantitative analysis of eumelanin and pheomelanin in humans, mice, and other animals: a comparative review. *Pigment Cell Research*, **16**: 523-531.

Ito, S.; Nakanishi, Y.; Valenzuela, R. K.; Brilliant, M. H.; Kolbe, L. and Wakamatsu, K. (2011) Usefulness of alkaline hydrogen peroxide oxidation to analyze eumelanin and pheomelanin in various tissue samples: application to chemical analysis of human hair melanins. *Pigment Cell & Melanoma Research*, **24**: 605-613.

Ito, S. and Wakamatsu, K. (2011) Diversity of human hair pigmentation as studied by chemical analysis of eumelanin and pheomelanin. *Journal of the European Academy of Dermatology and Venereology*, **25**: 1369-1380.

Ito, S.; Pilat, A.; Gerwat, W.; Skumatz, C. M. B.; Ito, M.; Kiyono, A.; Zadlo, A.; Nakanishi, Y.; Kolbe, L.; Burke, J. M.; Sarna, T. and Wakamatsu, K. (2013a) Photoaging of human retinal pigment epithelium is accompanied by oxidative modifications of its eumelanin. *Pigment Cell & Melanoma Research*, **26**: 357-366.

Ito, S.; Wakamatsu, K.; Glass, K. and Simon, J. D. (2013b) High-performance liquid chromatography estimation of cross-linking of dihydroxyindole moiety in eumelanin. *Analytical Biochemistry*, **434**: 221-225.

Kear, A. J.; Briggs, D. E. G. and Donovan, D. T. (1995) Decay and fossilization of nonmineralized tissue in coleoid cephalopods *Palaeontology*, **38**: 105-131.

Kenig, F.; Hayes, J. M.; Popp, B. N. and Summons, R. E. (1994) Isotopic biogeochemistry of the Oxford Clay Formation (Jurassic), UK. *Journal of the Geological Society*, **151**: 139-152.

Knicker, H. and Hatcher, P. G. (1997) Survival of protein in an organic-rich sediment: Possible protection by encapsulation in organic matter. *Naturwissenschaften*, **84**: 231-234.

Kollias, N.; Sayre, R. M.; Zeise, L. and Chedekel, M. R. (1991) Photoprotection by melanin. *Journal of Photochemistry and Photobiology B-Biology*, **9**: 135-160.

Kvenvolden, K. A.; Peterson, E. and Pollock, G. E. (1971) Geochemistry of amino acid enantiomers: gas chromatography of their diastereomeric derivatives. In *Advances in Organic Geochemistry* Eds.) pp. 387-401. New York: Pergamon Press.

Land, E. J. and Riley, P. A. (2001) Pulse radiolysis studies of *ortho*-quinone chemistry relevant to melanogenesis. *Journal of Photochemistry and Photobiology B: Biology*, **64**: 123-135.

Lang, W. D. (1924) The Blue Lias of the Devon and Dorset Coasts. *Proceedings of the Geologists' Association London*, **35**: 169-185.

Larsson, B. and Tjalve, H. (1978) Studies on melanin-affinity of metal-ions. *Acta Physiologica Scandinavica,* **104**: 479-484.

Li, Q.; Gao, K.-Q.; Vinther, J.; Shawkey, M. D.; Clarke, J. A.; D'Alba, L.; Meng, Q.; Briggs, D. E. G. and Prum, R. O. (2010) Plumage color patterns of an extinct dinosaur. *Science,* **327**: 1369-1372.

Lindahl, T. (1993) Instability and decay of the primary structure of DNA. *Nature,* **362**: 709-715.

Lindgren, J.; Uvdal, P.; Sjovall, P.; Nilsson, D. E.; Engdahl, A.; Schultz, B. P. and Thiel, V. (2012) Molecular preservation of the pigment melanin in fossil melanosomes. *Nature Communications,* **3**.

Lindgren, J.; Kaddumi, H. F. and Polcyn, M. J. (2013) Soft tissue preservation in a fossil marine lizard with a bilobed tail fin. *Nature Communications,* **4**.

Lindgren, J.; Sjovall, P.; Carney, R. M.; Uvdal, P.; Gren, J. A.; Dyke, G.; Schultz, B. P.; Shawkey, M. D.; Barnes, K. R. and Polcyn, M. J. (2014) Skin pigmentation provides evidence of convergent melanism in extinct marine reptiles. *Nature*: 5.

Lindqvist, C.; Schuster, S. C.; Sun, Y. Z.; Talbot, S. L.; Qi, J.; Ratan, A.; Tomsho, L. P.; Kasson, L.; Zeyl, E.; Aars, J.; Miller, W.; Ingolfsson, O.; Bachmann, L. and Wiig, O. (2010) Complete mitochondrial genome of a Pleistocene jawbone unveils the origin of polar bear. *Proceedings of the National Academy of Sciences of the United States of America,* **107**: 5053-5057.

Littke, R.; Rotzal, H.; Leythaeuser, D. and Baker, D. R. (1991) Lower Toarcian Posidonia Shale in southern Germany (Schwabische-Alb) - organic facies, depositional environment, and maturity *Erdol & Kohle Erdgas Petrochemie,* **44**: 407-414.

Liu, Y. and Simon, J. D. (2003) The effect of preparation procedures on the morphology of melanin from the ink sac of Sepia officinalis. *Pigment Cell Research,* **16**: 72-80.

Liu, Y.; Hong, L.; Kempf, V. R.; Wakamatsu, K.; Ito, S. and Simon, J. D. (2004) Ion-exchange and adsorption of Fe(III) by Sepia melanin. *Pigment Cell Research,* **17**: 262-269.

Liu, Y.; Hong, L.; Wakamatsu, K.; Ito, S.; Adhyaru, B.; Cheng, C. Y.; Bowers, C. R. and Simon, J. D. (2005) Comparison of structural and chemical properties of black and red human hair melanosomes. *Photochemistry and Photobiology*, **81**: 135-144.

Liu, Y. and Simon, J. D. (2005) Metal-ion interactions and the structural organization of Sepia eumelanin. *Pigment Cell Research*, **18**: 42-48.

Manning, P. L.; Edwards, N. P.; Wogelius, R. A.; Bergmann, U.; Barden, H. E.; Larson, P. L.; Schwarz-Wings, D.; Egerton, V. M.; Sokaras, D.; Mori, R. A. and Sellers, W. I. (2013) Synchrotron-based chemical imaging reveals plumage patterns in a 150 million year old early bird. *Journal of Analytical Atomic Spectrometry*, **28**: 1024-1030.

Mason, H. S. (1948) The chemistry of melanin. III. Mechanisms of the oxidation of dihydroxyphenylalanine by tyrosinase. *Journal of Biological Chemistry*, **172**: 83-92.

McCarthy, K.; Rojas, K.; Niemann, M.; Palmowski, D.; Peters, K. and Stankiewicz, A. (2011) Basic petroleum geochemistry for source rock evaluation. *Oilfield Reviews*, **23**: 32-43.

McDonald, J. H., (2008) *Handbook of Biological Statistics*, Baltimore: Sparky House.

McGraw, K. J. and Wakamatsu, K. (2004) Melanin basis of ornamental feather colors in male Zebra Finches. *Condor*, **106**: 686-690.

McNamara, M. E. (2013) The taphonomy of colour in fossil insects and feathers. *Palaeontology*, **56**: 557-575.

McNamara, M. E.; Briggs, D. E. G.; Orr, P. J.; Field, D. J. and Wang, Z. (2013) Experimental maturation of feathers: implications for reconstructions of fossil feather colour. *Biology Letters*, **9**.

Meng, S. and Kaxiras, E. (2008) Theoretical models of eumelanin protomolecules and their optical properties. *Biophysical Journal*, **94**: 2095-2105.

Meredith, P. and Sarna, T. (2006) The physical and chemical properties of eumelanin. *Pigment Cell Research,* **19**: 572-594.

Minale, L.; Fattorusso, E.; Cimino, G.; De Stefano, S. and Nicolaus, R. A. (1967) Structure and biogenesis of pheomelanins. II. Degradation products. *Gazzetta Chimica Italiana,* **97**: 1636-1663.

Moyer, A. E.; Zheng, W.; Johnson, E. A.; Lamanna, M. C.; Li, D.-q.; Lacovara, K. J. and Schweitzer, M. H. (2014) Melanosomes or Microbes: Testing an Alternative Hypothesis for the Origin of Microbodies in Fossil Feathers. *Sci. Rep.,* **4**.

Napolitano, A.; Vincensi, M. R.; Di Donato, P.; Monfrecola, G. and Prota, G. (2000) Microanalysis of melanins in mammalian hair by alkaline hydrogen peroxide degradation: Identification of a new structural marker of pheomelanins. *Journal of Investigative Dermatology,* **114**: 1141-1147.

Neuberger, A. (1948) Stereochemistry of amino acids. In *Advances in protein chemistry* (Anson, M.L. and Edsall, J.T., Eds.), 4: pp. 297-383. New York: Academic Press.

Ni, M. and Ratner, B. D. (2008) Differentiating calcium carbonate polymorphs by surface analysis techniques - an XPS and TOF-SIMS study. *Surface and Interface Analysis,* **40**: 1356-1361.

Nicolaus, R. A., (1968) *Melanins*, Paris: Hermann Press.

Nielsen-Marsh, C. M. (2002) Biomolecules in fossil remains. *The Biochemist*: 12-14.

Nofsinger, J. B.; Liu, Y. and Simon, J. D. (2002) Aggregation of eumelanin mitigates photogeneration of reactive oxygen species. *Free Radical Biology and Medicine,* **32**: 720-730.

Oliveira, H. P.; Graeff, C. F. O.; Brunello, C. A. and Guerra, E. M. (2000) Electrochromic and conductivity properties: a comparative study between melanin-like/V2O5 center dot nH(2)O and polyaniline/V2O5 center dot nH(2)O hybrid materials. *Journal of Non-Crystalline Solids,* **273**: 193-197.

Ozeki, H.; Ito, S. and Wakamatsu, K. (1996a) Chemical characterization of melanins in sheep wool and human hair. *Pigment Cell Research,* **9**: 51-57.

Ozeki, H.; Ito, S.; Wakamatsu, K. and Thody, A. J. (1996b) Spectrophotometric characterization of eumelanin and pheomelanin in hair. *Pigment Cell Research,* **9**: 265-270.

Palumbo, A. (2003) Melanogenesis in the ink gland of *Sepia officinalis*. *Pigment Cell Research,* **16**: 517-522.

Panizzi, L. and Nicolaus, R. A. (1952) Ricerche sulle melanine. *Gazzetta Chimica Italiana,* **82**: 435-460.

Panzella, L.; Manini, P.; Monfrecola, G.; d'Ischia, M. and Napolitano, A. (2007) An easy-to-run method for routine analysis of eumelanin and pheomelanin in pigmented tissues. *Pigment Cell Research,* **20**: 128-133.

Peles, D. N.; Hong, L.; Hu, D. N.; Ito, S.; Nemanich, R. J. and Simon, J. D. (2009) Human Iridal Stroma Melanosomes of Varying Pheomelanin Contents Possess a Common Eumelanic Outer Surface. *Journal of Physical Chemistry B,* **113**: 11346-11351.

Penn, I. E.; Cox, B. M. and Gallois, R. W. (1986) Towards precision in statigraphy - geophysical log correlation of upper Jurassic (including Callovian) strata of the eastern England shelf. *Journal of the Geological Society*, **143**: 381-410.

PerkinElmer (2013) *Material Safety Data Sheet*, Soluene-350. http://www.perkinelmer.com/Catalog/Product/ID/6003038.

Pezzella, A.; dIschia, M.; Napolitano, A.; Palumbo, A. and Prota, G. (1997) An integrated approach to the structure of Sepia melanin. Evidence for a high proportion of degraded 5,6-dihydroxyindole-2-carboxylic acid units in the pigment backbone. *Tetrahedron,* **53**: 8281-8286.

Piatelli, M.; Fattorusso, E.; Magno, S. and Nicolaus, R. A. (1962) The structure of melanins and melanogenesis. II. Sepiomelanin and synthetic pigments. *Tetrahedron*, **18**: 941-949.

Potts, A. M. and Au, P. C. (1976) Affinity of melanin for inorganic-ions. *Experimental Eye Research,* **22**: 487-491.

Prauss, M.; Ligouis, B. and Luterbacher, H. (1991) Organic matter and palynomorphs in the 'Posidonienschiefer' (Toarcian, Lower Jurassic) of southern Germany. *Modern and Ancient Continental Shelf Anoxia*, **58**: 335-351.

Prota, G.; Piatelli, M. and Nicolaus, R. A. (1966) Preliminary results in the study of phaeomelanins. *Rendiconto dell'Accademia delle Scienze Fisiche e Matematiche*, **33**: 146-150.

Prota, G. and Nicolaus, R. A. (1967a) On the biogenesis of phaeomelanins. In *Advances in Biology of Skin* (Montagna, W. and Hu, F.E., Eds.), 8: pp. 323-328. New York: Pergamon Press.

Prota, G. and Nicolaus, R. A. (1967b) Structtura e biogenesi delle feomelanine. Nota I. Isolamento e propprieta dei pigmenti delle piume. *Gazzetta Chimica Italiana*, **97**: 665-684.

Prota, G., (1992) *Melanins and Melanogenesis*, San Diego: Academic Press, Inc. .

Qian, Y. R.; Engel, M. H.; Macko, S. A.; Carpenter, S. and Deming, J. W. (1993) Kinetics of peptide hydrolysis and amino-acid decomposition at high-temperature. *Geochimica Et Cosmochimica Acta*, **57**: 3281-3293.

Raper, H. S. (1927) The tyrosinase-tyrosine reaction. VI. Production from tyrosine of 5,6-dihydroxyindole and 5,6-dihydroxyindole-2-carboxylic acid the precursor of melanin. *Biochemical Journal*, **90**: 4137-4144.

Riley, P. A. (1997) Melanin. *International Journal of Biochemistry & Cell Biology*, **29**: 1235-1239.

Rohl, H. J.; Schmid-Rohl, A.; Oschmann, W.; Frimmel, A. and Schwark, L. (2001) The Posidonia Shale (Lower Toarcian) of SW-Germany: an oxygen-depleted ecosystem controlled by sea level and palaeoclimate. *Palaeogeography Palaeoclimatology Palaeoecology*, **165**: 27-52.

Rutherfurd, S. M. and Gilani, G. S. (2001) Amino Acid Analysis. In *Current Protocols in Protein Science* Eds.) pp. 1-37 John Wiley & Sons, Inc.

Salamon, M.; Tuross, N.; Arensburg, B. and Weiner, S. (2005) Relatively well preserved DNA is present in the crystal aggregates of fossil bones. *Proceedings of the National Academy of Sciences of the United States of America*, **102**: 13783-13788.

Sarna, T.; Hyde, J. S. and Swartz, H. M. (1976) Ion-exchange in melanin - electron-spin resonance study with lanthanide probes. *Science*, **192**: 1132-1134.

Sarna, T. and Sealy, R. C. (1984) Photoinduced oxygen-consumption in melanin systems - action spectra and quantum yields for eumelanins and synthetic melanin. *Photochemistry and Photobiology*, **39**: 69-74.

Sarna, T. (1992) Properties and function of the ocular melanin - a photobiophysical view. *Journal of Photochemistry and Photobiology B-Biology*, **12**: 215-258.

Sarna, T. and Swartz, H. A. (2006) The Physical Properties of Melanins. In *The Pigmentary System* (Norlund, J.J.; Boissy, R.E.; Hearing, V.J.; King, R.A.; Oetting, W.S. and Ortonne, J.-P., Eds.) pp. 311-341. Malden: Blackwell Publishing.

Sarzanini, C.; Mentasti, E.; Abollino, O.; Fasano, M. and Aime, S. (1992) Melanin-ion content in *Sepia officinalis* melanin *Marine Chemistry*, **39**: 243-250.

Schraermeyer, U. (1994) Fine structure of melanogenesis in the ink sac of *Sepia officinalis* *Pigment Cell Research*, **7**: 52-60.

Schroeder, R. A. and Bada, J. L. (1976) Review of geochemical application of amino-acid racemization reaction. *Earth-Science Reviews*, **12**: 347-391.

Schweitzer, M. H.; Suo, Z.; Avci, R.; Asara, J. M.; Allen, M. A.; Arce, F. T. and Horner, J. R. (2007a) Analyses of soft tissue from Tyrannosaurus rex suggest the presence of protein. *Science*, **316**: 277-280.

Schweitzer, M. H.; Wittmeyer, J. L. and Horner, J. R. (2007b) Soft tissue and cellular preservation in vertebrate skeletal elements from the Cretaceous to the present (vol 274, pg 183, 2006). *Proceedings of the Royal Society B-Biological Sciences*, **274**: 3183-3183.

Schweitzer, M. H.; Avci, R.; Collier, T. and Goodwin, M. B. (2008) Microscopic, chemical and molecular methods for examining fossil preservation. *Comptes Rendus Palevol*, **7**: 159-184.

Schweitzer, M. H.; Zheng, W. X.; Organ, C. L.; Avci, R.; Suo, Z. Y.; Freimark, L. M.; Lebleu, V. S.; Duncan, M. B.; Heiden, M. G. V.; Neveu, J. M.; Lane, W. S.; Cottrell, J. S.; Horner, J. R.; Cantley, L. C.; Kalluri, R. and Asara, J. M. (2009) Biomolecular Characterization and Protein Sequences of the Campanian Hadrosaur B. canadensis. *Science*, **324**: 626-631.

Schweitzer, M. H. (2011) Soft Tissue Preservation in Terrestrial Mesozoic Vertebrates. In *Annual Review of Earth and Planetary Sciences, Vol 39* (Jeanloz, R. and Freeman, K.H., Eds.), 39: pp. 187-216.

Sealy, R. C.; Hyde, J. S.; Felix, C. C.; Menon, I. A. and Prota, G. (1982) Eumelanins and pheomelains - characterization by electron-spin resonance spectroscopy. *Science*, **217**: 545-547.

Sherman Hsu, C. P. (1997) Infrared spectroscopy. In *Handbook of Instrumental Techniques for Analytical Chemistry* (Seattle, F.A., Eds.) pp. 247-284. Englewood Cliffs: Prentice-Hall.

Simon, J. D.; Peles, D.; Wakamatsu, K. and Ito, S. (2009) Current challenges in understanding melanogenesis: bridging chemistry, biological control, morphology, and function. *Pigment Cell & Melanoma Research*, **22**: 563-579.

Simon, J. D. and Peles, D. N. (2010) The Red and the Black. *Accounts of Chemical Research*, **43**: 1452-1460.

Simpson, M. J.; Glass, K. E.; Wilson, J. W.; Wilby, P. R.; Simon, J. D. and Warren, W. S. (2013) Pump-Probe Microscopic Imaging of Jurassic-Aged Eumelanin. *Journal of Physical Chemistry Letters*, **4**: 1924-1927.

Simpson, M. J.; Wilson, J. W.; Robles, F. E.; Dall, C. P.; Glass, K.; Simon, J. D. and Warren, W. S. (2014) Near-Infrared Excited State Dynamics of Melanins: The Effects of Iron Content, Photo-Damage, Chemical Oxidation, and Aggregate Size. *The Journal of Physical Chemistry A*, **118**: 993-1003.

Stankiewicz, B. A.; Briggs, D. E. G.; Evershed, R. P.; Flannery, M. B. and Wuttke, M. (1997) Preservation of chitin in 25-million-year-old fossils. *Science,* **276**: 1541-1543.

Stankiewicz, B. A.; Poinar, H. N.; Briggs, D. E. G.; Evershed, R. P. and Poinar, G. O. (1998) Chemical preservation of plants and insects in natural resins. *Proceedings of the Royal Society B-Biological Sciences,* **265**: 641-647.

Stankiewicz, B. A.; Briggs, D. E. G.; Michels, R.; Collinson, M. E.; Flannery, M. B. and Evershed, R. P. (2000) Alternative origin of aliphatic polymer in kerogen. *Geology,* **28**: 559-562.

Stepien, K.; Dzierzega-Lecznar, A.; Kurkiewicz, S. and Tam, I. (2009) Melanin from Epidermal Human Melanocytes: Study by Pyrolytic GC/MS. *Journal of the American Society for Mass Spectrometry,* **20**: 464-468.

Swartz, W. E. (1973) X-ray photoelectron spectroscopy *Analytical Chemistry,* **45**: 788-800.

Tegelaar, E. W.; Deleeuw, J. W.; Derenne, S. and Largeau, C. (1989) A reappraisal of kerogen formation. *Geochimica Et Cosmochimica Acta,* **53**: 3103-3106.

Thompson, M. (2008) *CHNS Elemental Anaysers*. Analytical Methods Committee, AMC Technical Briefs

Tiemann, T. K. (2010) F-test and one-way anova. In *Introduction to Business Statistics* (Tiemann, T.K.; Drexel, M.; Sharman, J. and Walton, L., Eds.) pp. 52-58. Zurich: Global Text.

Traub, W.; Arad, T. and Weiner, S. (1993) Mineralization of collagen fibrils. *Journal of Cellular Biochemistry*: 145-145.

Vinther, J.; Briggs, D. E. G.; Prum, R. O. and Saranathan, V. (2008) The colour of fossil feathers. *Biology Letters,* **4**: 522-525.

Vinther, J.; Briggs, D. E. G.; Clarke, J.; Mayr, G. and Prum, R. O. (2010) Structural coloration in a fossil feather. *Biology Letters,* **6**: 128-131.

Wakamatsu, K. and Ito, S. (1988) Preparation of eumelanin-related metabolites 5,6-dihydroxyindole, 5,6-dihydroxyindole-2-carboxylic acid, and their *o*-methyl derivatives. *Analytical Biochemistry*, **170**: 335-340.

Wakamatsu, K. and Ito, S. (2002) Advanced chemical methods in melanin determination. *Pigment Cell Research*, **15**: 174-183.

Wakamatsu, K.; Kavanagh, R.; Kadekaro, A. L.; Terzieva, S.; Sturm, R. A.; Leachman, S.; Abdel-Malek, Z. and Ito, S. (2006) Diversity of pigmentation in cultured human melanocytes is due to differences in the type as well as quantity of melanin. *Pigment Cell Research*, **19**: 154-162.

Wakamatsu, K.; Ohtara, K. and Ito, S. (2009) Chemical analysis of late stages of pheomelanogenesis: conversion of dihydrobenzothiazine to a benzothiazole structure. *Pigment Cell & Melanoma Research*, **22**: 474-486.

Wakamatsu, K.; Nakanishi, Y.; Miyazaki, N.; Kolbe, L. and Ito, S. (2012) UVA-induced oxidative degradation of melanins: fission of indole moiety in eumelanin and conversion to benzothiazole moiety in pheomelanin. *Pigment Cell & Melanoma Research*, **25**: 434-445.

Ward, W. C.; Lamb, E. C.; Gooden, D.; Chen, X.; Burinsky, D. J. and Simon, J. D. (2008) Quantification of naturally occurring pyrrole acids in melanosomes. *Photochemistry and Photobiology*, **84**: 700-705.

Weiner, S. and Traub, W. (1986) Organization of hydroxyapatite crystals within collagen fibrils. *Febs Letters*, **206**: 262-266.

Wenczl, E.; Van der Schans, G. P.; Roza, L.; Kolb, R. M.; Timmerman, A. J.; Smit, N. P. M.; Pavel, S. and Schothorst, A. A. (1998) (Pheo)melanin photosensitizes UVA-induced DNA damage in cultured human melanocytes. *Journal of Investigative Dermatology*, **111**: 678-682.

Wilby, P. R.; Hudson, J. D.; Clements, R. G. and Hollingworth, N. T. J. (2004) Taphonomy and origin of an accumulate of soft-bodied cephalopods in the Oxford Clay Formation (Jurassic, England). *Palaeontology*, **47**: 1159-1180.

Wogelius, R. A.; Manning, P. L.; Barden, H. E.; Edwards, N. P.; Webb, S. M.; Sellers, W. I.; Taylor, K. G.; Larson, P. L.; Dodson, P.; You, H.; Da-Qing, L. and Bergmann, U. (2011) Trace Metals as Biomarkers for Eumelanin Pigment in the Fossil Record. *Science,* **333**: 1622-1626.

Wolbarsht, M. L.; Walsh, A. W. and George, G. (1981) Melanin, a unique biological absorber. *Applied Optics,* **20**: 2184-2186.

Yalçin Erik, N.; Özçelik, O. and Altunsoy, M. (2006) Interpreting Rock-Eval pyrolysis data using graphs of S2 vs. TOC: Middle Triassic-Lower Jurassic units, eastern part of SE Turkey. *Journal of Petroleum Science and Engineering,* **53**: 34-46.

Zareba, M.; Bober, A.; Korytowski, W.; Zecca, L. and Sarna, T. (1995) The effect of a synthetic neuromelanin on yield of free hydroxyl radicals generated in model systems. *Biochimica Et Biophysica Acta-Molecular Basis of Disease,* **1271**: 343-348.

Zemlyanov, D. (2011) A new window opens. *Nature Nanotechnology,* **6**: 612-613.

Zhang, F.; Kearns, S. L.; Orr, P. J.; Benton, M. J.; Zhou, Z.; Johnson, D.; Xu, X. and Wang, X. (2010) Fossilized melanosomes and the colour of Cretaceous dinosaurs and birds. *Nature,* **463**: 1075-1078.

Zhang, J. Z. (2009a) Spectroscopic techniques for studying optical properties of nanomaterials. In *Optical properties and spectroscopy of nanomaterials* (Zhang, J.Z., Eds.) pp. Hackensack: World Scientific.

Zhang, J. Z. (2009b) Other experimental techniques: electron microscopy and x-ray. In *Optical Properties and Spectroscopy of Nanomaterials* (Zhang, J.Z., Eds.) pp. Hackensack: World Scientific

Zhou, W.; Apkarian, R. P.; Wang, Z. L. and Joy, D. (2007) Fundamentals of scanning electron microscopy. In *Scanning Microscopy for Nanotechnology: Techniques and Applications* (Zhou, W. and Wang, Z.L., Eds.) pp. 1-40. New York: Springer.

Biography

Keely Elizabeth Glass

Personal

Born December 29, 1987 in Thousand Oaks, California, USA

Education

B.S.,	Chemistry with Biochemistry	Wake Forest University	December 2008
Ph.D.,	Chemistry	Duke University	May 2014

Publications

Keely Glass, Shosuke Ito, Philip R. Wilby, Takayuki Sota, Atsushi Nakamura, C. Russell Bowers, Jakob Vinther, Suryendu Dutta, Roger Summons, Derek E. G. Briggs, Kazumasa Wakamatsu, and John D. Simon, (2012) Direct chemical evidence for eumelanin pigment from the Jurassic period, *Proceedings of the National Academy of Sciences*, **109**(26): 10218-10223.

Shosuke Ito, Kazumasa Wakamatsu, Keely Glass, and John D. Simon, (2013) High-performance liquid chromatography estimation of cross-linking of dihydroxyindole moiety in eumelanin, *Analytical Biochemistry*, **434**(2): 221-225.

Mary Jane Simpson, Keely E. Glass, Jesse W. Wilson, Philip R. Wilby, John D. Simon, and Warren S. Warren, (2013) Pump-probe microscope imaging of Jurassic-aged eumelanin, *Journal of Physical Chemistry Letters*, **4**(11): 1924-1927.

Keely Glass, Shosuke Ito, Philip R. Wilby, Takayuki Sota, Atsushi Nakamura, C. Russell Bowers, Kristen E. Miller, Suryendu Dutta, Roger E. Summons, Derek E. G. Briggs, Kazumasa Wakamatsu, and John D. Simon, (2013) Impact of diagenesis and maturation on the survival of eumelanin in the fossil record, *Organic Geochemistry*, **64**: 29-37.

Mary Jane Simpson, Jesse W. Wilson, Francisco E. Robles, Christopher P. Dall, Keely Glass, John D. Simon, and Warren S. Warren, (2014) Near-infrared excited state dynamics of melanins: the effects of iron content, photo-damage, chemical oxidation, and aggregate size, *Journal of Physical Chemistry A*, **118**(6): 993-1003.